

**Springer Theses**

Recognizing Outstanding Ph.D. Research

Evdokiya Georgieva Kostadinova

# Spectral Approach to Transport Problems in Two-Dimensional Disordered Lattices

Physical Interpretation and  
Applications

 Springer

# **Springer Theses**

Recognizing Outstanding Ph.D. Research

## **Aims and Scope**

The series “Springer Theses” brings together a selection of the very best Ph.D. theses from around the world and across the physical sciences. Nominated and endorsed by two recognized specialists, each published volume has been selected for its scientific excellence and the high impact of its contents for the pertinent field of research. For greater accessibility to non-specialists, the published versions include an extended introduction, as well as a foreword by the student’s supervisor explaining the special relevance of the work for the field. As a whole, the series will provide a valuable resource both for newcomers to the research fields described, and for other scientists seeking detailed background information on special questions. Finally, it provides an accredited documentation of the valuable contributions made by today’s younger generation of scientists.

### **Theses are accepted into the series by invited nomination only and must fulfill all of the following criteria**

- They must be written in good English.
- The topic should fall within the confines of Chemistry, Physics, Earth Sciences, Engineering and related interdisciplinary fields such as Materials, Nanoscience, Chemical Engineering, Complex Systems and Biophysics.
- The work reported in the thesis must represent a significant scientific advance.
- If the thesis includes previously published material, permission to reproduce this must be gained from the respective copyright holder.
- They must have been examined and passed during the 12 months prior to nomination.
- Each thesis should include a foreword by the supervisor outlining the significance of its content.
- The theses should have a clearly defined structure including an introduction accessible to scientists not expert in that particular field.

More information about this series at <http://www.springer.com/series/8790>

Evdokiya Georgieva Kostadinova

# Spectral Approach to Transport Problems in Two-Dimensional Disordered Lattices

Physical Interpretation and Applications

Doctoral Thesis accepted by  
Baylor University, Waco, Texas, USA

 Springer

Evdokiya Georgieva Kostadinova  
Center for Astrophysics  
Space Physics and Engineering Research  
Baylor University  
Waco, TX, USA

ISSN 2190-5053

ISSN 2190-5061 (electronic)

Springer Theses

ISBN 978-3-030-02211-2

ISBN 978-3-030-02212-9 (eBook)

<https://doi.org/10.1007/978-3-030-02212-9>

Library of Congress Control Number: 2018960269

© Springer Nature Switzerland AG 2018

This work is subject to copyright. All rights are reserved by the Publisher, whether the whole or part of the material is concerned, specifically the rights of translation, reprinting, reuse of illustrations, recitation, broadcasting, reproduction on microfilms or in any other physical way, and transmission or information storage and retrieval, electronic adaptation, computer software, or by similar or dissimilar methodology now known or hereafter developed.

The use of general descriptive names, registered names, trademarks, service marks, etc. in this publication does not imply, even in the absence of a specific statement, that such names are exempt from the relevant protective laws and regulations and therefore free for general use.

The publisher, the authors, and the editors are safe to assume that the advice and information in this book are believed to be true and accurate at the date of publication. Neither the publisher nor the authors or the editors give a warranty, express or implied, with respect to the material contained herein or for any errors or omissions that may have been made. The publisher remains neutral with regard to jurisdictional claims in published maps and institutional affiliations.

This Springer imprint is published by the registered company Springer Nature Switzerland AG  
The registered company address is: Gewerbestrasse 11, 6330 Cham, Switzerland

*To my father, Georgy Dimitrov Kostadinov.  
Every day I wake up and know I can do  
anything in a world where you love me and  
have my back. Look how far we've gone, and  
this is only the beginning!*

# Supervisor's Foreword

From our earliest observations of lightning to the most recent achievements in nanoelectronics, electrical phenomena have been transformative to human life. This is not surprising, given that the fundamental physics behind electromagnetics is closely related to the very nature and properties of matter itself. Although the *effects* of the electric field force were known to the ancient Egyptians, Arabs, and Greeks, it was not until the eighteenth and nineteenth centuries before such phenomena were investigated using scientific methods and mathematical techniques. Early on, the groundbreaking work of Franklin, Volta, Ampère, Faraday, and Maxwell paved the way for the discovery of the electric charge in 1896 by J. J. Thomson. Later, the realization that the electric field is directly related to the guided motion of individual particles led to the development of the Drude model for conductivity in 1900 and the understanding that free electrons scatter from positive ions in metal lattice sites, much like steel balls in a pinball machine. This led to the expectation that conductivity should be directly proportional to the average distance an electron travels between collisions with an ion. However, a few decades later, quantum mechanics showed that due to the wave-particle duality of matter, electrons actually diffract from positive ions in an ideal crystal and collisions occur only when impurities (or lattice defects) are present.

The above led Philip Anderson in 1958 to argue that electron localization in a lattice potential is possible, given a critical level of disorder. In this case, the scattering or the resistance in the crystal increases and the traveling wave-particle experiences a transition from an extended to a localized state.

The resulting (now standard) approach to the Anderson localization problem, called scaling theory, has proved widely successful for both 1D and 3D systems. However, in the critical 2D case, scaling theory predicts that all energy states are localized for any (nonzero) amount of disorder. Since metallic behavior has been both numerically predicted and experimentally observed for various 2D systems, including electron gases, cold atoms, and photonic lattices, this immediately leads to an interesting conundrum known as the Anderson 2D localization problem. With the recent discovery of graphene and other two-dimensional materials, the resolution of this contradiction is more pressing than ever.

Eva Kostadinova chose to conduct her doctoral research at this intersection of fundamental physics. The Anderson 2D localization problem has been left unsolved for over 50 years at least in part due to the need to master material across multiple disciplines before one can even consider approaching it. In order to accomplish the research that ended up comprising her dissertation, Eva had to first become familiar with a number of diverse research areas crossing physics, mathematics, and statistics. Most students, once aware of the magnitude of such an endeavor, would have redirected their research toward a less demanding problem. Eva instead simply began working with Dr. Constanze Liaw (then in the Department of Mathematics at Baylor and now at the University of Delaware) to discover how a spectral method Dr. Liaw had recently developed might be repurposed to provide data on the problem. Along the way, she also introduced herself to Dr. Mandy Hering (Baylor Department of Statistical Science) who provided the statistical analysis she needed to help with the numerical work involved.

In her dissertation, Eva argues that this novel mathematical technique, the spectral approach, provides a possible solution to the Anderson localization problem. The spectral approach predicts the existence of extended states in 2D crystals with nonzero disorder, in qualitative agreement with existing experimental results. Although recognized among mathematicians, this method is little known to the physics community. The present work offers the first attempt to provide physical interpretation of the spectral approach and explores its application to transport problems in various 2D-disordered lattices.

This interdisciplinary work provides important new insights in the transport behavior of 2D materials by building a bridge between semiclassical physics, materials science, and mathematics. The result is a valuable study that leads us ever closer to a solution of the Anderson 2D localization problem.

Center for Astrophysics,  
Space Physics & Engineering Research  
and Department of Physics  
Baylor University  
Waco, TX, USA

Dr. Truell Hyde

# Acknowledgments

This work was supported by the Simons Foundation/NSF/DMS (Simons Foundation grant number 426258 and NSF/DMS grant number 1700204, Constanze Liaw) and NASA/NSF (NASA grant number 1571701 and NSF grant numbers 1414523, 1740203, and 1262031, Lorin Matthews and Truell Hyde).

The author gratefully acknowledges the contribution of Dr. Amanda Hering, who provided valuable advice on the statistical analysis of our data.

# Contents

<b>1</b>	<b>Introduction</b> . . . . .	<b>1</b>
<b>2</b>	<b>Theoretical Background</b> . . . . .	<b>13</b>
<b>3</b>	<b>Spectral Approach</b> . . . . .	<b>27</b>
<b>4</b>	<b>Delocalization in 2D Lattices of Various Geometries</b> . . . . .	<b>43</b>
<b>5</b>	<b>Transport in the Two-Dimensional Honeycomb Lattice with Substitutional Disorder</b> . . . . .	<b>55</b>
<b>6</b>	<b>Transport in 2D Complex Plasma Crystals</b> . . . . .	<b>73</b>
<b>7</b>	<b>Conclusions</b> . . . . .	<b>87</b>
	<b>Appendix A: Basic Materials Science Terms</b> . . . . .	<b>91</b>
	<b>Appendix B: Mathematical Preliminaries</b> . . . . .	<b>95</b>
	<b>Curriculum Vitae</b> . . . . .	<b>103</b>

**Parts of this thesis have been published in the following journal articles:**

1. Kostadinova, E. G., Liaw, C. D., Matthews, L. S., & Hyde, T. W. (2016). Physical interpretation of the spectral approach to delocalization in infinite disordered systems. *Materials Research Express*, 3(12), 125904.
2. Kostadinova, E. G., Busse, K., Ellis, N., Padgett, J., Liaw, C. D., Matthews, L. S., & Hyde, T. W. (2017). Delocalization in infinite disordered two-dimensional lattices of different geometry. *Physical Review B*, 96(23), 235408.
3. Kostadinova, E. G., Guyton, F., Cameron, A., Busse, K., Liaw, C., Matthews, L. S., & Hyde, T. W. (2018). Transport properties of disordered two-dimensional complex plasma crystal. *Contributions to Plasma Physics*, 58(2–3), 209–216.

# Chapter 1

## Introduction



In condensed matter physics, a crystal without impurities is often described by the one-electron model (Fig. 1.1), where the transport properties of the material are studied using the energy spectrum of a single electron moving under the influence of a periodic array of atoms [1]. Neglecting interaction between electrons, the one-electron Hamiltonian is given by

$$H_0 \equiv K + V_0, \quad (1.1)$$

where  $K$  is the kinetic energy of the particle and  $V_0$  is the periodic potential function of the lattice. Throughout this work, we take  $K \equiv -\Delta$ , where  $\Delta$  is the discrete Laplacian<sup>1</sup> on the Hilbert space  $\mathcal{H}$ . A crucial assumption of the one-electron model is that the medium is infinite in space, which allows for the use of statistical mechanics without considerations of finite size and boundary effects. However, a common practice is to approximate the infinite system by a finite one, where one examines the dependence of relevant properties on system size. Such methods are incomplete without a proper scaling approach, which extends the finite volume back to infinity and recovers the properties of the extended system. A primary goal of this book is to point out possible issues related to scaling and propose an alternative approach to transport problems, which does not require finite-size approximations.

The one-electron model has shown remarkable success in the theoretical analysis of basic transport features in unperturbed lattices. However, ‘real’ crystals (such as those produced in a laboratory or semiconductor manufacturing facility) are characterized by a variety of imperfections, which interact with the traveling electron and affect significantly the transport properties of the material. As lattice disorder increases to a critical value, the electron wave-particle may experience a transition from an extended to a localized state; this is an example of a metal-to-insulator

---

<sup>1</sup>The discrete Laplacian is the analogue of the continuous Laplacian on a graph or a discrete grid. Here, it represents the energy transfer term (nearest neighbor interaction) of the Hamiltonian.

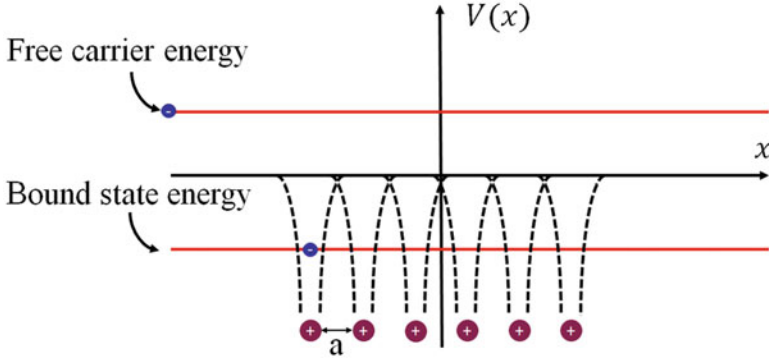


**Fig. 1.1** In the one-electron model, the transport behavior of the system is described by the energy spectrum of a single electron moving through a periodic array of identical atoms. Despite its success in describing some important features of conductivity, the one-electron model does not account for the effects produced by lattice impurities

transition (MIT) in the medium (see Fig. 1.2). In 1958 P.W. Anderson [2] proposed that at zero temperature<sup>2</sup> the quantum-mechanical motion of a wave-particle may come to a halt due to sufficiently large spatial disorder within the system. This phenomenon is now known as Anderson localization. Due to its wide applicability, the subject of Anderson localization and the related transport problems arising from it has grown into a rich field in both physics and mathematics.

Most of the numerical results presented in this work examine transport problems in the static-lattice, zero-temperature limit, which is the case originally considered by the Anderson model. The importance of studying transport in this regime is best summarized by David Thouless (winner of the 2016 Nobel Prize for physics) [3]:

“This restriction is made not because we think that effects of dynamics and correlations are unimportant but because we believe that a thorough understanding of the restricted problem is necessary before real progress can be made with the more general problem.”

It has been shown that various aspects of the static scenario can be incorporated into a class of perturbation problems described by the so-called Anderson-type Hamiltonians (first introduced in [4]). In general, the Anderson-type Hamiltonian on the Hilbert space  $\mathcal{H}$  can be defined as a self-adjoint linear operator of the form

$$H_\epsilon = H_0 + V_\epsilon, \quad (1.2)$$

where  $H_0$  is the Hamiltonian of the unperturbed crystal as given in Eq. (1.1) and  $V_\epsilon$  is a distribution of random variables, representing the disorder within the system. To

<sup>2</sup>The zero-temperature approximation is an important limitation of the Anderson model as it neglects the contact of the system with any external thermal bath. Since thermal fluctuations often play important role in real experiments, they should be accounted for in a comprehensive theory of transport.

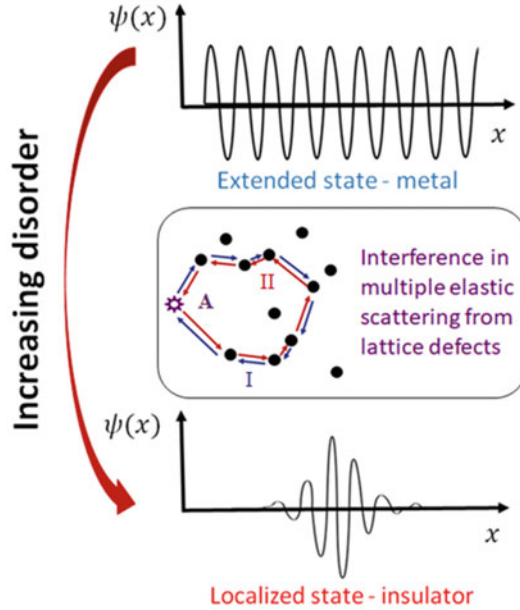


**Fig. 1.2** A simplified illustration of a metal-to-insulator transition (MIT) caused by critical amount of disorder in the system. In the quantum regime, an electron wave-particle traveling through a disordered medium is scattered from successive lattice defects. Consider two waves following the same path through the crystal but wave I (blue arrows) travels in the clockwise direction, while wave II (red arrows) propagates counterclockwise. Upon return to the initial point A, the two paths interfere constructively, which increases the probability for the electron to be found on lattice site A. Such constructive interference of multiple wave paths can lead to spatial localization of the electron

model different (but related) transport problems, once can vary the choice of distribution type in the perturbative term  $V_\epsilon$ . Anderson-type Hamiltonians possess properties required by the spectral approach, which is the focus of this work. Here we introduce the spectral method by considering the discrete random Schrödinger operator (see Eq. (1.3)), which is an important special case of an Anderson-type Hamiltonian with wide application in condensed matter physics.

Examination of a realistic transport problem in a disordered system should account for both static effects (such as zero-temperature interactions with hot solid and topological disorder) and dynamical phenomena (such as random lattice excitations and stochastic processes). In Chaps. 3–5, we investigate numerically the static-lattice problem for various infinite disordered lattices. The dynamical aspects of disorder are briefly discussed in Chap. 6 in the context of travelling lattice waves in a 2D complex plasma crystal. There, the numerical simulations carried out for a (realistic) semi-classical dust crystal are compared against the predictions for a (theoretical) static case scenario. This allows for determination of the regime

where the spectral analysis of the idealized system is a good approximation for the realistic one. A future goal of our research will be to use these results to fully adapt the spectral approach to the time-dependent scenario.

## 1.1 Formulation of the Transport Problem

The static lattice, zero temperature transport problem, where a charge carrier is travelling through a disordered medium is where we begin. For simplicity, we consider the 2D separable Hilbert space  $\mathcal{H} = l^2(\mathbb{Z}^2)$  of square summable sequences on the square<sup>3</sup> lattice  $\mathbb{Z}^2$ . In this case, the discrete random Schrödinger operator is given by the self-adjoint Hamiltonian  $H_\epsilon$

$$H_\epsilon = -\Delta + \sum_{i \in \mathbb{Z}^2} \epsilon_i \delta_i \langle \delta_i | \quad (1.3)$$

where  $\Delta$  is the discrete Laplacian in 2D,  $\{\delta_i\}_{i \in \mathbb{Z}^2}$  are the standard orthonormal base vectors of the Hilbert space  $\mathcal{H}$  (namely,  $\delta_n(m) = \delta_{nm}$ , where  $\delta_{nm}$  is the Kronecker delta), and  $\{\epsilon_i\}_{i \in \mathbb{Z}^2}$  is a set of random variables on a probability space  $(\Omega, \mathcal{P})$ . The random variables  $\epsilon_i$  are independent identically distributed (i.i.d.) in the interval  $[-W/2, W/2]$  with probability density  $\chi$ . In this work, we examine three choices for  $\chi$ : uniform, Gaussian, and bimodal distributions, which can be used to model various lattice defects.

The discrete random Schrödinger operator in Eq. (1.3) describes a 2D arrangement of atoms located at the integer points of the square lattice  $\mathbb{Z}^2$ . The perturbative part of the operator assigns a random amount of energy  $\epsilon_i$  from the interval  $[-W/2, W/2]$  according to the prescribed probability distribution  $\chi$ . Thus, the amount of disorder in the system can be varied either by changing the magnitude of  $W$  or by choice of distribution type. Except for degenerate cases, the perturbative term in Eq. (1.3) is non-compact almost surely,<sup>4</sup> which indicates that the spectra of  $H_\epsilon$  cannot be easily studied using the results from classical perturbation theory [5]. A more adequate treatment of problems involving non-compact operators can be found in spectral theory.

In Chap. 3, we present a general introduction of the spectral approach, which does not require the choice of Kronecker delta functions as the base vectors for the Hilbert space. However, in this study, we use  $\{\delta_i\}_{i \in \mathbb{Z}^2}$  for two main reasons: computational simplicity and ability to compare our approach with some of the most fundamental works in the field. The base vector  $\delta_i$  assumes the value 1 in the  $i^{\text{th}}$  entry and 0 in all other entries. This corresponds to the tight-binding approximation, where the

---

<sup>3</sup>The same analysis can easily be generalized to any dimension and lattice geometry.

<sup>4</sup>Note that in probability theory an event happens almost surely if it happens with probability 1. In this book, we use the two phrases interchangeably.

wavefunction is expanded as a sum over orthogonalized atomic wave amplitudes. In this approximation, the Schrödinger equation becomes a matrix equation for the amplitudes. Combined with the (common) assumption that there is only one atomic orbital at each lattice site, the tight-binding model facilitates the computation of a transport problem on a larger lattice. The single-orbital and tight-binding approximations were used both by Anderson in his original paper on localization [2] and Abrahams et al. in the development of scaling theory [6], which motivates us to introduce the innovative spectral approach using the same assumptions. However, the generalized definition of the spectral method can be used with a different choice of base vectors, which allows for analysis of physical systems with long-range interaction in the potential. An example of such a system is the complex plasma crystal (discussed in Chap. 6).

In the static lattice case, one is interested in the amount of disorder that triggers a phase transition from an extended to a localized state in the crystal. These two phase states correspond to distinct modes of charge transport: tunneling and hopping. In the unperturbed periodic crystal, quantum mechanical tunneling from one site to another spreads the eigenstates over the entire system, which corresponds to delocalization in the form of metallic conductivity. As the amount of disorder passes the critical value, transport of electrons may only occur through hopping from one localized state to another with the help of energy transfer from the phonon system. This regime corresponds to exponential localization in the form of hopping conductivity. The transition from one phase state to the other may not occur at a single critical value of the disorder. Instead, it has been suggested that there exists a transition region of disordered values, where the energy states of the Hamiltonian are neither extended, nor exponentially localized. This topic will be further discussed in Chap. 3.

## 1.2 Nature of Disorder

In condensed matter, disordered materials are sometimes defined as crystals with lack of long-range order in their atomic distributions [7]. Thus, a broader definition of lattice perturbation is the absence of periodicity in the crystalline structure. Most of this work focuses on *short-range* (or local) disorder for which lattice site interaction is limited to the nearest neighbor (i.e., the tight-binding approximation). Short-range impurities often occur as localized neutral scatterers, randomly distributed throughout the crystal. In contrast, *long-range* disorder is usually represented by charged impurities for which the interaction decreases according to a shielded Coulomb law. In Chap. 6, we discuss the 2D dusty plasma crystal, where both short-range and long-range disorder effects can be observed. Specifically, we will examine a 2D complex plasma crystal formed by negatively charged micron-sized particles suspended in low-density plasma gas. The interplay between the Coulomb repulsion among the particles and the external radial confinement in the system naturally introduces both Coulomb defects (i.e., a charge gradient throughout the crystal) and geometrical lattice imperfections (such as defect lines and domains of various orientation).

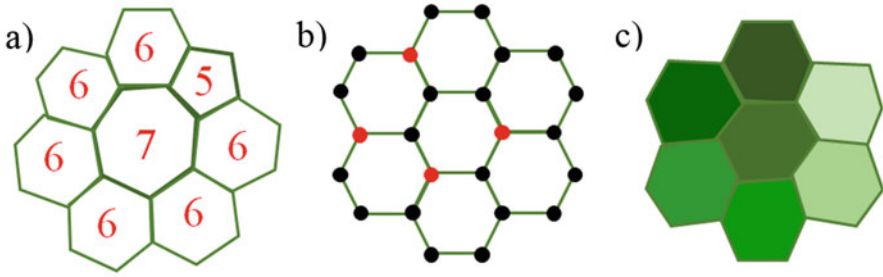


**Fig. 1.3** Examples of (a) positional, (b) substitutional, and (c) topological disorder on the 2D honeycomb lattice. The red numbers in part (a) provide the number of nearest neighbors for the corresponding cell. The red dots in part (b) represent the dopant atoms. In part (c), the different shades of the cells indicate various spatial orientation

Before we can provide an adequate discussion of the dynamics in realistic systems, such as the complex plasma crystal, we need a thorough understanding of the local and global transport phenomena characteristic of the time-independent, “frozen” lattice. One advantage of this case is that in the static lattice approximation, the hot solid type disorder can be distinguished from the topological disorder. The former describes a periodic lattice in which some atoms are shifted from their regular position due to a mechanical defect (static positional disorder shown in Fig. 1.3a) or replaced by a different type of atom through doping (substitutional disorder shown in Fig. 1.3b). The Anderson localization problem (see Chap. 4) is useful in modeling positional defects, while the quantum percolation model (see Chap. 5) is often applied in the study of doping.

In the case of a topologically disordered system, long-range order in the atomic distribution is completely broken, i.e. uniform periodicity cannot be assumed throughout the lattice. However, short-range order is preserved in the sense that the number of nearest neighbors (for the corresponding unperturbed lattice) remain intact although bond lengths and angles can fluctuate. Crystals exhibiting this type of perturbation present significant challenges to all scaling models relying on periodic boundary conditions. Topological disorder can be represented by a system whose domains exhibit various orientations with respect to a primitive axis (see Fig. 1.3c). In this paper, such lattice imperfections are studied with the help of numerical simulations of dust lattice waves in the complex plasma crystal. A second mechanism for accomplishing topological disorder is to introduce a high density of dislocations into a solid, which is the description of a liquid used in the dislocation theory of melting. In a future work, we will examine this case using the solid-to-liquid phase transition in a complex plasma crystal.

A third, usually neglected problem, is the stochastic-type disorder, where time-dependent fluctuations contribute to the transport properties of the material. Stochastic processes are often considered “noise”, which is subtracted or averaged depending on the length and time scales of the examined system. Nevertheless, there are cases where the accuracy of experimental results is sensitive to the constant

interaction with the environment. Self-organization and stability of crystal structures is dependent on the interplay between initial conditions (which are deterministic) and randomness in the system (in the sense of stochastic behavior). The effect of stochastic processes in various systems requires deep understanding of deterministic chaos theory and examination of complex dynamical systems. The spectral method presented in this work (Chap. 3) relies on a decomposition of the measure<sup>5</sup> in the examined Hilbert space. The analogous approach to the case of stochastic processes is called the Lévy-Itô decomposition. Another future goal of our research is to develop a spectral approach to the analysis of random processes and apply it in the study of thermal and charge fluctuations in the complex plasma crystal.

The above definitions of disorder are all motivated by physical application. In the case where the Schrödinger equation assumes a matrix form, a mathematical distinction should be made between diagonal and off-diagonal types of disorder. The former, describes perturbation of the on-site parameters, such as fluctuation of lattice site ground state energy. This type of disorder will be considered in Chap. 3, where we introduce the spectral approach. Alternatively, a defect can be represented by an off-diagonal fluctuation, to describe, for example, changes in the hopping potential between two neighboring sites. In the present work, we assume that the interaction potential is constant and normalize it to unity.

### 1.3 Relevance to Physical Systems

Since the discovery of the electric charge, the question of conductivity in various materials has been a topic of research for mathematicians, physicists, and engineers. Only a few decades ago, the theory of electron transport in disordered materials relied on the classical Drude model, in which free electrons were assumed to scatter off lattice site impurities in proportion to the mean free path. It was later recognized by P. W. Anderson, that the quantum-mechanical wave character of electrons introduces essential modifications to this simplistic ballistic picture. The implementation of quantum mechanics into the classical theory paved the way for the development of the semiconductor industry, which is the backbone of modern technology. In a semiconductor crystal, both the concentration and type of lattice impurity determines conductivity. In the low concentration limit, isolated impurities produce discrete bound energy states located between the valence and conduction bands. Due to Coulomb repulsion, such discrete intermediate levels have slightly different energies from one another. In this case, electron excitation, relaxation, or trapping can be achieved only upon interaction with the phonon system when external energy is supplied. This mode of transport is referred to as hopping conductivity, or localization. As the concentration of impurities increases, isolated intermediate states form a continuous band, where the electrons move freely from

---

<sup>5</sup>See Appendix B for a definition of measure.

one state to another. This provides an alternative mode of transport in the system, which corresponds to metallic conductivity. It was argued by Mott [8] that the passage from a discrete to a continuous spectrum of the impurity levels constitutes a simple example of a metal-to-insulator transition (MIT).<sup>6</sup>

The subject of Anderson localization and related transport problems has grown into a rich field of research for both physicists [9–12] and mathematicians [13–17]. Anderson localization is currently well understood for the 1D [18–20] and 3D [21–26] cases, where the problem has been studied in both quantum mechanical [10, 21, 24, 27–29] and classical [30–36] systems. However, as mentioned in the previous section, the existence of extended states in the critical 2D case is still a topic of heated debate due to a disagreement between the theoretical predictions of scaling theory (see Sect. 2.4) and experimental observation. This issue was limited to the theoretical realm before the discovery of graphene in 2004 [37, 38]. Graphene is the world’s first truly two-dimensional material making it an ideal candidate for the development of flexible and durable semi-transparent technology, improved energy storage units, high-efficiency solar panels, and water purification systems. However, the realization of such applications is extremely sensitive to a proper understanding of conductivity in this 2D material.

According to scaling theory [6], all energy states are localized in a 2D crystal for any (nonzero) amount of disorder, i.e. an Anderson-type MIT should not occur. For the case of a 2D carbon lattice in the tight-binding limit, it was established numerically that the energy states are localized with large localization length (in the range of several hundred nanometers to microns) [39–41]. In contrast, analytical calculations by Lherbier et al. [42] indicated the existence of minimum conductivity in graphene characterized by short-range interactions. Further evidence for delocalization was analytically obtained for a single graphene sheet with long-range interactions [43] or off-diagonal disorder [44].

A crossover from extended to localized states has been experimentally established for graphene doped with hydrogen [45]. The origins of this transition remain unclear. One possible explanation is that doped graphene exhibits a localization length longer than the size of current numerical simulations, which leads to the “apparent” existence of delocalized states [46–48]. The other major hypothesis, which will be the one examined in this work, is that scaling theory does not yield reliable results for all dimensions and system sizes [49, 50], and that its limitations come to play in the critical 2D case.

Apart from classical semiconductors, there is a variety of other disordered systems (such as isotropic mixtures and substitutional alloys), where adequate analysis of transport phenomena is important. Of special interest is the case of semiconducting glasses, which form domains of various orientation upon

---

<sup>6</sup>Note that in this description the unperturbed crystal is an isolator and the impurities act to facilitate transport. Alternatively, one can consider a conducting regular lattice with impurities acting as (almost) perfect barriers that impede transport. In this work, we focus on the second formulation of the problem.

crystallization. The structure of such materials exhibits only local symmetry, presenting a significant challenge to any scaling approach to conductivity. A second important class of problems is related to electron transport in amorphous elementary materials forming disordered rings and chains of atoms [51]. The study of conductivity in such non-crystalline systems requires consideration of nonlinear interactions and the dynamical aspects of disorder. One interesting representative phenomenon is the crossover from a crystalline to an amorphous solid and its dependence on the impurity concentration. In this problem, the non-crystalline system may be viewed as a limiting case of an ordered lattice, where a high concentration of random defects causes a phase transition to an amorphous solid. A proper theory of conductivity must account for such transition.

The class of Anderson-type problems is not limited solely to electron transport in materials. In fact, the original work by P. W. Anderson was motivated by the magnetic resonance experiments of Feher [52], which showed anomalously long relaxation times of electron spins in doped semiconductors. Since then, numerous techniques and results from the analysis of electron transport have been applied to the study of spin waves in disordered systems. The connection between the two phenomena is apparent from the Schrödinger equation for the tight-binding model, which is analogous to the equations for the spin waves. Such analogy can be further extended to the classical realm, where the Anderson localization and related transport problems can be studied using electromagnetic or sound wave equations. Diffusion of both quantum mechanical and classical waves through a disordered medium obeys Ohm's law, where the conductance/transmission decreases linearly with system size [35]. Once the amount of scattering from defects passes a critical value, Anderson localization brings classical diffusion to a complete halt. In this case, the transmission coefficient in the localized regime decreases exponentially, which can be easily detected in a macroscopic experiment. The topic of wave transport in classical systems will be further examined in Chap. 6.

Finally, transport in real materials depends on the interplay between the interaction with impurities and the correlations among electrons. Strongly correlated systems (SCSs) are systems that cannot be effectively described by the physics of free-particle ensembles. They exhibit anomalous (often technologically useful) collective behavior, which is a result of the strong interactions among the entities involved [53, 54]. As in the case of the crystalline-to-amorphous phase transition, a comprehensive theory of the simpler non-correlated problem represents a valuable step toward better understanding of the more complex case, where strong correlations cannot be neglected.

## Bibliography

1. L.H. Hoddeson, G. Baym, The development of the quantum mechanical electron theory of metals: 1900-28. *Proc. R. Soc. Lond. Ser. Math. Phys. Sci.* **371**(1744), 8–23 (1980)

2. P.W. Anderson, Absence of diffusion in certain random lattices. *Phys. Rev.* **109**(5), 1492–1505 (1958)
3. D.J. Thouless, Electrons in disordered systems and the theory of localization. *Phys. Rep.* **13**(3), 93–142 (1974)
4. V. Jakšić, Y. Last, Spectral structure of Anderson type Hamiltonians. *Invent. Math.* **141**(3), 561–577 (2000)
5. C. Liaw, Approach to the extended states conjecture. *J. Stat. Phys.* **153**(6), 1022–1038 (2013)
6. E. Abrahams, P. Anderson, D. Licciardello, T. Ramakrishnan, Scaling theory of localization. *Phys. Rev. Lett.* **42**(10) (1979)
7. F. Yonezawa, T. Ninomiya, Introduction, in *Topological Disorder in Condensed Matter*, (Springer, Berlin, Heidelberg, 1983), pp. 1–11
8. N.F. Mott, Conduction in non-crystalline systems IX. The minimum metallic conductivity. *Philos. Mag.* **26**(4), 1015–1026 (1972)
9. T. Brandes, S. Kettenmann, *The Anderson Transition and Its Ramifications—Localization, Quantum Interference, and Interactions* (Springer, 2003)
10. J. Chabé, G. Lemarié, B. Grémaud, D. Delande, P. Szriftgiser, J.C. Garreau, Experimental observation of the Anderson metal-insulator transition with atomic matter waves. *Phys. Rev. Lett.* **101**(25), 255702 (2008)
11. B. Kramer, A. MacKinnon, Localization: theory and experiment. *Rep. Prog. Phys.* **56**(12), 1469–1564 (1993)
12. A. Lagendijk, B. van Tiggelen, D.S. Wiersma, Fifty years of Anderson localization. *Phys. Today* **62**(8), 24–29 (2009)
13. M. Aizenman, S. Molchanov, Localization at large disorder and at extreme energies: an elementary derivations. *Commun. Math. Phys.* **157**(2), 245–278 (1993)
14. P. Hartmann et al., Crystallization dynamics of a single layer complex plasma. *Phys. Rev. Lett.* **105**, 115004 (2010)
15. L.A. Pastur, Spectral properties of disordered systems in the one-body approximation. *Commun. Math. Phys.* **75**(2), 179–196 (1980)
16. J. Fröhlich, T. Spencer, Absence of diffusion in the Anderson tight binding model for large disorder or low energy. *Commun. Math. Phys.* **88**(2), 151–184 (1983)
17. V. Jakšić, Y. Last, Simplicity of singular spectrum in Anderson-type Hamiltonians. *Duke Math. J.* **133**(1), 185–204 (2006)
18. A. Furusaki, N. Nagaosa, Single-barrier problem and Anderson localization in a one-dimensional interacting electron system. *Phys. Rev. B* **47**(8), 4631–4643 (1993)
19. F.A.B.F. de Moura, M.L. Lyra, Delocalization in the 1D Anderson model with long-range correlated disorder. *Phys. Rev. Lett.* **81**(17), 3735–3738 (1998)
20. J. Bertolotti, S. Gottardo, D.S. Wiersma, M. Ghulinyan, L. Pavesi, Optical necklace states in Anderson localized 1D systems. *Phys. Rev. Lett.* **94**(11), 113903 (2005)
21. G. Semeghini et al., Measurement of the mobility edge for 3D Anderson localization. *Nat. Phys.* **11**(7), 554–559 (2015)
22. A.W. Stadler, A. Kusy, R. Sikora, Numerical studies of the Anderson transition in three-dimensional quantum site percolation. *J. Phys. Condens. Matter* **8**(17), 2981 (1996)
23. C. Conti, A. Fratallocchi, Dynamic light diffusion, three-dimensional Anderson localization and lasing in inverted opals. *Nat. Phys.* **4**(10), 794–798 (2008)
24. S.E. Skipetrov, A. Minguzzi, B.A. van Tiggelen, B. Shapiro, Anderson localization of a Bose-Einstein condensate in a 3D random potential. *Phys. Rev. Lett.* **100**(16), 165301 (2008)
25. S.S. Kondov, W.R. McGehee, J.J. Zirbel, B. DeMarco, Three-dimensional Anderson localization of ultracold matter. *Science* **334**(6052), 66–68 (2011)
26. S.E. Skipetrov, B.A. van Tiggelen, Dynamics of Anderson localization in open 3D media. *Phys. Rev. Lett.* **96**(4), 043902 (2006)
27. A.M.M. Pruisken, Universal singularities in the integral quantum hall effect. *Phys. Rev. Lett.* **61**(11), 1297–1300 (1988)

28. S. Fishman, D.R. Grempel, R.E. Prange, Chaos, quantum recurrences, and Anderson localization. *Phys. Rev. Lett.* **49**(8), 509–512 (1982)
29. K. Whitham, J. Yang, B.H. Savitzky, L.F. Kourkoutis, F. Wise, T. Hanrath, Charge transport and localization in atomically coherent quantum dot solids. *Nat. Mater.* **15**(5), 557–563 (2016)
30. S. Faez, A. Strybulevych, J.H. Page, A. Lagendijk, B.A. van Tiggelen, Observation of multifractality in Anderson localization of ultrasound. *Phys. Rev. Lett.* **103**(15), 155703 (2009)
31. H. Hu, A. Strybulevych, J.H. Page, S.E. Skipetrov, B.A. van Tiggelen, Localization of ultrasound in a three-dimensional elastic network. *Nat. Phys.* **4**(12), 945–948 (2008)
32. O. Richoux, V. Tourmat, T. Le Van Suu, Acoustic wave dispersion in a one-dimensional lattice of nonlinear resonant scatterers. *Phys. Rev. E* **75**(2), 026615 (2007)
33. M. Störzer, P. Gross, C.M. Aegerter, G. Maret, Observation of the critical regime near Anderson localization of light. *Phys. Rev. Lett.* **96**(6), 063904 (2006)
34. A.A. Chabanov, A.Z. Genack, Photon localization in resonant media. *Phys. Rev. Lett.* **87**(15), 153901 (2001)
35. D.S. Wiersma, P. Bartolini, A. Lagendijk, R. Righini, Localization of light in a disordered medium. *Nature* **390**(6661), 671–673 (1997)
36. A.C. Hladky-Hennion, J.O. Vasseur, S. Degraeve, C. Granger, M. de Billy, Acoustic wave localization in one-dimensional Fibonacci phononic structures with mirror symmetry. *J. Appl. Phys.* **113**(15), 154901 (2013)
37. K.S. Novoselov et al., Electric field effect in atomically thin carbon films. *Science* **306**(5696), 666–669 (2004)
38. K.S. Novoselov et al., Two-dimensional atomic crystals. *Proc. Natl. Acad. Sci. U. S. A.* **102**(30), 10451–10453 (2005)
39. A. Cresti et al., Charge transport in disordered graphene-based low dimensional materials. *Nano Res.* **1**(5), 361–394 (2008)
40. A. Lherbier, B. Biel, Y.-M. Niquet, S. Roche, Transport length scales in disordered graphene-based materials: strong localization regimes and dimensionality effects. *Phys. Rev. Lett.* **100**(3), 036803 (2008)
41. N. Leconte, A. Lherbier, F. Varchon, P. Ordejon, S. Roche, J.-C. Charlier, Quantum transport in chemically modified two-dimensional graphene: from minimal conductivity to Anderson localization. *Phys. Rev. B* **84**(23), 235420 (2011)
42. A. Lherbier, S.M.-M. Dubois, X. Declerck, S. Roche, Y.-M. Niquet, J.-C. Charlier, Two-dimensional graphene with structural defects: elastic mean free path, minimum conductivity, and Anderson transition. *Phys. Rev. Lett.* **106**(4), 046803 (2011)
43. H. Suzuura, T. Ando, Weak-localization in metallic carbon nanotubes. *J. Phys. Soc. Jpn.* **75**(2), 024703 (2006)
44. S.-J. Xiong, Y. Xiong, Anderson localization of electron states in graphene in different types of disorder. *Phys. Rev. B* **76**(21), 214204 (2007)
45. A. Bostwick et al., Quasiparticle transformation during a metal-insulator transition in graphene. *Phys. Rev. Lett.* **103**(5), 056404 (2009)
46. I. Amanatidis, S.N. Evangelou, Quantum chaos in weakly disordered graphene. *Phys. Rev. B* **79**(20), 205420 (2009)
47. J.E. Barrios-Vargas, G.G. Naumis, Critical wavefunctions in disordered graphene. *J. Phys. Condens. Matter* **24**(25), 255305 (2012)
48. E. Amanatidis, I. Klefogiannis, D.E. Katsanos, S.N. Evangelou, Critical level statistics for weakly disordered graphene. *J. Phys. Condens. Matter* **26**(15), 155601 (2014)
49. K. Nomura, M. Koshino, S. Ryu, Topological delocalization of two-dimensional massless Dirac fermions. *Phys. Rev. Lett.* **99**(14), 146806 (2007)
50. J.H. Bardarson, J. Tworzydło, P.W. Brouwer, C.W.J. Beenakker, One-parameter scaling at the Dirac point in graphene. *Phys. Rev. Lett.* **99**(10), 106801 (2007)
51. H. Fritzsche, Electronic properties of amorphous semiconductors, in *Amorphous and Liquid Semiconductors*, (Springer, Boston, 1974), pp. 221–312

52. G. Feher, Observation of nuclear magnetic resonances via the electron spin resonance line. *Phys. Rev.* **103**(3), 834–835 (1956)
53. A.O. Gogolin, A.A. Nersesyan, A.M. Tsvelik, *Bosonization and Strongly Correlated Systems* (Cambridge University Press, 2004)
54. Strongly Correlated Systems—Theoretical Methods | Adolfo Avella | Springer. [Online]. <http://www.springer.com/us/book/9783642218309>. Accessed 7 Aug 2016

# Chapter 2

## Theoretical Background



### 2.1 Localization Criteria

In his original paper on localization [1], Anderson considered a very general case of a 3D lattice space, where sites  $j$  can be distributed either regularly or randomly. Lattice site energies  $E_j$  are stochastic variables randomly selected from a probability distribution  $P(E)dE$  where the width of the distribution  $W$  is used to vary the amount of disorder in the system. The hopping energy between neighboring lattice states is represented by an interaction matrix element  $V_{jk}(\mathbf{r}_{jk})$ , which can also be chosen to vary randomly according to a predetermined probability distribution. The basic approach to analyzing transport in this setup is to place a single entity, for instance, the spin of an electron, on site  $n$  at time  $t = 0$  and study the time evolution of its wavefunction.

*The Anderson theorem states that if  $V_{jk}(\mathbf{r}_{jk})$  falls off at large distances faster than  $1/r^3$  and if the average value of  $V$  is less than a certain critical  $V_c \sim W$ , then transport comes to a halt.*

In other words, localization occurs when the hopping matrix element provides only short-range interaction and when the magnitude of the hopping energy is on the order of the variation in lattice site energies. If these conditions are satisfied, the amplitude of the wavefunction around site  $n$  falls off rapidly with distance as  $t \rightarrow \infty$ , whereas the amplitude located on site  $n$  itself remains finite. The Anderson theorem leaves two regions of uncertainty; namely, the case where  $V_{jk}(\mathbf{r}_{jk})$  falls off as  $1/r^3$  and the regime where  $V \sim W$  (also called the high-concentration limit). Due to its general formulation, this criterion for the metal-to-insulator transition was not originally well understood. This led to a series of simplifications and special cases that were later introduced.

An important addition to the theory of localization is the idea of a minimum conductivity, originally suggested by Mott [2–4]. He argued that the mean free path  $l$  between successive interactions with impurities in a material cannot be smaller than the lattice constant  $a$ . Thus, the value of the conductivity of a metal has its minimum

when  $l \approx a$ . Since the wavelength  $\lambda$  of electrons at the Fermi surface is on the order of  $2\pi a$ , this provides a requirement for extended states to exist, which is given by

$$l \geq a \quad \text{or} \quad l \geq \lambda/2\pi = 1/k, \quad (2.1)$$

where  $k$  is the wave vector. Similar reasoning was independently developed by Ioffe and Regel [5], who argued that *localization is expected to occur for  $kl \leq 1$* . The physical interpretation of this criterion comes from the realization that below  $kl = 1$ , the electric field cannot perform even a single oscillation before it is scattered again by successive impurities. Thus, in this limit, the wave collapses into a localized state. It is important to note the subtle difference between the Mott and Ioffe-Regel criteria, which is apparent from the sign of the two inequalities. Mott identifies the critical value of the mean free path above which *extended states exist* in any dimension, whereas Ioffe and Regel discuss the regime, where *delocalization cannot occur*. Technically, Mott's minimum conductivity disagrees with scaling theory (see Sect. 2.4), which predicts that in the critical 2D case true metallic conductivity does not exist. On the contrary, the Ioffe-Regel criterion does not deal with extended states and is, thus, still widely used in localization problems, especially in those related to localization in the classical regime.

One of the first measures of localization employed numerically was given by Bell, Dean and Hibbins-Butler [6, 7], who studied the propagation of atomic vibrations in vitreous silica, germania, and beryllium fluoride. Bell et al. pointed out that the spatial extent of modes, which largely determines the thermal conductivity of a glass, can be considered analogous to the spatial extension of electron states, which influences the electrical conductivity in a crystalline solid. Therefore, they examined the transport properties of the normal modes in various spectral bands of chalcogenide glasses. As a measure of localization, Bell et al. introduced a parameter  $N_{EFF}(\omega)$ , which is a rough estimate of the number of atoms effectively participating in a normal mode with frequency  $\omega$ . The definition of  $N_{EFF}(\omega)$  is related to the energy-moments of a normal mode, given by

$$M_n \equiv M_n(\omega) = \sum_{i=1}^N (\epsilon_i)^n, \quad (2.2)$$

where  $\epsilon_i(\omega) = m_i |r_i|^2$  is the mean kinetic energy of the  $i^{\text{th}}$  atom (with mass  $m_i$  and real vector displacement amplitude  $r_i$ ), which participates in a normal mode with frequency  $\omega$ . In particular,  $M_0 = N$ , where  $N$  is the total number of atoms in the vibrating system while  $M_1$  is proportional to the total vibrational energy of the mode in question. The parameter  $N_{EFF}(\omega)$  is then defined as

$$N_{EFF}(\omega) = (M_1)^2/M_2. \quad (2.3)$$

In other words,  $N_{EFF}(\omega)$  is the ratio of the total mean vibrational kinetic energy squared to the sum of the squared mean kinetic energies of the participating atoms. Therefore,  $N_{EFF}(\omega)$  lies between  $N$  (the limiting case where all atoms vibrate with

equal amplitude, which corresponds to pure translational motion) and 1 (the limiting case where only one atom participates in the mode, i.e. the vibration is localized). If  $N_{EFF}(\omega)$  is normalized by the number of atoms in the system  $N$ , one obtains the so called ‘participation ratio’

$$p(\omega) = N_{EFF}(\omega)/N = (M_1)^2/(NM_2). \quad (2.4)$$

One way to distinguish the localized from the delocalized regime in the system is to calculate the dependence of the participation ratio on system size.

Bell et al. aimed to provide an experimentally measurable distinction between the localized and delocalized regimes thus quantifying the concept of degree of localization. *The Bell et al. criterion states that if  $p(\omega)$  tends to a constant value as  $N \rightarrow \infty$ , the vibrational mode is extended, while if  $p(\omega)$  tends to zero, the vibration stays localized.*

Arguably, the most important contribution of this criterion is that it provided the first suggestion that conductivity can be studied using scaling techniques.

Some of the first numerical experiments explicitly using a scaling criterion for localization were conducted by Edwards and Thouless [8] in 1972. Edwards and Thouless pointed out that the energy of a localized state in a large system should be insensitive to the boundary conditions, provided the center of localization is not located near a boundary. In contrast, any change in the boundary conditions should affect significantly the energy spectrum of an extended wave. Therefore, one can compute the energy states for a given system using one set of boundary conditions, then repeat the calculation using another set of boundary condition and then examine the energy shift  $\Delta E$  between corresponding levels (as derived from the two calculations) to determine the transport regime of the examined system. Specifically, Edwards and Thouless assumed periodic boundary conditions in their first calculation and then repeated the calculations using anti-periodicity across one of the borders. In the localized regime,  $\Delta E$  should be exponentially small, while in the extended states regime, the energy differences should be comparable to the spacing between levels, roughly given by  $\eta = W/N$ , where  $W$  is the width of the energy fluctuations (introduced in the Anderson theorem above) and  $N$  is the number of atoms in the system.

Since the electron wavefunction in the disordered lattice can be localized in an area with more than one atom, the spatial extent of the localization must be determined by increasing the system size to infinity or letting  $N \rightarrow \infty$ . *The Edwards and Thouless criterion states that if the ratio  $\Delta E/\eta$  tends to a constant as  $N \rightarrow \infty$ , then the system is in the delocalized regime, while if  $\Delta E/\eta$  decreases with system size, the system is in the localized regime.*

Numerically, the size of a system may be increased by stacking identical  $d$ -dimensional cubes of  $N$  sites each assuming periodic boundary conditions. The resulting system consists of  $N$  energy bands of width  $d\Delta E$ , where  $d$  is the dimensionality of the system. For the case when unit cell cubes are not identical but randomly chosen from a predetermined distribution, the strength of the coupling

(or hopping energy) between states on neighboring cubes is given by the quantity  $V = (1/2)\Delta E$ . The quantity of interest in this model is the ratio of the available hopping energy to the mean spacing between energy levels

$$\frac{V}{\eta} = \frac{N\Delta E}{2W}. \quad (2.5)$$

Note that the numerical factor of  $1/2$  has been neglected in the Edwards and Thouless criteria given above.

## 2.2 Anderson Model

The Anderson localization problem examines the propagation of a mobile entity through a  $d$ -dimensional disordered lattice. As a representative example, we consider an electron traveling in the 3D lattice, where each site  $j$  is randomly assigned energy  $E_j$  from a probability distribution  $P(E)dE$  with a characteristic width which determines the degree of disorder in the system. Assume that the energies  $E_j$  are independent and identically distributed (i.i.d.) random variables and let  $V_{jk}(\mathbf{r}_{jk})$  be the hopping energy between neighboring states. Assuming only one orbital per lattice site, the electron wavefunction can be expanded as a sum over orthogonalized atomic wavefunctions. In this approximation, the probability amplitude  $a_j$  that the electron is found at the site  $j$  satisfies the time-dependent Schrödinger equation of the form

$$i\dot{a}_j = E_j a_j + \sum_{k \neq j} V_{jk} a_k \quad (2.6)$$

with the Hamiltonian at site  $j$  given by:

$$H_j = E_j + \sum_{k \neq j} V_{jk}. \quad (2.7)$$

(In Eq. 2.7, the energies are measured in frequency units therefore,  $\hbar = 1$ .) If the probability distribution  $|a_j(0)|^2$  at  $t = 0$  is known to be appreciable over a specific range of energies  $E_j$  or spatial coordinates  $\mathbf{r}_j$ , the salient question becomes how rapidly (if at all) this distribution diffuses away from that region. The time evolution of the amplitude can be determined using the Laplace transform of Eq. (2.6)

$$i[sf_j(s) - a_j(0)] = E_j f_j + \sum_{k \neq j} V_{jk} f_k, \quad (2.8)$$

where

$$f_j(s) = \int_0^\infty e^{-st} a_j(t) dt \quad (2.9)$$

is the Laplace transform of  $a_j(t)$ . The variable  $s$  is an arbitrary complex variable with either positive or zero real part. The behavior of  $f_j$  as  $s \rightarrow 0+$  is equivalent to the behavior of  $a_j$  as  $t \rightarrow \infty$ . For simplicity, we assume  $a_0(0) = 1$  for  $j = 0$ , i.e. the electron wavefunction is initially localized (with probability 1) at a single atom at the origin. Solving (2.8) for  $f_j(s)$  yields

$$f_j(s) = \frac{i\delta_{0j}}{is - E_j} + \sum_{k \neq j} \frac{V_{jk} f_k(s)}{is - E_j}, \quad (2.10)$$

where  $a_j(0) = \delta_{0j}$ . Equation (2.10) not involving  $f_0(s)$  can be solved for  $f_j(s)$  in terms of  $f_0(s)$  using an iterative approach, which gives

$$f_j(s) = \frac{V_{j0} f_0(s)}{is - E_j} + \sum_{k \neq j} \frac{V_{jk}}{is - E_j} \frac{V_{k0} f_0(s)}{is - E_k} + \dots \quad (2.11)$$

Thus, the zeroth equation becomes

$$f_0(s) = \frac{i}{is - E_0} + \sum_{\substack{k \neq 0 \\ l \neq k}} \frac{V_{0k}}{is - E_0} \left[ \frac{V_{k0}}{is - E_k} + \sum_{\substack{l \neq 0 \\ l \neq k}} \frac{V_{kl}}{is - E_k} \frac{V_{l0}}{is - E_l} + \dots \right] f_0(s) \quad (2.12)$$

or

$$f_0(s) = \frac{i}{is - E_0} \left\{ 1 + \left[ \sum_k \frac{(V_{k0})^2}{is - E_k} + \sum_{k,l} \frac{V_{0k} V_{kl} V_{l0}}{(is - E_k)(is - E_l)} + \dots \right] f_0(s) \right\} \quad (2.13)$$

In both (2.12) and (2.13), the expression  $\frac{i}{is - E_0}$  is the Laplace transform of  $e^{-iE_0 t}$ , which represents a plane wave of energy  $E_0$ . Terms within the curly brackets in Eq. (2.13) represent the evolution operator for a pure discrete spectrum in time-dependent perturbation theory. The perturbed energy as  $t \rightarrow \infty$  can be defined as

$$V_c(0) = \sum_{k \neq 0} \frac{(V_{k0})^2}{is - E_k} + \sum_{k,l} \frac{V_{0k} V_{kl} V_{l0}}{(is - E_k)(is - E_l)} + \dots \quad (2.14)$$

In many cases, the first term in Eq. (2.14) is a good approximation for the value of  $V_c$ . In this approximation, the perturbed energy can be rewritten as

$$V_c(0) \approx \sum_{k \neq 0} \frac{(V_{0k})^2}{is - E_k} = \sum_k (V_{0k})^2 \left( \frac{E_k}{s^2 + E_k^2} - \frac{is}{s^2 + E_k^2} \right). \quad (2.15)$$

In the limit  $s \rightarrow 0$ , the first term on the right-hand side is the second-order perturbation  $-\Delta E^{(2)}$  of the initial energy  $E_0$

$$\lim_{s \rightarrow 0} \sum_k (V_{0k})^2 \left( \frac{E_k}{s^2 + E_k^2} \right) = - \sum_k (V_{0k})^2 \left( \frac{1}{E_k} \right) = -\Delta E^{(2)}. \quad (2.16)$$

The second term on the right-hand side of Eq. (2.15) can be written as

$$\begin{aligned} \lim_{s \rightarrow 0} \left( - \sum_k (V_{0k})^2 \frac{is}{s^2 + E_k^2} \right) &= -i \sum_k (V_{0k})^2 \delta(E_k) \\ &\quad - is \sum_{k, E_k \neq 0} \frac{(V_{0k})^2}{E_k^2} = -\frac{i}{\tau} - isK, \end{aligned} \quad (2.17)$$

where  $\sum_k (V_{0k})^2 \delta(E_k) = 1/\tau$  and  $\sum_{k, E_k \neq 0} \frac{(V_{0k})^2}{E_k^2} = K$ . Equation (2.13) now becomes

$$f_0(s) = \frac{i}{is(1+K) + \left(\frac{i}{\tau}\right) - (E_0 - \Delta E^{(2)})}. \quad (2.18)$$

When  $\tau$  is finite, the  $K$  term is indeterminate, and the solution is

$$f_0(s) = \frac{1}{s + \left(\frac{1}{\tau}\right) + i(E_0 - \Delta E^{(2)})}. \quad (2.19)$$

Taking the inverse Laplace transform of Eq. (2.19) gives

$$\lim_{t \rightarrow \infty} a_0(t) = e^{-\frac{t}{\tau}} e^{-i(E_0 - \Delta E^{(2)})t}. \quad (2.20)$$

Equation (2.20) represents a state of perturbed energy  $E_0 - \Delta E^{(2)}$  decaying at a rate  $e^{-\frac{t}{\tau}}$ , i.e. a delocalized state. For the case where  $\tau$  is infinite, the constant  $K$  is preserved and the solution becomes

$$f_0(s) = \frac{1}{s(1+K) + i(E_0 - \Delta E^{(2)})}. \quad (2.21)$$

The inverse Laplace transform of Eq. (2.21) has the form

$$\lim_{t \rightarrow \infty} a_0(t) = \frac{1}{1+K} e^{-\frac{i(E_0 - \Delta E^{(2)})t}{(1+K)}}. \quad (2.22)$$

This represents a localized state of (the same) perturbed energy which does not decay, having a finite amplitude  $a_0(t \rightarrow \infty)$  reduced from unity by the ratio  $1/(1+K)$ . The parameter  $K$  measures the spread of the initial state due to virtual transitions.

The technique suggested by Anderson to tackle the above was to study the infinite series expansion of the perturbed energy  $V_c(s)$  by treating  $V_c(s)$  as a probability variable. Once the arbitrary energy of the initial atom  $j = 0$  is determined, the investigation of the probability distribution for  $V_c$  resolves itself into three parts: (1) Study the first term in Eq. (2.14), (2) Discuss the convergence of the series of higher order perturbations, and (3) Decide whether this kind of convergence in a probability sense is meaningful, and whether the choice of arbitrary energy is correct.

In the above analysis, we saw that the important quantity for accomplishing step 1 is to determine the imaginary part<sup>1</sup> of  $V_c$  given by

$$\text{Im}(V_c) = -s \sum_k \frac{(V_{0k})^2}{s^2 + E_k^2} = -sX(s). \quad (2.23)$$

In the limit where  $s \rightarrow 0$ , a finite value of the quantity  $X(s)$  implies localization. In the analysis of the  $X(s)$  series, one runs into the issue of repeated indices, which can be eliminated in a self-consistent way by including the perturbed energy  $V_c(k)$  in the energy denominator for atom  $k$ . This means that the ‘‘propagator’’ for state  $k$  is given by

$$e_k = \frac{1}{is - E_k - V_c(k)} \quad (2.24)$$

with a (first-order) perturbed energy given by

$$V_c(0) = \sum_{k \neq 0} \frac{(V_{0k})^2}{is - E_k - V_c(k)} = \sum_{k \neq 0} \frac{(V_{0k})^2}{e_k}. \quad (2.25)$$

Assuming the  $V_{0k}$  terms have the same order of magnitude and that the  $E_k$  terms are of order  $W$  (the characteristic width of the probability distribution of the on-site energies) the series in Eq. (2.25) converges only if  $V_{0k} \leq W$ .

In summary, the Anderson method uses perturbation theory to calculate the time evolution of the electron wavefunction. Series expansion of the perturbed energies

---

<sup>1</sup>Remember that the real part of  $V_c$  is the ordinary second order energy perturbation and the imaginary part is the one that gave rise to the localized solution.

given in Eq. (2.14) therefore is an indication of the transport regime in the system. A converging series corresponds to a regime where the electron wavefunction may decrease but does not go to zero with time, i.e. the particle remains localized, whereas a diverging series indicates that the system is in the extended regime. There are two important limitations to the Anderson model. First, the use of perturbation theory implies that the series expansion method is only valid for impurity bands in the low-concentration limit and with low-energy tail. Thus, such reasoning does not apply to highly disordered systems. Second, the calculation does not account for contact with any external thermal reservoir, which is an important restriction for both relaxation and transport processes.

### 2.3 Edwards and Thouless Model

In 1972, Edwards and Thouless [8] conducted numerical simulations where the Anderson localization is examined using a scaling criterion. In their formulation of the problem, the hopping amplitude  $V_{ij}$  between neighboring sites is assumed constant while the on-site energies are allowed to vary. The resulting equation for the amplitudes  $a_i$  associated with an eigenstate of energy  $E$  is

$$Ea_i = -V \sum_l a_{i+l} + \epsilon_i a_i \quad (2.26)$$

with the Hamiltonian at site  $i$  given by

$$H_i = -ZV + \epsilon_i. \quad (2.27)$$

Here, the constant hopping amplitude is normalized to unity and the displacement vector/ranges over the  $Z$  nearest neighbors. Thus, the first term in the Hamiltonian is the discrete Laplacian, or the graph representation of the kinetic energy term.<sup>2</sup> The on-site energies  $\epsilon_i$  are independent identically distributed (i.i.d.) variables selected from the interval  $(-\frac{1}{2}W, \frac{1}{2}W)$ , where  $W$  represents the amount of disorder in the system as defined earlier. In other words, the energy band is given by:

$$-\frac{1}{2}W - ZV < E < \frac{1}{2}W + ZV. \quad (2.28)$$

---

<sup>2</sup>The Hamiltonian in Eq. (2.27) can be rewritten in the more general operator form of Eq. (1.3) from Chap. 1. The formulation of the problem presented in this section involves a discrete random Schrödinger operator. Thus, in Chap. 3, we provide a physical interpretation of the spectral approach through a comparison with the Edwards and Thouless model.

Using this approach, Edwards and Thouless examined the dependence of conductivity on the amount of disorder  $W$  in the limit of increasing number of lattice sites  $N$ . As discussed in Sect. 2.1, Edwards and Thouless argued that in the localized regime, the energy eigenvalues for a wave-particle in the bulk of the crystal are not (appreciably) affected by a change at the boundary, which is not the case in the extended state regime. Specifically, if the ratio  $\Delta E/\eta^3$  decreases as  $N \rightarrow \infty$ , the system is in the localized regime.

To obtain the shift  $\Delta E$ , David and Thouless calculated the energy levels once with periodic and again with antiperiodic boundary conditions. For a periodic system of period  $L$ , they assumed the following solution of the Schrödinger equation

$$\psi_k(\mathbf{r}) = \phi(\mathbf{r})e^{iKx}, \quad (2.29)$$

where  $\phi(\mathbf{r})$  is a function having the same periodicity as the crystal and  $K$  is the reciprocal lattice vector. For this general form of the wavefunction, the amplitude changes by a factor of  $\exp(iKL)$  when the coordinate  $x$  is increased by amount  $L$ . Thus, if  $K$  is an integer multiple of  $2\pi/L$ , the solution is periodic and if  $K$  is an integer multiple of  $\pi/L$ , the solution becomes antiperiodic. The change from periodic to antiperiodic boundary conditions is equivalent to adding the term

$$\frac{\hbar K \widehat{p}_x}{m} + \frac{\hbar^2 K^2}{2m} \quad (2.30)$$

to the Hamiltonian for the periodic system. In the operator formulation of the problem, the momentum operator  $\widehat{p}_x$  must be replaced by the corresponding difference operator  $(\widehat{p}_x)_{ij}$  as required by the tight-binding approximation. With this substitution, perturbation theory gives an energy shift of the form

$$\Delta E_\alpha = \frac{\hbar^2 K^2}{m^2} \sum_{\beta \neq \alpha} \frac{|(\widehat{p}_x)_{\alpha\beta}|^2}{E_\alpha - E_\beta} + \frac{\hbar^2 K^2}{2m}. \quad (2.31)$$

This energy shift deviates from zero only if the fluctuations in the summation term on the right are appreciable. In the localized regime, the fluctuations are small and  $\Delta E_\alpha$  is close to zero (except for exponentially small terms). In the delocalized regime, assuming  $(\widehat{p}_x)_{\alpha\beta}$  does not depend strongly on the energy difference  $E_\alpha - E_\beta$ , the mean square value of the matrix element  $(\widehat{p}_x)_{ij}$  can be taken from the Kubo-Greenwood formula for the electrical conductivity of a cube of side  $L$  given by

---

<sup>3</sup>Remember that  $\Delta E$  is the energy shift (the difference between corresponding energy levels calculated with two different boundary conditions) and  $\eta$  is the energy spacing (roughly given by  $W/N$ ).

$$\sigma = \frac{2\pi e^2 \hbar L^3}{m^2} \left| (\hat{p}_x)_{\alpha\beta} \right|_{\text{avg}}^2 [D(E)]^2, \quad (2.32)$$

where  $D(E)$  is the density of states per unit volume at the Fermi surface. In the case, where the energy levels,  $E_\alpha$  and  $E_\beta$ , are uncorrelated, the geometric mean of the energy shift is given by

$$\overline{\Delta E_\alpha} = \frac{\pi \hbar^2 K^2 L^3 D(E)}{m^2} \left| (\hat{p}_x)_{\alpha\beta} \right|_{\text{avg}}^2 = \frac{\sigma \hbar K^2 L^3}{2e^2} \eta, \quad (2.33)$$

where  $\eta = 1/L^3 D(E)$  is the spacing between energy levels. Thus, for a 3D cubic lattice, the ratio of interest in Edwards and Thouless's criterion for localization becomes

$$\frac{\overline{\Delta E_\alpha}}{\eta} = \frac{\sigma \hbar K^2 L^3}{2e^2}. \quad (2.34)$$

In terms of the mean free path  $l$ , the conductivity can be expressed as  $\sigma = (e^2 k^2 \lambda) / (3\pi \hbar)$  so that Eq. (2.34) becomes

$$\frac{\overline{\Delta E_\alpha}}{\eta} = \frac{k^2 K^2 L^3 \lambda}{6\pi^2}. \quad (2.35)$$

In the two-dimensional case, similar reasoning gives

$$\frac{\overline{\Delta E_\alpha}}{\eta} = \frac{k K^2 L^2 \lambda}{4\pi^2}. \quad (2.36)$$

Assuming  $KL = 2$ , the general form of Eq. (2.34) becomes

$$\frac{\overline{\Delta E_\alpha}}{\eta} = \frac{2\sigma \hbar L^{d-2}}{e^2}, \quad (2.37)$$

where  $d$  is the dimensionality of the system.

Edward and Thouless studied the Anderson localization in the two-dimensional square and the three-dimensional diamond lattices using equations (2.36) and (2.35), respectively. Their numerical simulations, together with later work by Thouless [9], predicted that exponential localization should occur for  $W \geq 6$  for the 2D case and for  $W \geq 15$  in the 3D case. They also established that in the 3D diamond lattice, the calculated energy states corresponding to disorder  $5 \leq W \leq 15$  are neither extended, nor exponentially localized. Similar conclusion was reached in a further study by Last and Thouless [10], which suggested that the metal-to-insulator transition is not abrupt. Instead, there is a transitional interval of disorder values, in which the wave function

decays according to a power law or slower. Thouless argued that similar phenomenon occurs in 2D but the effect is less prominent [9].

## 2.4 Scaling Theory

In 1979 Abrahams et al. [11] introduced the scaling theory of localization, which examines how, close to the mobility edge, the conductivity depends on system size. In this approach, transport is studied with the help of a generalized dimensionless parameter, called the ‘‘Thouless number’’, which is the scale-dependent version of Eq. (2.37)

$$g(L) = \frac{\overline{\Delta E_\alpha(L)}}{\eta(L)} = \frac{2\hbar G(L)}{e^2}, \quad (2.38)$$

where  $L$  is the side of a small finite hypercube and  $G(L) = \sigma L^{d-2}$  is the conductance in the limit  $L \gg l$  (i.e. the cube size is much larger than the mean free path). The conductance  $G$  is assumed independent of the conductivity  $\sigma$  and only a function of system size. In the case where  $L \gg l$ , the phase relationships for arbitrary integration of the Schrödinger equation across the cube are as random as the phase relationships across different cubes. In this limit, the Thouless number  $g(L)$  represents the change of energy levels when two hypercubes are fitted together.

The major assumption here is that the conductance of a hypercube of size  $2L$  depends on a single parameter, namely, the conductance of the hypercube of size  $L$  from which the larger one was built, i.e.  $g(2L) = f(g(L))$  (as shown in Fig. 2.1).

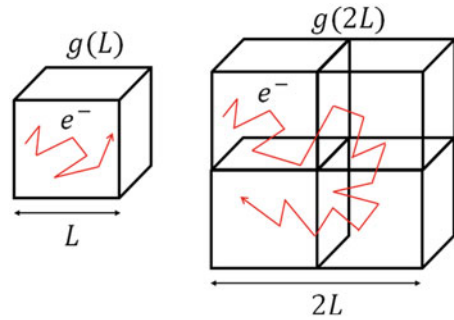
To obtain the conductivity of a larger crystal, one combines  $b^d$  hypercubes into blocks of side  $bL$  and computes the new value of  $g(bL) = f(b, g(L))$ . As the size of the system is extended to infinity by successive stacking of blocks, the scaled expression becomes

$$\beta(g(L)) = \frac{d \ln g(L)}{d \ln L}. \quad (2.39)$$

Employing the above, Abrahams et al. used perturbation theory in  $g$  to obtain the asymptotes of  $\beta$  and a plot of  $\beta$  as a function of  $\ln g$ . They established that there is no real transition from a localized to extended states for either one-dimensional or two-dimensional systems. In the 2D case, the calculation predicted that instead of a sharp mobility edge, there is a universal crossover from logarithmic to exponential decay induced by increasing amount of disorder.

While it is natural to assume that any amount of disorder in a one-dimensional system (with only nearest neighbor interactions) will localize all possible energy states, such conclusion remains controversial for the two-dimensional case, where the function  $\beta$  exhibits critical behavior. As a result, the existence of extended states for infinite disordered systems has remained a topic of debate for the past several

**Fig. 2.1** Visual representation of one-parameter scaling theory in 3D



decades primarily due to the argument that the scaling approach is limited due to the use of boundary conditions and perturbation theory.

Throughout the 1980s, key aspects of scaling theory were confirmed numerically. Those include the explicit derivation of the scaling function  $\beta(g(L))$  for arbitrary dimension  $d$  [12] and the dependence of the dimensionless conductance  $g(L)$  of system size [13]. Experimental evidence in support of these numerical calculations was initially obtained using thin metallic films [14] and 2D electron systems fabricated on semiconductor surfaces [15].

However, later studies demonstrated the existence a transition between the metallic and conducting phases in two-dimensional systems close to zero temperature using disordered fermion thin films [16, 17]. The emergence of metallic behavior in the strongly coupled regime (where Coulomb interaction energy is much larger than the Fermi energy) was established in 2D systems characterized by large electron density [18–21]. In the finite-temperature limit, metal-to-insulator transition was shown for 2D system of charged traps [22] and electron structures in silicon [23].

In the next chapter, we introduce a new mathematical technique, called the spectral approach, which examines transport in disordered systems without the use of scaling arguments. Thus, we expect that this new method can contribute to the study of the Anderson localization in the critical two-dimensional case.

## Bibliography

1. P.W. Anderson, Absence of diffusion in certain random lattices. *Phys. Rev.* **109**(5), 1492–1505 (1958)
2. S.N.F. Mott, H. Jones, *The Theory of the Properties of Metals and Alloys* (Courier Corporation, 1958)
3. N.F. Mott, Conduction in non-crystalline systems IX. The minimum metallic conductivity. *Philos. Mag.* **26**(4), 1015–1026 (1972)
4. N. Mott, Metal-insulator transitions. *Phys. Today* **31**(11) (1978)
5. A.F. Ioffe, Non-crystalline, amorphous, and liquid electronic semiconductors. *Prog. Semicond.* **4**, 237–291 (1960)

6. R.J. Bell, P. Dean, Atomic vibrations in vitreous silica. *Discuss. Faraday Soc.* **50**(0), 55–61 (1970)
7. R.J. Bell, P. Dean, D.C. Hibbins-Butler, Localization of normal modes in vitreous silica, germania and beryllium fluoride. *J. Phys. C Solid State Phys.* **3**(10), 2111 (1970)
8. J.T. Edwards, D.J. Thouless, Numerical studies of localization in disordered systems. *J. Phys. C Solid State Phys.* **5**(8), 807 (1972)
9. D.J. Thouless, Electrons in disordered systems and the theory of localization. *Phys. Rep.* **13**(3), 93–142 (1974)
10. B.J. Last, D.J. Thouless, Evidence for power law localization in disordered systems. *J. Phys. C Solid State Phys.* **7**(4), 699 (1974)
11. E. Abrahams, Scaling theory of localization: absence of quantum diffusion in two dimensions. *Phys. Rev. Lett.* **42**(10), 673–676 (1979)
12. D. Vollhardt, P. Wölfle, Scaling equations from a self-consistent theory of Anderson localization. *Phys. Rev. Lett.* **48**(10), 699–702 (1982)
13. P.A. Lee, D.S. Fisher, Anderson localization in two dimensions. *Phys. Rev. Lett.* **47**(12), 882–885 (1981)
14. G.J. Dolan, D.D. Osheroff, Nonmetallic conduction in thin metal films at low temperatures. *Phys. Rev. Lett.* **43**(10), 721–724 (1979)
15. D.J. Bishop, D.C. Tsui, R.C. Dynes, Nonmetallic conduction in electron inversion layers at low temperatures. *Phys. Rev. Lett.* **44**(17), 1153–1156 (1980)
16. M.P.A. Fisher, G. Grinstein, S.M. Girvin, Presence of quantum diffusion in two dimensions: universal resistance at the superconductor-insulator transition. *Phys. Rev. Lett.* **64**(5), 587–590 (1990)
17. M. Y. Azbel, “Quantum particle in a random potential: exact solution and its implications,” *Phys. Rev. B*, vol. 45, no. 8, pp. 4208–4216, 1992
18. D. Popović, A.B. Fowler, S. Washburn, Metal-insulator transition in two dimensions: effects of disorder and magnetic field. *Phys. Rev. Lett.* **79**(8), 1543–1546 (1997)
19. S.J. Papadakis, M. Shayegan, Apparent metallic behavior at  $B = 0$  of a two-dimensional electron system in AlAs. *Phys. Rev. B* **57**(24), R15068–R15071 (1998)
20. P.T. Coleridge, R.L. Williams, Y. Feng, P. Zawadzki, Metal-insulator transition at  $B = 0$  in p-type SiGe. *Phys. Rev. B* **56**(20), R12764–R12767 (1997)
21. A. Punnoose, Metal-insulator transition in disordered two-dimensional electron systems. *Science* **310**(5746), 289–291 (2005)
22. B.I. Altshuler, D.I. Maslov, V.m. Pudalov, Metal–insulator transition in 2D: Anderson localization in temperature-dependent disorder? *Phys. Status Solidi B* **218**(1), 193–200 (2000)
23. S.V. Kravchenko, G.V. Kravchenko, J.E. Furneaux, V.M. Pudalov, M. D’Iorio, Possible metal-insulator transition at  $B = 0$  in two dimensions. *Phys. Rev. B* **50**(11), 8039–8042 (1994)

# Chapter 3

## Spectral Approach



### 3.1 Essence of the Spectral Method

In Chap. 2, we reviewed several theoretical formulations of the Anderson-type transport problem. Here we classify the various localization criteria in three broad categories: dynamical, statistical, and spectral. In the dynamical formulation of the problem, localization of the traveling electron is represented by an exponential decay of the corresponding wave function, satisfying the time-dependent Schrödinger equation. In the statistical case, one is interested in the energy eigenvalues of the system's Hamiltonian, which is represented by a finite-sized random matrix. In this formulation, localization occurs when the computed eigenvalues are discrete and infinitely close to one another. As the dynamical and statistical formulations have clear interpretations in the language of quantum mechanics, they are often applied as localization criteria by both physicists [1–4] and mathematicians [5–7].

In contrast, the spectral formulation, which is well-known to mathematicians [8–11], has not yet been implemented by the physics community. In this approach the spectrum of the Hamiltonian is decomposed in a singular part corresponding to localization and an absolutely continuous part indicating the existence of scattering states (or delocalization). In 2013 Liaw [12] developed a mathematical technique, suited for detection of delocalization in infinite disordered systems of any dimension and geometry. Her spectral model has been well explained in the language of mathematics but has yet to be understood physically and applied to natural-world problems.

The primary goal of this chapter is to provide a brief mathematical formulation and a physical interpretation of this new approach to transport problems. We also discuss its applicability to physical experiments. A major advantage of the spectral model is that, unlike the dynamical and statistical formulations, it avoids issues

---

This chapter published as: E. G. Kostadinova, C. D. Liaw, L. S. Matthews, and T. W. Hyde, "Physical interpretation of the spectral approach to delocalization in infinite disordered systems," *Mater. Res. Express*, vol. 3, no. 12, p. 125904, 2016.

related to the use of periodic boundary conditions and finite-size scaling. Thus, we expect that spectral theory will contribute to the analysis of the critical 2D Anderson localization case, where previous experimental results [13–16] have shown disagreement with scaling theory predictions [17].

It is important to note that the discussion in this chapter does not aim to contradict scaling theory. Rather, our goal is to introduce an alternative mathematical approach to Anderson-type transport problems that provides additional insight into the theory while improving agreement between numerical and experimental results.

### 3.1.1 Cyclic Subspaces and Equivalence Classes

Consider the Hilbert space  $\mathcal{H}$  and let the operator  $\hat{A}$  be a linear transformation on that space. The operator  $\hat{A}$  has a cyclic vector  $\mathbf{f}$  in the Hilbert space if the linear span (set of all linear combinations) of the vectors  $\{\mathbf{f}, \hat{A}\mathbf{f}, \hat{A}^2\mathbf{f}, \dots\}$  is dense in  $\mathcal{H}$ . Equivalently,  $\mathbf{f}$  is a cyclic vector for the operator  $\hat{A}$  if the set of all vectors of the form  $p(\hat{A})\mathbf{f}$ , where  $p$  varies over all polynomials, is dense in  $\mathcal{H}$ . In other words, when  $\mathbf{f}$  is cyclic for  $\hat{A}$ , one can generate the subspace  $S \equiv \text{span}\{\mathbf{f}, \hat{A}\mathbf{f}, \hat{A}^2\mathbf{f}, \dots\}$ , such that every point in the Hilbert space,  $h \in \mathcal{H}$ , is either contained in the subspace  $S$  or is its limiting point. If the operator  $\hat{A}$  is a finite Hermitian matrix, then a necessary and sufficient condition that  $\hat{A}$  has a cyclic vector is that its eigenvalues are *distinct*. In contrast, if they are not distinct, nothing is sufficient to make any vector  $\mathbf{f}$  cyclic for the operator  $\hat{A}$ . In the context of quantum mechanics, one can employ similar reasoning and use cyclicity to study the spectrum of a given operator, such as the Hamiltonian.

For example, consider the (time-independent) Hamiltonian  $\hat{H}$  on the Hilbert space  $\mathcal{H}$ , represented by a finite-dimensional discrete operator, whose spectrum consists of a finite number of eigenvalues  $\lambda_i$ . If  $\hat{H}$  only has nondegenerate eigenvalues, i.e.  $\lambda_i \neq \lambda_j$  when  $i \neq j$ , then the eigenvector-eigenvalue equation is given by

$$\hat{H}\mathbf{v}_i = \lambda_i\mathbf{v}_i, \quad (3.1)$$

where  $\mathbf{v}_i$  is the only eigenstate corresponding to the eigenvalue  $\lambda_i$ . Thus, if the value of the energy in the quantum system is measured to be  $\lambda_i$ , then the corresponding state  $\mathbf{v}_i$  is assumed to be known. Physically, nondegenerate (or distinct) eigenvalues indicate lack of overlap among the possible energy states. In other words, the electron wave function can only assume quantized states, as in the case of a particle trapped in a simple harmonic oscillator or an infinite potential well. Based on the above definitions, we expect that in these cases, all vectors in the Hilbert space (representing the possible states of the quantum system) are cyclic for the examined Hamiltonian.

On the other hand, if  $\hat{H}$  has degenerate eigenvalues, then the measurement of a specific energy  $\lambda_i$  can be associated with several possible states of the quantum

system. In this case, no vector in the Hilbert space is cyclic for the examined Hamiltonian.

### 3.1.2 Spectral Decomposition of Normal Operators

To analyze transport in a periodic structure, such as a  $d$ -dimensional lattice  $\Gamma$ , it is convenient to let the separable Hilbert space  $\mathcal{H}$  be the set of square summable sequences  $l^2(\Gamma)$  defined on the  $d$ -dimensional space. In this space, the time-independent Hamiltonian characterized by a spectrum of discrete eigenvalues, yields possible states of the quantum system that either correspond to eigenvectors or a linear combination of them. Therefore, the Hamiltonian can easily be diagonalized by a change of basis<sup>1</sup>

$$H = U^{-1}DU, \quad \text{where} \quad D = \begin{pmatrix} \lambda_1 & \cdots & 0 \\ \vdots & \ddots & \vdots \\ 0 & \cdots & \lambda_n \end{pmatrix}, \quad (3.2)$$

where  $U$  is the unitary matrix that contains the orthonormalized eigenvectors in its columns. In operator theory, the generalization of this procedure to a larger class of operators is called the Spectral Theorem. Broadly speaking, the Spectral Theorem provides the conditions under which a general operator or a matrix can be diagonalized. Specifically, it identifies a class of linear operators that can be modeled by multiplication operators.<sup>2</sup>

Now consider diagonalization of the general Hamiltonian  $H$  acting on a vector  $v \in l^2(\Gamma)$ . If  $H$  is linear, then we must also have  $Hv \in l^2(\Gamma)$ . According to the Spectral Theorem, when  $H$  is self-adjoint and cyclic, a unitary operator  $U$  exists so that

$$H = U^{-1}M_{\xi}U, \quad (3.3)$$

where  $M_{\xi}f(\xi) = \xi f(\xi)$  is the multiplication by the independent variable on another square-integrable Hilbert space  $L^2(\mu)$ . The new space  $L^2(\mu)$  stands for the square-integrable functions with respect to a measure  $\mu$

<sup>1</sup>For notational simplicity, in the following sections we omit the hats on top of the operators and we denote vectors with ordinary letters instead of bold ones.

<sup>2</sup>In operator theory, a multiplication operator is an operator  $T$  defined on some vector space of functions and whose value at a function  $f$  is given by a fixed function  $h(\xi)$ . That is, when  $T$  acts on  $f$ , the result is  $h(\xi)f(\xi)$ :

$$T(f)(\xi) = h(\xi)f(\xi)$$

for all  $f$  in the function space and all  $\xi$  in the domain of  $f$  (which is the same as the domain of  $h$ ). In Eq. (3.6) we encounter a multiplication operator for which  $h(\xi) = \xi$ .

$$L^2(\mu) = \left\{ f : \mathbb{R} \rightarrow \mathbb{R} \mid \int_{\mathbb{R}} |f(\xi)|^2 d\mu(\xi) < \infty \right\}. \quad (3.4)$$

This new space  $L^2(\mu)$  can be decomposed into two orthogonal Hilbert spaces,  $L^2(\mu_{ac})$  and  $L^2(\mu_{sing})$ , where the spectral measure  $\mu$  is decomposed into an absolutely continuous part and a singular part

$$d\mu = d\mu_{ac} + d\mu_{sing}, \quad (3.5)$$

where

1.  $d\mu_{ac}$ —the absolutely continuous part of the spectrum of  $H$ , which corresponds to the scattering states of the system (or the conducting band of a semiconductor). By the RAGE Theorem [11], the existence of  $d\mu_{ac} \neq 0$  means that there is delocalization in terms of transport.
2.  $d\mu_{sing}$ —the singular part of the spectrum of  $H$  that represents “everything else”, including the discrete eigenvalues, where the eigenvalues are included as Dirac  $\delta$  point masses. For example, if  $H$  only has one eigenvalue at  $\lambda$ , then  $\mu$  equals a Dirac  $\delta$  mass at  $\lambda$ :

$$\int_{\mathbb{R}} f d\mu = \int_{\mathbb{R}} f \delta_{\lambda} d\xi = f(\lambda). \quad (3.6)$$

It is important to note that the singular part of the spectrum  $d\mu_{sing}$  also contains very poorly behaved pieces, called the singular continuous part.<sup>3</sup> Here, the space  $L^2(\mu)$  (on which  $H$  acts by  $M_{\xi}$ ) can be decomposed into two orthogonal Hilbert spaces:

$$L^2(\mu) = L^2(\mu_{ac}) \oplus L^2(\mu_{sing}). \quad (3.7)$$

Thus, in this case the Hamiltonian has a part  $H_{ac}$  that comes from  $L^2(\mu_{ac})$  and a part  $H_{sing}$  that comes from  $L^2(\mu_{sing})$ .

In the general formulation of a transport problem, the spectrum of the Hamiltonian operator is not limited to a collection of discrete eigenvalues. Instead, since the spectrum can also include an absolutely continuous part, the Spectral Theorem should be employed to map the action of the operator from the square summable Hilbert space to the square-integrable Hilbert space whose measure accounts for all possible solutions. (Naturally, continuous solutions require an integrable space and cannot be contained in a summable one.)

---

<sup>3</sup>It is not known what physical property/state corresponds to the singular continuous part (see p. 23 of [18]). We saw a hint for a possible answer in Edwards and Thouless’ model, where it was pointed out that there are solutions to the problem corresponding to an intermediate region in which the particle states are neither localized, nor describable in terms of weakly coupled plane waves [19–21]. However, these “intermediate” states found in theory have not yet been observed experimentally or given a solid physical interpretation.

### 3.1.3 Extended States Conjecture and the Distance Formula

In this work, we are mostly interested in applying the spectral approach to the special case of a two-dimensional disordered lattice. However, the mathematical technique is not limited by dimension or geometry. In the general introduction of the method presented below,  $v_0$  and  $v_1$  are any two (different) vectors in the Hilbert space of interest. Later, (in all numerical simulations) we chose  $v_0 = \delta_0$  and  $v_1 = \delta_1$ , where  $\delta_0$  and  $\delta_1$  are the standard basis vectors of the integer lattice under consideration.

The method we introduce in this section relies on the connection between cyclicity and spectral decomposition. The following theorems hold.

*Theorem 1 [10]: For any vector  $v_0$  in the lattice space,  $v_0$  is cyclic for the singular part  $(H_\epsilon)_{sing}$  with probability 1.*

*Theorem 2 [12]: If one shows that  $v_0$  is not cyclic for  $H_\epsilon$  with non-zero probability, then almost surely<sup>4</sup>*

$$(H_\epsilon)_{sing} \neq H_\epsilon. \quad (3.8)$$

In other words, if Eq. (3.8) holds, the spectrum of  $H_\epsilon$  is not limited to the singular part but also includes an absolutely continuous part, which corresponds to the existence of extended states.

*Essence of the Spectral Method:* For a system described by an Anderson-type Hamiltonian

1. Chose a random vector, say  $v_0$ , corresponding to the initial state of the quantum mechanical system in the space, and generate the sequence  $\{v_0, H_\epsilon v_0, (H_\epsilon)^2 v_0, \dots, (H_\epsilon)^n v_0\}$  where  $n \in \{0, 1, 2, \dots\}$  is the number of iterations of  $H_\epsilon$  and is used as a timestep. Physically, this sequence represents the time-evolution of energy in the lattice.
2. Apply a Gram-Schmidt orthogonalization process (without normalization) to the members of the sequence and denote the new sequence  $\{m_0, m_1, m_2, \dots, m_n\}$ .
3. Calculate the distance from *another* vector from the same Hilbert space, say  $v_1$  and decompose it into a projection along sequence  $\{m_0, m_1, m_2, \dots, m_N\}$  and an orthogonal component

$$v_1 = \sum_{n=0}^N \langle m_n | v_1 \rangle |m_n\rangle + (v_1)_\perp \quad (3.9)$$

By the Pythagorean Theorem, we can rewrite Eq. (3.9) in terms of probability amplitudes

---

<sup>4</sup>Note that in probability theory an event happens *almost surely* if it happens *with probability 1*. In this paper, we use the two phrases interchangeably.

$$\begin{aligned} \|v_1\|^2 = 1 &= \left\| \sum_{n=0}^N \langle m_n | v_1 \rangle |m_n\rangle + (v_1)_\perp \right\|^2 \\ &= \left\| \sum_{n=0}^N \langle m_n | v_1 \rangle |m_n\rangle \right\|^2 + \|(v_1)_\perp\|^2, \end{aligned} \quad (3.10)$$

where  $\|\cdot\|_2$  is the Euclidean norm and  $\langle \cdot | \cdot \rangle$  is the inner product in the space. Solving for  $(v_1)_\perp$  gives

$$(v_1)_\perp = \sqrt{1 - \left\| \sum_{n=0}^N \langle m_n | v_1 \rangle |m_n\rangle \right\|^2}, \quad (3.11)$$

4. Define the distance parameter in the spectral approach as

$$D_{\epsilon, W}^n = \sqrt{1 - \sum_{k=0}^n \frac{\langle m_k | v_1 \rangle^2}{\|m_k\|_2^2}}, \quad (3.12)$$

where  $\left\| \sum_{n=0}^N \langle m_n | v_1 \rangle |m_n\rangle \right\|^2 \equiv \sum_{k=0}^n \langle m_k | v_1 \rangle^2 / \|m_k\|_2^2$  as the sequence  $\{m_0, m_1, m_2, \dots, m_n\}$  is orthogonal. It can be shown [12, 22] that extended states exist with probability 1 if

$$\lim_{n \rightarrow \infty} D_{\epsilon, W}^n > 0. \quad (3.13)$$

## 3.2 Simplified Numerical Model (“Toy Model”)

### 3.2.1 Application to the Discrete Random Schrödinger Operator

Consider the discrete random Schrödinger operator,<sup>5</sup> which is a special case of the Anderson-type Hamiltonian

---

<sup>5</sup>The discrete Random Schrödinger operator on the 2D honeycomb lattice was introduced in Eq. (1.3) in Chap. 1.

$$H_\epsilon = -\Delta + \sum_{i \in \Gamma} \epsilon_i \delta_i \langle \delta_i |, \quad (3.14)$$

where  $\Delta$  is the discrete Laplacian,  $\delta_i$  are the standard basis vectors of the space  $\Gamma$ , and the  $\epsilon_i$  are random variables selected from the interval  $(-W/2, W/2)$  according to a prescribed probability distribution function  $\chi$ . For any vector  $\delta_i \in l^2(\Gamma)$ , say  $\delta_0$ , one can prove the existence of extended states by showing that  $\delta_0$  is noncyclic for the given  $H_\epsilon$ . To accomplish this numerically, we fix the dimension  $d$  in Eq. (3.14) and we let  $\Delta = -ZV$ . Here  $Z$  is the number of nearest neighbors and is thus determined by the geometry of the lattice. The hopping potential  $V$  is taken to be unity. Next, for a given value of the disorder  $W$ , we generate one realization of the random variables  $\epsilon_i$  according to the chosen probability distribution  $\chi$ . For the Anderson localization problem, the variables  $\epsilon_i$  are independent identically distributed (i.i.d.) according to the uniform distribution

$$\chi(\tau) = \begin{cases} 0, & \tau \notin (-W/2, W/2) \\ 1/W, & \tau \in (-W/2, W/2) \end{cases}. \quad (3.15)$$

In other words, the random variables are uniformly distributed, so that  $\epsilon_i$  takes each value in  $(-W/2, W/2)$  with equal probability. Here we have

$$\int_0^{W/2} \chi(\epsilon) d\epsilon = \frac{1}{2}. \quad (3.16)$$

Throughout this chapter and in Chap. 4, the assumed distribution will be the one in Eq. (3.15). In Chap. 5, we will examine various choice for  $\chi$  corresponds to modeling different transport problems, which are related to the Anderson localization.

The next step in the numerical calculation is to fix a random vector  $\delta_0$  in the  $d$ -dimensional space and generate the sequence  $\{\delta_0, H\delta_0, H^2\delta_0, \dots, H^n\delta_0\}$ , where  $n \in \{0, 1, 2, \dots\}$  is the number of iterations of the Hamiltonian and is used as a timestep. Here one iteration of the Hamiltonian corresponds to the time needed for the energy of the particle in the initial state to propagate to its nearest neighbors; thus, the plot  $D_{\epsilon, W}^n$  vs.  $n$  is analogous to determining the evolution of the distance value over time. Figure 3.1 shows an (intuitive) visual representation of this process on the two-dimensional triangular lattice.

The Gram-Schmidt orthogonalization process (without normalization) is then applied to the members of the sequence and the resulting subspace is denoted by  $\{m_0, m_1, m_2, \dots, m_n\}$ . The distance from *any other* general vector  $\delta_1$  in the chosen space to the  $n$ -dimensional orthogonal subspace  $\{m_0, m_1, m_2, \dots, m_n\}$  is then numerically calculated using Eq. (3.12). Once the distance values at each timestep are generated for one realization of the random variables  $\epsilon_i \in (-W/2, W/2)$ , the same process is repeated for several other realizations of the on-site energies (keeping the same  $W$ ). This step is adopted to eliminate possible numerical errors introduced by

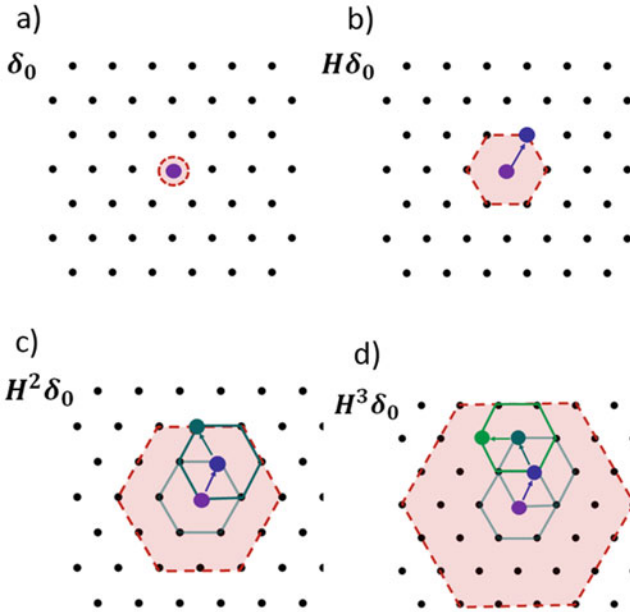


**Fig. 3.1** Visual representation of the first three iterations of the Hamiltonian on a triangular lattice. In each picture, the shaded area indicates the number of particles which have potentially been affected by the corresponding iteration of the Hamiltonian. The small hexagons show possible energy transfer to the nearest neighbors and the enlarged dots connected with arrows indicate one possible path for propagation. The particle in (a) is in some initial energy state. After one iteration of the Hamiltonian (b), energy has been transferred to its nearest neighbors. In the second iteration (c), the nearest neighbors (the vertices of the shaded hexagon in (b)) can also transfer energy to their nearest neighbors, including back to the original particle. A subsequent iteration is shown in (d) (reprinted with permission)

the random generator. Finally, the discrete time evolution of the averaged  $D_{c,W}^n$  values is plotted and various methods are employed to establish whether the distance parameter limits to a positive nontrivial value at infinity.

It is important to keep in mind that the requirement for delocalization given by the spectral approach is  $D_{c,W}^n > 0$  at  $n = \infty$ . The case where  $D_{c,W}^n \leq 0$  does not necessarily prove localization. However, it is reasonable to expect that this case indicates the lack of extended states.

### 3.2.2 Preliminary Results in 2D and 3D

Although the spectral approach can be applied to infinite disordered systems of any dimension or geometry, here we report preliminary results for the 2D square and 3D diamond lattices, which were the ones examined by Edwards and Thouless [19]. We

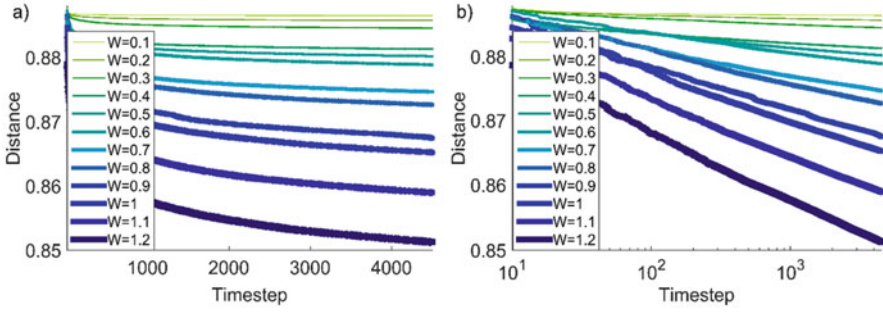


**Fig. 3.2** (a) Time evolution plot of  $D_{c,W}^n$  for the 2D weak disorder case. (b) Corresponding log-log plot (reprinted with permission)

used the raw data from the 2D and 3D numerical simulations conducted by Liaw et al. [12, 22] to obtain discrete time evolution plots of the distance  $D$  for various values of the disorder  $W$ . In this section, we define weak disorder as  $W < 1$ , medium disorder as  $1 \leq W \leq 5$ , and strong disorder as  $W > 5$ . (Similar definitions can be found in [23, 24].) The number of iterations of the Hamiltonian in the numerical calculation is represented by a discrete timestep  $n \in \{0, 1, 2, \dots\}$ . Thus, the plot of  $D_{c,W}^n$  vs.  $n$  represents a time evolution of the distance parameter.

In the 2D case, the examined range of disorder was  $W = 0.1, 0.2, \dots, 1.2$  with four realizations for each  $W$  and  $n = 4500$  timesteps. Figure 3.2a shows the plots the (averaged) distance parameter for each disorder value along with corresponding log-log plots (Fig. 3.2b). As can be seen from the graphs, the distance parameter does not rapidly tend to zero for  $W \leq 0.6$ , implying the existence of extended states. For  $0.8 \leq W$ , the slope of the lines gradually increases and it becomes less obvious whether  $D_{c,W}^n$  will cross the zero axis at infinity. For  $W \geq 0.9$ , the slopes of the lines become even greater, suggesting that transition to localization may have occurred. These trends can also be seen in the log-log plots (Fig. 3.2b), where the large slope of the lines for  $W > 0.6$  implies faster decay of the distance vector towards zero.

Another feature of Fig. 3.2 is an observed gap between the limiting values of  $D$  as the disorder increases from  $W = 0.3$  to  $W = 0.4$ , from  $W = 0.6$  to  $W = 0.7$ , and from  $W = 0.8$  to  $W = 0.9$ , which may imply some type of splitting in the allowed energy states of the system. This phenomenon will be examined in detail in a future paper.

In the 3D case, the simulations were carried over a wide range of  $W$  values. This time, however, the used timestep was  $n = 500$  due to data requirement restrictions. Figure 3.3 shows distance time evolution plots and log-log plots for the three types of disorder: weak, medium, and strong. The total variation of the disorder ranged from  $W = 0.1$  to  $W = 40$  in different steps. For small and medium disorder (Fig. 3.3a–d) it seems that the distance tends to nonzero values and the corresponding log-log plots have constant slopes, implying no significant decrease of  $D$  over time.

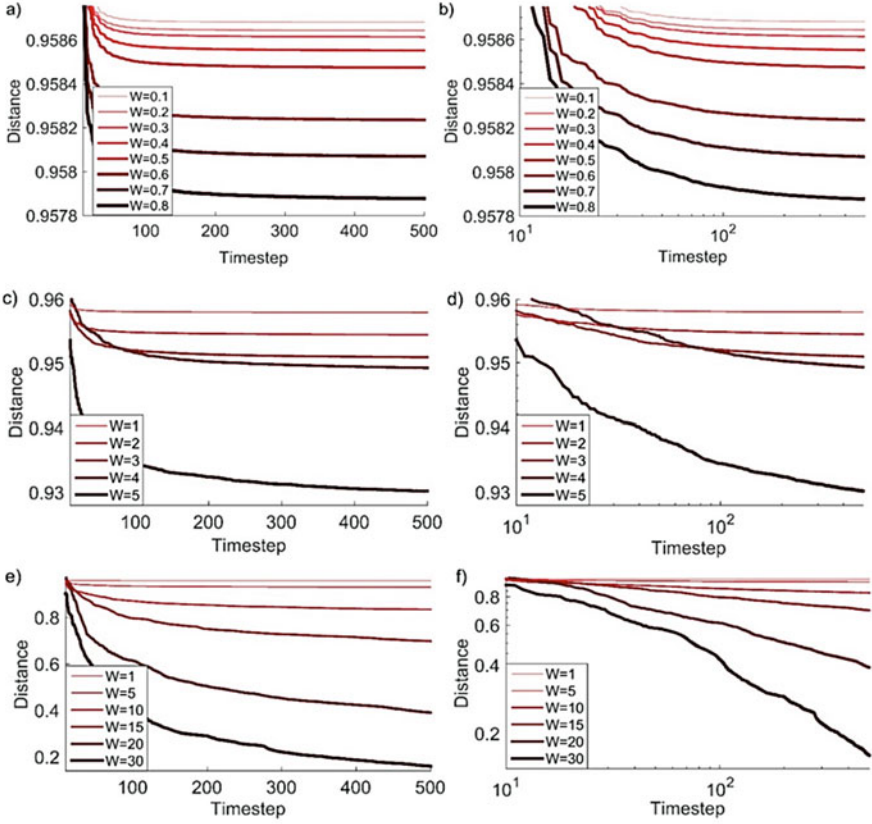


**Fig. 3.3** Time evolution plot of  $D$  for a 3D case with: (a) weak disorder, (c) medium disorder, and (e) strong disorder. The plots in (b), (d), and (f) show the corresponding log-log plots (reprinted with permission)

For large disorder, Fig. 3.3e, f show that for  $W \geq 10$  the distance lines approach the horizontal axis rapidly and the slopes of the corresponding log-log plots become increasingly negative. In this case, the model gives inconclusive results, i.e. a crossover to localization may have occurred. The graphs also indicate that the transition point distinguishing extended from localized states occurs in the interval  $5 \leq W \leq 15$ .

Our preliminary results for the 2D square lattice disagree with the numerical simulations of David and Thouless by an order of 10 (see last paragraph of Sect. 2.3) In the 3D diamond lattice case, we confirm their prediction that the transition point occurs in the range  $5 \leq W \leq 15$ .

### 3.3 Physical Interpretation

As we mentioned earlier, the spectral approach to transport problems involving Anderson-type Hamiltonians is well known and accepted in the mathematical community. However, the techniques of spectral theory are often neglected in favor of more “traditional” methods, such as the perturbative approach in Kubo-Greenwood (KG) theory [25, 26] and the recursive Green’s function technique (RGT) [27, 28]. In this section, we provide a discussion of the spectral approach through a comparison with the well-known Edwards and Thouless model. The discussion aims to create an initial physics intuition, which will help researchers apply the spectral method to their numerical and experimental studies. A comprehensive interpretation of the mathematics will hopefully be obtained once the spectral techniques becomes a common tool for the analysis of transport problems in the physics community.

#### 3.3.1 Band Structure and the Spectrum of the Hamiltonian

As previously mentioned, in this book we apply the spectral technique (Sect. 3.1) to the discrete random Schrodinger operator (Eq. 1.3) in the tight binding approximation, which allows us to make a comparison with the model developed by David and Thouless (Sect. 2.3). The formulation of the Anderson localization problem in both cases assumes constant (and normalized to unity) hopping amplitudes  $V$  and random on-site energies  $\epsilon_i$  distributed uniformly in an interval of disorder  $(-W/2, W/2)$ . Thus, one can study how the transport properties in the system change as the width of the disorder interval is varied. The key distinction between the spectral techniques and the methods discussed in Chap. 2 is the transport regime of interest. Historically, scientists have been interested in the critical amount of system disorder that will yield localization. Thus, the common numerical techniques used in the physics community start with finite systems and examine how conductivity behaves as the size of the simulation is increased. Although these methods are successful in establishing exponential localization, they may not be fully suitable for establishing the existence of extended states. In contrast, the spectral approach is designed to study delocalization in an infinite system, which makes it appropriate for investigating the critical Anderson 2D case.

As noted before, Edwards and Thouless examine the ratio of the energy shift  $\Delta E$  to the energy spacing  $\eta = W/N$  of a large (or infinite) system created by stacking together identical  $d$ -dimensional cubes of side  $N$ . The transition towards exponential localization occurs when the ratio  $\Delta E/\eta = N\Delta E/W$  goes to zero as the system size increases, i.e. the energy shift is expected to be exponentially small. This definition makes sense when one recognizes that  $N\Delta E$  represents  $N$  energy bands of width  $\Delta E$ . Thus, as the system size increases, the energy band is represented by narrow discrete energy levels and transport is only allowed through hopping. In the delocalized regime, the ratio  $\Delta E/\eta$  approaches a constant value for the scaled system, which

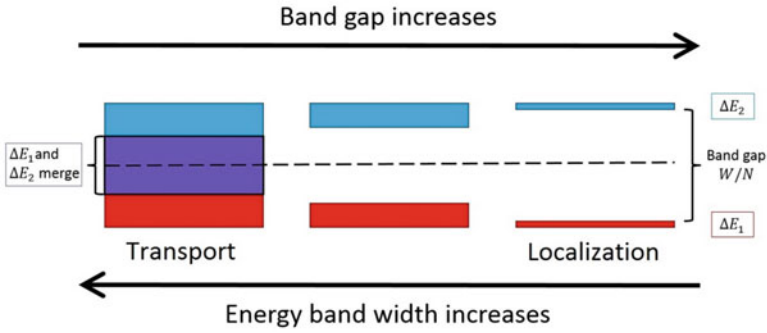


**Fig. 3.4** Visual representation of the metal-to-insulator transition in terms of energy band structure (reprinted with permission)

implies a large value of  $\Delta E$ . In this case, the spectrum consists of broad (possibly overlapping) energy bands, allowing for metallic transport. Figure 3.4 gives a simplified picture of the metal-to-insulator transition.

The band structure of a given system provides a visual representation of the spectrum of possible energies. Thus, one can see the parallel between the above discussion and the spectral approach, where the existence of extended states corresponds to the presence of an absolutely continuous part in the spectrum of the Hamiltonian.

From the perspective of spectral theory, Edwards and Thouless's model examines the singular spectrum of the Hamiltonian (which includes the discrete eigenvalues and the poorly behaved pieces that are neither discrete, nor continuous). In this sense, the limit where the width of the energy bands  $\Delta E$  becomes exponentially small corresponds to the limit where the spectrum of energy eigenvalues becomes discrete.<sup>6</sup> Mathematically, this corresponds to a pure point spectrum of the Hamiltonian (i.e., only discrete eigenvalues or poorly behaved pieces that are neither discrete nor continuous). In the case of a pure point spectrum, the random nature of the system ensures non-degeneracy of the eigenvalues with probability one. For example, even if two eigenvalues  $\lambda_1$  and  $\lambda_2$  are equal for a given realization of the random variables  $\epsilon_i$ , the effect of slightly changing just one of these random variables will split  $\lambda_1$  and  $\lambda_2$  into distinct eigenvalues. In such a system, by the Kolmogorov zero-one law, all eigenvalues are distinct.

In the spectral model, extended states exist with probability 1 when the spectrum of the Hamiltonian is not limited to its singular component, but also has a continuous part. This is a strong definition of transport called dynamical delocalization [11]. In this regime, the energy bands already overlap by a non-trivial amount, which indicates some degeneracy. Thus, the effect of slightly changing the random

<sup>6</sup>It is known that even if the energy bands are narrow, they can still have internal structure. However, Edwards and Thouless' model cannot distinguish structure inside the bands. Thus, for the purpose of their simulation, each band behaved as a discrete energy value.

variables induces a “wiggling” of the band edges, but does not change the overlapping property. In this sense, degeneracy (i.e. overlap) of the absolutely continuous spectrum is somewhat more stable than is the pure point spectrum case.

### 3.3.2 *Bounded Operators and the Hilbert Space*

Although both Edwards and Thouless’s model and the spectral approach employ the same form of the Hamiltonian, the two techniques make different assumptions on the corresponding domain in the Hilbert space. However, Edwards and Thouless use an *unbounded Hamiltonian*, which requires the application of boundary conditions to the wavefunction. In contrast, the spectral approach starts with a *bounded  $H_c$* , which can be applied to the Schrödinger equation without the assumption of boundary conditions. Thus, an important distinction between the two treatments is in the domain of the applied operator. However, Edwards and Thouless use an *unbounded Hamiltonian*, which requires the application of boundary conditions to the wavefunction. In contrast, the spectral approach starts with a *bounded  $H_c$* , which can be applied to the Schrödinger equation without the assumption of boundary conditions. Thus, an important distinction between the two treatments is in the domain of the applied operator.

A subtle but crucial step in the analysis of a quantum mechanical transport problem is the choice of restrictions on the Hamiltonian operator and the Hilbert space. Many physical problems are defined by a time-evolution differential equations for which the Hamiltonian is not necessarily self-adjoint (for example, there is no self-adjoint momentum operator for a particle moving on a half-line). Thus, it is a common practice in the physics community to define an unbounded Hamiltonian  $H$  and then attempt to find self-adjoint extensions of  $H$ , corresponding to boundary conditions or conditions at infinity. Although this approach is standard in the formulation of quantum mechanics and quantum field theory, the assumption of unbounded Hamiltonian is not necessarily defined on the entire Hilbert space  $\mathcal{H}$ . Instead, such operator is restricted to the dense subspaces of  $\mathcal{H}$ . Although this approach is successful in solving some problems in quantum mechanics, it causes incompleteness in the theory as important physical properties of the self-adjoint operators (representing the observables in quantum mechanics) are sensitive to the choice of the domain. Thus, the restriction of the domain of  $H$  to the dense subspaces of  $\mathcal{H}$  can cause loss of information about the transport behavior of the system [29].

The algebras of bounded operators has been shown to form an equivalent treatment of quantum mechanics [30] and quantum field theory [31]. Here we avoid the (rather unphysical) application of boundary conditions using an Anderson-type bounded Hamiltonian operator, which is defined on the entire Hilbert space. Thus, we expect that the proposed spectral approach accounts for wavefunction solutions that are omitted by scaling theory due to the restricted domain of the unbounded Hamiltonian used there.

### 3.4 Scope and Limitations of the Spectral Analysis

The spectral method is designed to test for the existence of extended states in infinite disordered lattices of any dimension or geometry. Thus, it is applicable to a variety of physical systems and mathematical problems. In the application chapters of this work, we use the spectral method in the analysis of the following transport problems: (1) Anderson localization in 2D lattices of various geometries (Chap. 4), (2) Quantum percolation and binary alloy problems (Chap. 5), and (3) Lattice wave transport in a complex plasma crystal (Chap. 6). Our goal is to show that the spectral method can be adapted to both the quantum and classical regimes, where Anderson-type Hamiltonians are relevant.

In all numerical simulations, we use the discrete random Schrödinger operator, where the Laplacian is a constant hopping potential  $V$  ranging over the  $Z$  nearest neighbors (i.e.,  $\Delta = ZV$ ) and the on-site energies  $\epsilon_i$  are uncorrelated (since  $\delta_i$  assumes the value 1 in the  $i^{\text{th}}$  entry and zero in all other entries). However, the spectral approach can be applied to a more general form of the Anderson-type Hamiltonian, where the Laplacian involves more neighbors and the on-site energies are correlated, i.e. the  $\delta_i$  are not Kronecker delta functions but general vectors  $v_i$  in the space  $\Gamma$ .

The suggested spectral approach relies on the limiting value of the distance parameter  $D_{\epsilon,w}^n$  as time go to infinity. However, in all 2D simulations, the chosen number of iterations of the Hamiltonian is  $n = 4500$ . Thus, the numerical experiments may be limited by the length of the computation.

## Bibliography

1. T. Brandes, S. Kettenmann, *The Anderson Transition and Its Ramifications—Localization, Quantum Interference, and Interactions* (Springer, 2003)
2. J. Chabé, G. Lemarié, B. Grémaud, D. Delande, P. Szriftgiser, J.C. Garreau, Experimental observation of the Anderson metal-insulator transition with atomic matter waves. *Phys. Rev. Lett.* **101**(25), 255702 (2008)
3. B. Kramer, A. MacKinnon, Localization: theory and experiment. *Rep. Prog. Phys.* **56**(12), 1469–1564 (1993)
4. A. Lagendijk, B. van Tiggelen, D.S. Wiersma, Fifty years of Anderson localization. *Phys. Today* **62**(8), 24–29 (2009)
5. M. Aizenman, S. Molchanov, Localization at large disorder and at extreme energies: an elementary derivations. *Commun. Math. Phys.* **157**(2), 245–278 (1993)
6. L.A. Pastur, Spectral properties of disordered systems in the one-body approximation. *Commun. Math. Phys.* **75**(2), 179–196 (1980)
7. J. Fröhlich, T. Spencer, Absence of diffusion in the Anderson tight binding model for large disorder or low energy. *Commun. Math. Phys.* **88**(2), 151–184 (1983)
8. M. Aizenman, R. Sims, S. Warzel, Absolutely continuous spectra of quantum tree graphs with weak disorder. *Commun. Math. Phys.* **264**(2), 371–389 (2006)
9. V. Jakšić, Y. Last, Spectral structure of Anderson type Hamiltonians. *Invent. Math.* **141**(3), 561–577 (2000)

10. V. Jakšić, Y. Last, Simplicity of singular spectrum in Anderson-type Hamiltonians. *Duke Math. J.* **133**(1), 185–204 (2006)
11. D. Hundertmark, A short introduction to Anderson localization, in *Analysis and Stochastics of Growth Processes and Interface Models*, (Oxford University Press, Oxford, 2008), pp. 194–218
12. C. Liaw, Approach to the extended states conjecture. *J. Stat. Phys.* **153**(6), 1022–1038 (2013)
13. S.V. Kravchenko, G.V. Kravchenko, J.E. Furneaux, V.M. Pudalov, M. D’Iorio, Possible metal-insulator transition at  $B = 0$  in two dimensions. *Phys. Rev. B* **50**(11), 8039–8042 (1994)
14. D. Popović, A.B. Fowler, S. Washburn, Metal-insulator transition in two dimensions: effects of disorder and magnetic field. *Phys. Rev. Lett.* **79**(8), 1543–1546 (1997)
15. S.J. Papadakis, M. Shayegan, Apparent metallic behavior at  $B = 0$  of a two-dimensional electron system in AlAs. *Phys. Rev. B* **57**(24), R15068–R15071 (1998)
16. A. Punnoose, Metal-insulator transition in disordered two-dimensional electron systems. *Science* **310**(5746), 289–291 (2005)
17. E. Abrahams, Scaling theory of localization: absence of quantum diffusion in two dimensions. *Phys. Rev. Lett.* **42**(10), 673–676 (1979)
18. M. Reed, B. Simon, *Functional Analysis* (Academic, New York, 1980)
19. J.T. Edwards, D.J. Thouless, Numerical studies of localization in disordered systems. *J. Phys. C Solid State Phys.* **5**(8), 807 (1972)
20. D.J. Thouless, Electrons in disordered systems and the theory of localization. *Phys. Rep.* **13**(3), 93–142 (1974)
21. B.J. Last, D.J. Thouless, Evidence for power law localization in disordered systems. *J. Phys. C Solid State Phys.* **7**(4), 699 (1974)
22. W. King, R.C. Kirby, C. Liaw, Delocalization for the 3-D discrete random Schrodinger operator at weak disorder. *J. Phys. A Math. Theor.* **47**(30), 305202 (2014)
23. S.-J. Xiong, Y. Xiong, Anderson localization of electron states in graphene in different types of disorder. *Phys. Rev. B* **76**(21), 214204 (2007)
24. A. Lherbier, B. Biel, Y.-M. Niquet, S. Roche, Transport length scales in disordered graphene-based materials: strong localization regimes and dimensionality effects. *Phys. Rev. Lett.* **100**(3), 036803 (2008)
25. R. Kubo, Statistical-mechanical theory of irreversible processes. I. General theory and simple applications to magnetic and conduction problems. *J. Phys. Soc. Jpn.* **12**(6), 570–586 (1957)
26. D.A. Greenwood, The Boltzmann equation in the theory of electrical conduction in metals. *Proc. Phys. Soc.* **71**(4), 585 (1958)
27. S. Rotter, J.-Z. Tang, L. Wirtz, J. Trost, J. Burgdörfer, Modular recursive Green’s function method for ballistic quantum transport. *Phys. Rev. B* **62**(3), 1950–1960 (2000)
28. C.H. Lewenkopf, E.R. Mucciolo, The recursive Green’s function method for graphene. *J. Comput. Electron.* **12**(2), 203–231 (2013)
29. A. Heathcote, Unbounded operators and the incompleteness of quantum mechanics. *Philos. Sci.* **57**(3), 523–534 (1990)
30. I.E. Segal, Postulates for general quantum mechanics. *Ann. Math.* **48**(4), 930–948 (1947)
31. H. Araki, Hamiltonian formalism and the canonical commutation relations in quantum field theory. *J. Math. Phys.* **1**(6), 492–504 (1960)

# Chapter 4

## Delocalization in 2D Lattices of Various Geometries



### 4.1 Transport in the Honeycomb, Triangular, and Square Lattices

We applied the spectral approach to the cases of 2D honeycomb, triangular, and square lattices (Fig. 4.1) using the discrete random Schrödinger operator  $H_\epsilon$  given in Eq. (1.3). Of course,  $\mathbb{Z}^2$  is now replaced by the honeycomb/triangular lattice. Each simulation was run for  $n = 4500$  iterations of the Hamiltonian. The difference in geometry was reflected in the Laplacian, which has the form  $\Delta = -ZV$ , where  $Z$  is the number of nearest neighbors. The hopping potential  $V$  was taken to be unity. Thus, the results from the numerical simulations are in units of  $V$ . For each lattice geometry, we considered disorders  $W = 0.10 : 0.05 : 1.20$ . To facilitate the discussion, in this work, we divide this range of values into small ( $W < 0.60$ ), medium ( $0.60 \leq W \leq 0.90$ ), and large ( $W > 0.90$ ) disorder. This convention is specific for our study and will be used throughout this chapter. In all 2D simulations we used timestep  $n = 4500$ .

To minimize numerical error and ensure randomness of the assigned values of  $\epsilon_i$ , five realizations were generated for each  $W$  and the resulting distances averaged at each iteration. Figure 4.2 shows the distance-time evolution of the (averaged) values of  $D$  obtained for each geometry. A qualitative examination of the plots indicates that for all three lattices the distance values for small disorder ( $W < 0.60$ ) quickly flatten out and appear as horizontal lines at  $n = 4500$ .

---

This chapter published as: E. G. Kostadinova, K. Busse, N. Ellis, J. Padgett, C. D. Liaw, L. S. Matthews, & T. W. Hyde (2017). Delocalization in infinite disordered 2D lattices of different geometry. *ArXiv preprint: 1706.02800*. (recommended for publication in *Phys. Rev. B*)

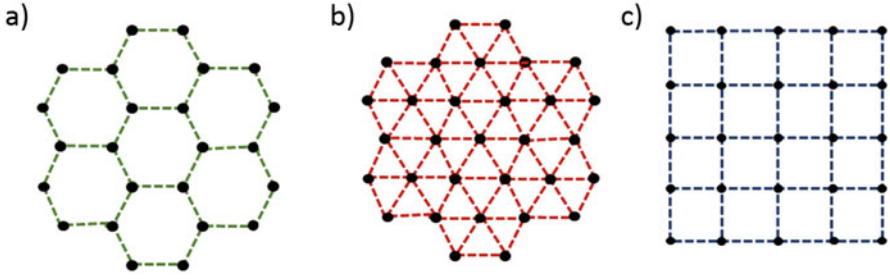


**Fig. 4.1** Honeycomb (a), triangular (b), and square (c) lattice geometry. Notice that the triangular symmetry is obtained by placing a lattice point at the center of each hexagon in the honeycomb lattice (reprinted with permission)

The corresponding log-log plots for these disorder values (see Fig. 4.3) are straight lines, suggesting that the distances are exponentially<sup>1</sup> decreasing towards finite nonzero values. According to the spectral approach, such behavior corresponds to the existence of extended states with probability 1.

As the amount of disorder is increased, the distance plots exhibit greater negative slopes and a quantitative analysis is needed to determine the transition from delocalized to localized states. In this analysis, the transition point represents the critical value of disorder for which the spectral approach can no longer show the existence of extended states with probability 1.

We emphasize that this transition point does not necessarily indicate a sharp metal-to-insulator transition; rather, it corresponds to the critical amount of disorder that marks the onset of the phase transition in the system. It has been previously argued by Thouless and Last [1] that (in both 2D and 3D) there is a transition interval of disorder values ( $W_{min}$ ,  $W_{max}$ ) (rather than a single point) for which the behavior of the wavefunction is characteristic of neither extended states nor exponential decay. Here we identify an analog of the lower bound  $W_{min}$  for such an interval. The upper bound is the critical amount of disorder above which the wavefunction decays exponentially and is the quantity commonly studied in the literature [2–4]. The intermediate region  $W_{min} < W < W_{max}$ , where the wavefunction may decay following a power law or logarithmically, is of significance for 2D materials, such as graphene.

As mentioned at the beginning of this section, we generated and averaged five different realizations for each examined disorder value. In each set of five realizations, the standard deviation from the mean value was used as error estimate in the quantitative analysis of the data. Figure 4.4 shows distance plots of the average values of  $D_{hc}$  (solid lines) together with the corresponding error estimates (shaded regions)

<sup>1</sup>Note that in the spectral approach an exponential decay of the distance plots to a finite nonzero value corresponds to delocalization. This *should not* be confused with the exponential decay of the electron wavefunction in scaling theory, which corresponds to localization. The  $D$  value is a mathematical construct that is used to test for cyclicity, not a physical wavefunction.

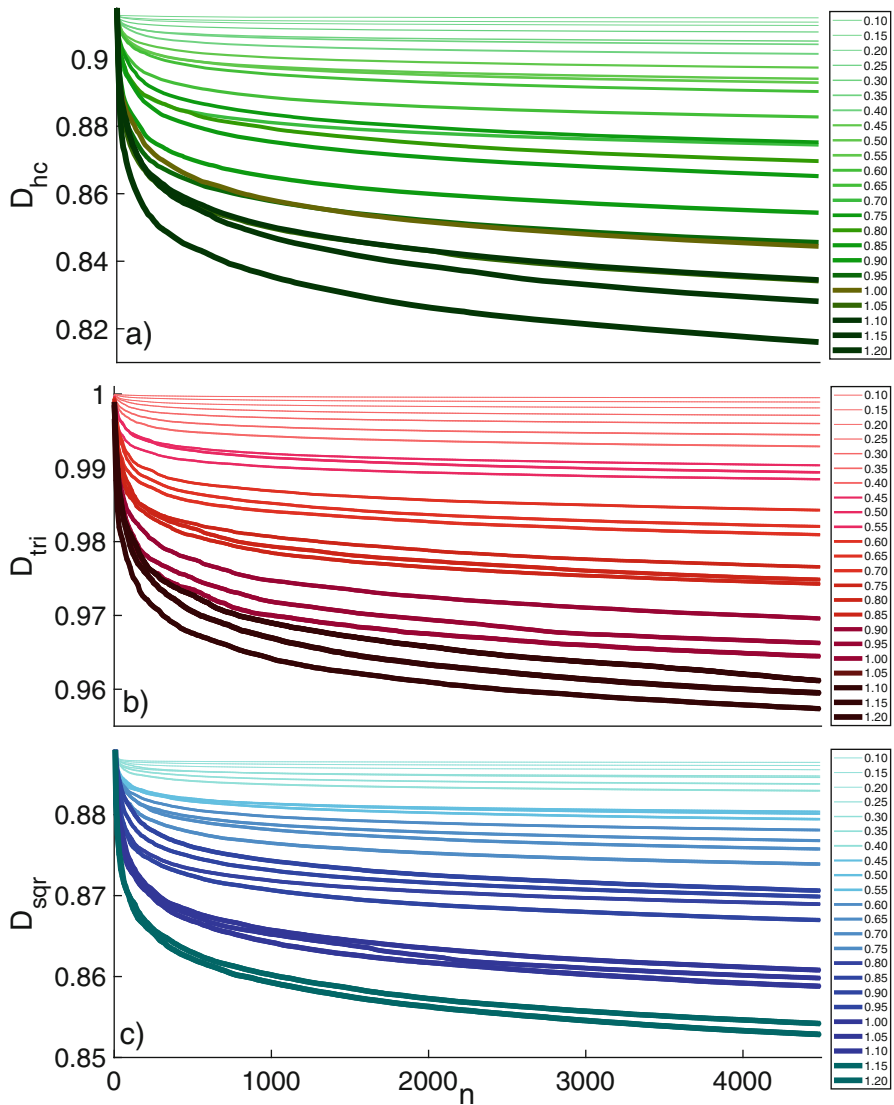


**Fig. 4.2** Distance time evolution plots for the honeycomb (a), triangular (b), and square (c) lattices with disorder  $W = 0.10 : 0.05 : 1.20$  (reprinted with permission)

for three disorder values for the honeycomb geometry. Small error estimates correspond to a small spread of  $D$  and higher certainty in the limiting distance value, whereas increasing error estimates indicate significant fluctuations in  $D$  and less certainty in the limiting value. As expected, the spread of the random realizations increases with increasing disorder, which indicates an onset of a transition in the limiting behavior of the distance values.

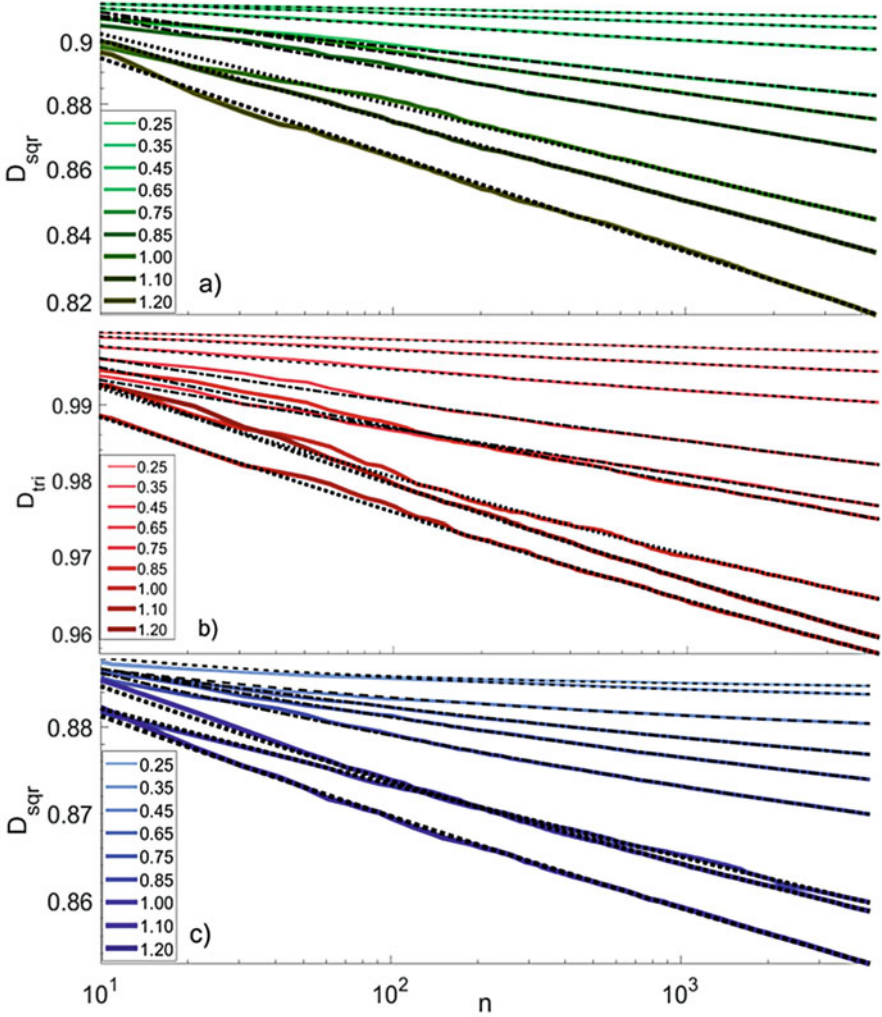


**Fig. 4.3** Log-log plots for the honeycomb (a), triangular (b), and square (c) lattices. For clarity of presentation, each graph displays only characteristic trends of the log-log plots for small disorder ( $W = 0.25, 0.35, 0.45$ ), medium disorder ( $W = 0.65, 0.75, 0.85$ ), and large disorder ( $W = 1.00, 1.10, 1.20$ ). In each plot, the dashed, dash-dotted, and dotted lines represent the fit to a nonlinear regression model (see Sect. 4.2) (reprinted with permission)

## 4.2 Orthogonality Check

It is known that in many instances Gram-Schmidt instability may occur in the algorithm we use to orthogonalize the sequence  $\{\delta_0, H\delta_0, H^2\delta_0, \dots, H^n\delta_0\}$ , which could cast doubt on the validity of our distance calculations. As discussed in [5], an *a posteriori* orthogonality check can be employed to test the accuracy of the results. The Krylov subspace was generated for a smaller problem ( $n = 250$ ) and its

**Fig. 4.4** Error estimates for small, medium, and large disorder values in the honeycomb lattice. The line gives the average distance at each iteration, while the shaded area indicates the standard deviation of the five realizations (reprinted with permission)

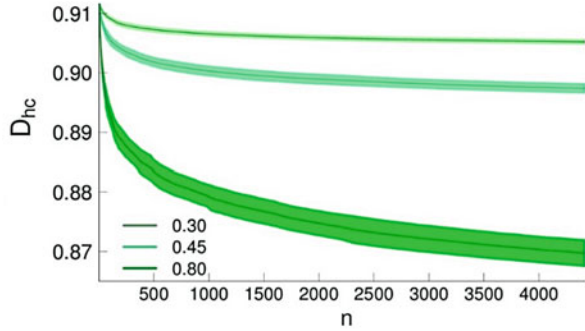


**Table 4.1** Orthogonality check results for the critical values of disorder in the honeycomb, triangular, and square lattices (reprinted with permission)

Geometry	Honeycomb	Triangular	Square
$W_c$	0.70	0.70	0.95
$Q$	$3.3632e-12$	$7.8317e-13$	$0^a$

<sup>a</sup>Calculations in the orthogonality check are made using 64-bit precision. Thus, we expect that the value of  $Q$  for the square lattice is on the order of  $10^{-64}$  or smaller

vectors stored as columns of a matrix  $K$ . The quantity  $Q = \|K^T K - I\|_\infty$  should deviate from zero in proportion to any loss of orthogonality and can be used as a check for the instability in the calculation. Since we expect the Gram-Schmidt instability to increase with increasing disorder, we applied the orthogonality check to the critical values of disorder  $W$  below which we claim delocalization with probability 1 for each geometry. In Table 4.1, we present the infinity-norm of the square matrix  $K$  for the critical values  $W_c = 0.70$  (in the honeycomb and triangular lattices) and  $W_c = 0.95$  (in the square lattice). As shown, the Krylov vectors in all three cases are in fact quite close to orthogonal indicating that the observed delocalization cannot be attributed to the instability of the Gram-Schmidt procedure.

### 4.3 Equation Fitting

For a given disorder, extended states exist if the corresponding distance parameter  $D$  approaches a nonzero value at infinity. As we need to extrapolate the limiting behavior for  $n \rightarrow \infty$ , we fit the data using an equation of the form

$$D = mn^{-\alpha} + b, \quad (4.1)$$

where the exponent term indicates how rapidly  $D$  tends to a finite value and  $b$  corresponds to the limiting value of  $D$  as  $n \rightarrow \infty$ . We applied a nonlinear regression model to Eq. (4.1) and performed hierarchical clustering of the resulting values for  $b$ , which allowed us to distinguish the delocalized regime for each geometry.

**Table 4.2** Equation parameters yielding the best fit for various amounts of disorder in the 2D honeycomb, triangular, and square lattices (reprinted with permission). Here  $R = (D(4500) - b)/bD$  (4500) measures the relative contribution of the exponential term at  $n = 4500$

$W$	Honeycomb		Triangular		Square	
	$b(\times 10^{-3})$	$R(\%)$	$b(\times 10^{-3})$	$R(\%)$	$b(\times 10^{-3})$	$R(\%)$
0.10	900 ± 2	1 ± 0	986 ± 3	1 ± 0	886 ± 0.1	0
0.15	897 ± 8	1 ± 1	984 ± 8	1 ± 1	886 ± 0.3	0
0.20	885 ± 10	3 ± 1	986 ± 10	1 ± 1	885 ± 0.1	0
0.25	877 ± 15	3 ± 2	978 ± 10	2 ± 1	884 ± 1	0
0.30	871 ± 21	4 ± 2	978 ± 13	2 ± 1	884 ± 0.5	0
0.35	839 ± 35	7 ± 4	967 ± 21	3 ± 2	882 ± 0.5	0
0.40	850 ± 34	6 ± 4	957 ± 15	4 ± 2	881 ± 0.6	0
0.45	825 ± 56	8 ± 6	968 ± 13	2 ± 1	878 ± 1	0
0.50	833 ± 42	7 ± 5	957 ± 29	3 ± 3	876 ± 2	0
0.55	756 ± 63	15 ± 7	933 ± 32	6 ± 3	873 ± 1	1 ± 0
0.60	700 ± 55	21 ± 6	952 ± 22	3 ± 2	866 ± 7	1 ± 1
0.65	745 ± 49	16 ± 6	922 ± 56	6 ± 6	864 ± 4	1 ± 1
0.70	756 ± 87	14 ± 10	908 ± 84	7 ± 9	844 ± 30	4 ± 3
0.75	585 ± 76	33 ± 9	850 ± 58	13 ± 6	854 ± 4	2 ± 1
0.80	483 ± 57	44 ± 7	830 ± 35	15 ± 4	850 ± 7	2 ± 1
0.85	517 ± 72	40 ± 8	867 ± 76	11 ± 8	842 ± 15	3 ± 2
0.90	641 ± 110	25 ± 13	839 ± 84	13 ± 9	825 ± 21	5 ± 2
0.95	486 ± 149	42 ± 18	831 ± 162	14 ± 17	833 ± 6	4 ± 1
1.00	246 ± 67	71 ± 8	765 ± 87	21 ± 9	771 ± 81	11 ± 9
1.05	265 ± 198	68 ± 24	803 ± 130	16 ± 14	780 ± 63	9 ± 7
1.10	344 ± 239	59 ± 29	828 ± 68	14 ± 7	806 ± 4	6 ± 1
1.15	173 ± 107	91 ± 18	735 ± 85	23 ± 9	763 ± 53	11 ± 6
1.20	155 ± 179	81 ± 22	801 ± 102	16 ± 10	737 ± 67	13 ± 8

Figure 4.2 shows that the values of  $D$  are rapidly changing for  $n < 1000$ ; accordingly, the data fit was performed using a nonlinear regression model for Eq. (4.1) with a weight function handle  $w = 1/\sqrt{4500 - n}$ . To further reduce data fluctuations, separate fits were generated for each of the five realizations of each considered disorder. The resulting values for  $b$  were then averaged and the standard deviation from the mean was used as an error estimate. Representative fits for small ( $W < 0.60$ ), medium ( $0.60 \leq W \leq 0.90$ ), and large ( $W > 0.90$ ) disorder are shown in Fig. 4.3. The extrapolated values of  $b$  as  $n \rightarrow \infty$  are provided in Table 4.2. For all considered cases, the root mean squared error<sup>2</sup> from the fit equation was consistently small ( $\sim 10^{-6} - 10^{-5}$ ), which indicates a good

<sup>2</sup>Note that there are two distinct errors in the discussion. The *error estimates* obtained from the spread of the random realizations for each disorder (the ones shown in Tables I and II) indicate the certainty with which we can determine the limiting behavior of the distance values. The *root mean squared error* shows the goodness of the fit.

agreement with the weighted regression model. Examination of the column containing the values of  $b$  for the honeycomb lattice indicates that these values experience a sharp drop when the disorder increases from  $W = 0.70$  to  $W = 0.75$  (highlighted in Table 4.2). This suggests the existence of two regions of disorder, where the distance values have distinct limiting behavior. The first region corresponds to the delocalized regime and  $W = 0.75$  marks the onset of the phase transition to a different transport behavior. Such sharp drops in the distance values are not as obvious for the triangular and the square lattice. However, regions corresponding to distinct behavior of the  $b$  values can be identified for all three geometries using a hierarchical clustering analysis introduced in the following section.

The second value in Table 4.2 is the ratio  $R = (D(4500) - b)/D(4500)$ , which quantifies the contribution of the exponential term in Eq. (4.1) to the value of  $D$  at  $n = 4500$ . Although the spectral model identifies the existence of extended states for *any* nonzero limiting value of  $D$  (i.e. the exact magnitude of  $D$  as  $n \rightarrow \infty$  is irrelevant), the simulations are finite ( $n = 4500$ ) and the value of  $R$  gives a good idea of how rapidly the distance  $D$  approaches the limiting value. Small  $R$  indicates rapid decay of  $D$  to its limiting value  $b$ , whereas increasing  $R$  suggests that the contribution of the exponential term is still significant after 4500 iterations. In the range of disorders for which  $R$  is large, the number of iterations may not be sufficient to extrapolate the limiting behavior of  $D$  at infinity. For both the honeycomb and the triangular lattice,  $R$  increases with increasing disorder and we can again identify the emergence of two regions (corresponding to smaller  $R$  and larger  $R$ ), where the rate of decay of  $D$  is different. In the square lattice case, the ratio remains small for almost all values of disorder considered, suggesting that the transition point for this geometry will be apparent if higher disorder values are included. In the next section, we identify the regions of distinct behavior of  $R$  using hierarchical clustering.

## 4.4 Cluster Analysis

Since every finite numerical simulation has limitations, a nonzero positive value for  $b$  is not the only criterion used in our analysis. Here, we claim the existence of extended states if, in addition to  $\lim_{n \rightarrow \infty} b > 0$ , the following two trends in the distance plots are observed: (1) consistency in the  $b$  values, and (2) consistency in the  $R$  values. For each geometry, we identify the region where extended states exist using hierarchical clustering of the values of  $b$  and  $R$  together with the corresponding error estimates (from Table 4.2). The clustering algorithm uses a Euclidean metric and Ward's minimum variance method.

The results for each geometry are represented by the dendrograms in Fig. 4.5. Dendrograms can be interpreted in two distinct ways: in terms of large-scale groups and in terms of variation among individual branches. The plots in Fig. 4.5 show the existence of two large-scale clusters for both  $b$  and  $R$  in each geometry case, which indicates that all examined 2D lattices experience a transition from one transport

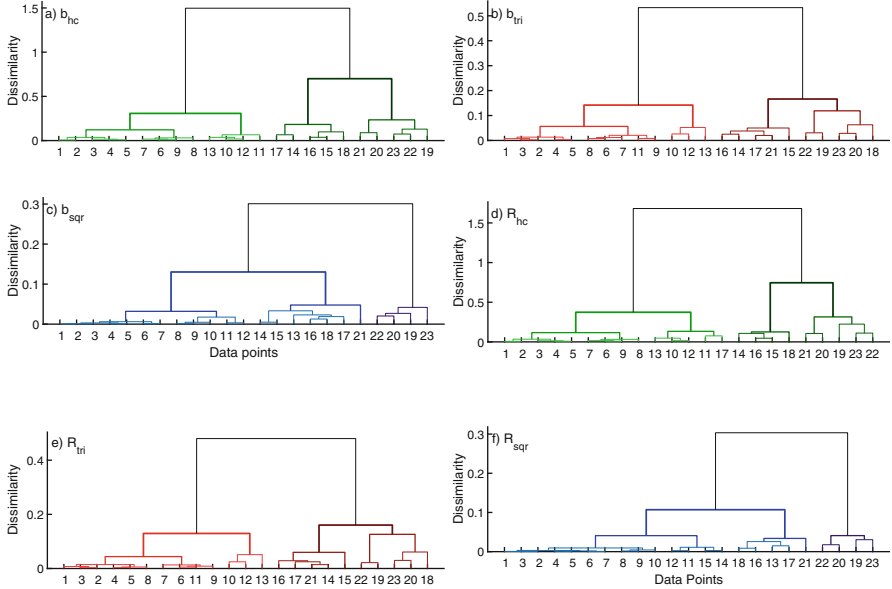


**Fig. 4.5** Dendrograms for the  $b$  and  $R$  values in the honeycomb, triangular, and square lattices. Each ordinal number on the horizontal axis corresponds to a given level of disorder, i.e.  $1 = 0.10$ ,  $2 = 0.15$ , etc. The height of each branch point (or clade) on the vertical axis represents the dissimilarity between clusters connected by that point. The dissimilarity criterion in Ward's method is the total within-cluster error sum of squares, which increases as we move up the tree (reprinted with permission)

regime to another as disorder increases. The left cluster in each dendrogram for  $b$  (Fig. 4.5a–c) groups together limiting distance values that exhibit small variation with increasing disorder and therefore correspond to the regime where extended states exist. The right clusters mark the formation of a second group of  $b$  values which exhibit distinctly different behavior from the first one. Data points within the second cluster correspond to values of disorder which trigger the onset of a phase transition towards different transport behavior. The dendrograms for  $R$  (Fig. 4.5c, d, e) confirm the trends established for the  $b$  values.

Comparison between Fig. 4.5a and Fig. 4.5b indicates key similarities between the triangular and the hexagonal lattices. In both cases, the left cluster includes all points in the range 1–13 (corresponding to  $0.10 \leq W \leq 0.70$ ) and the first point included in the right cluster is point 14 ( $W = 0.75$ ). In addition, each main cluster of both lattices has two sub-clusters, which group together similar disorder values. Thus, we conclude that in the honeycomb and triangular cases, extended states exist for  $W \leq 0.70$ . In contrast, the transition in the square lattice begins with point 19 ( $W = 1.00$ ), i.e. extended states in this geometry exist for  $W \leq 0.95$ . However,

since the right cluster in Fig. 4.5c consists of only four points, more data should be generated to confirm the transition point of the square lattice. In our previous work [6] (discussed in Chap. 3), we showed delocalization for  $W \leq 0.60$  in the square lattice. This result was obtained with a less robust method for data fit. The weaker method was compensated for by including a worst-case analysis argument. Altogether, this resulted in less resolution for the value of critical disorder. Here, we have improved on this result by generating more data and refining the fitting criteria.

It is interesting to note that for the honeycomb lattice there is an obvious dissimilarity between the two transport regimes (represented by the difference in cluster heights), which suggests an abrupt phase transition. In contrast, for the triangular case the heights of the two clusters are similar and for the square case, the right cluster is slightly lower than the left one. This indicates a more gradual transition in those two geometries. Such trends in the dendrograms suggest that the “sharpness” of the transition between transport regimes is affected by the number of nearest neighbors, which varies in each geometry.

A limitation of the current analysis is the number of realizations generated and averaged for each disorder value. Based on our previous work, we expect five realizations to be sufficient to identify the global regions of distinct transport behavior, i.e. to distinguish between localized and extended states. However, it is possible that occasionally, the randomly generated five realizations may not be ‘representative’ of the true behavior of the corresponding distance value. From both Table 4.1 and Fig. 4.5 we see that in the square lattice,  $W = 1.10$  (point 21) fall in the left cluster even though it is expected to appear in the right one. We assume that these ‘outliers’ result from the small number of realizations and do not affect significantly the group behavior of the clusters. Notice that the spectral method was inconclusive for those values since they are considered to lie past the transition points for that geometry.

## 4.5 Comparison Between the Honeycomb and the Triangular Lattices

In Sect. 4.3 we demonstrated that the honeycomb and triangular lattices experience onset of a phase transition for similar amounts of disorder. This phenomenon arises due to planar duality between the two geometries. Let  $\Lambda$  be a planar honeycomb graph in 2D space. The planar dual  $\Lambda^*$  of the honeycomb lattice is the graph constructed by placing a vertex at the center of every face of  $\Lambda$ . Connecting only pairs of vertices corresponding to adjacent faces shows that the dual of the honeycomb lattice is the triangular lattice (Fig. 4.6a).

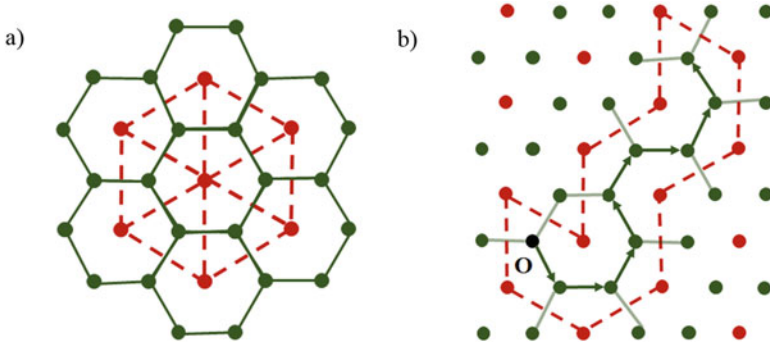


**Fig. 4.6** (a) The triangular lattice can be constructed as a dual of the honeycomb lattice. (b) If a finite open path in the honeycomb lattice (indicated by arrows) contains the origin  $O$ , then there exists a closed loop of closed edges (dashed lines) that also contains the origin. Here the lighter lines between points represent closed edges where transitions are not allowed (reprinted with permission)

In the Anderson localization problem, one can reflect the amount of disorder by either varying the on-site energies while keeping the hopping integral constant, or by fixing the on-site energies and allowing the hopping potential to vary. In a topological representation of a lattice, the lattice sites correspond to vertices and the hopping integrals—to bonds (or edges). Since every edge of the honeycomb lattice is crossed by a unique edge of the triangular lattice, there is a one-to-one correspondence between the bonds of the two. Thus, if an edge in the real lattice is open (closed), then the dual edge that crosses it, can also be defined as open (closed). It is reasonable to expect that the resulting transport problem in dual space will produce similar results, up to a transformation. The precise transition points and local behavior of the honeycomb and the triangular lattice differ due to the different number of nearest neighbors. However, the behavior of the two lattices in the extended states regime should be highly similar based on the following argument.

Graphically, an extended state can be represented by a cluster of open paths connecting the origin to infinity, while a localized state corresponds to a finite cluster of open paths or a loop. Figure 4.6b shows a finite cluster of open paths (solid green arrows) starting from the origin  $O$ . The cluster is finite because it is surrounded by closed edges (light solid green lines), i.e. transitions that are not allowed. Each closed edge is crossed by a unique edge of the dual lattice (red dashed lines). It has been proven [7] that if a finite open cluster contains the origin, then the corresponding edges of the dual form a closed loop, which also contain the origin. Conversely, if a closed loop in the dual contains the origin, then the corresponding open cluster (containing the origin) is finite. Thus, the existence of an infinite path from the origin to infinity in the real lattice occurs when the closed loop of the dual lattice stretches to infinity. From this discussion, it is reasonable to conclude that the delocalization properties of a honeycomb lattice can be examined with the help of a system with triangular symmetry and vice versa.

## Bibliography

1. B.J. Last, D.J. Thouless, Evidence for power law localization in disordered systems. *J. Phys. C Solid State Phys.* **7**(4), 699 (1974)
2. J. Chabé, G. Lemarié, B. Grémaud, D. Delande, P. Szriftgiser, J.C. Garreau, Experimental observation of the Anderson metal-insulator transition with atomic matter waves. *Phys. Rev. Lett.* **101**(25), 255702 (2008)
3. P.T. Coleridge, R.L. Williams, Y. Feng, P. Zawadzki, Metal-insulator transition at  $B = 0$  in p-type SiGe. *Phys. Rev. B* **56**(20), R12764–R12767 (1997)
4. A. Punnoose, Metal-insulator transition in disordered two-dimensional electron systems. *Science* **310**(5746), 289–291 (2005)
5. W. King, R.C. Kirby, C. Liaw, Delocalization for the 3-D discrete random Schroedinger operator at weak disorder. *J. Phys. Math. Theor.* **47**(30), 305202 (2014)
6. E.G. Kostadinova, C.D. Liaw, L.S. Matthews, T.W. Hyde, Physical interpretation of the spectral approach to delocalization in infinite disordered systems. *Mater. Res. Express* **3**(12), 125904 (2016)
7. H. Kesten, Unsolved problems, in *Percolation theory for mathematicians*, (Birkhäuser, Boston, 1982), pp. 380–385

# Chapter 5

## Transport in the Two-Dimensional Honeycomb Lattice with Substitutional Disorder



According to the well-established scaling theory [1], in a 2D crystal (characterized by an Anderson-type Hamiltonian), all energy states are either exponentially or logarithmically localized for any nonzero amount of disorder, i.e. there is no real metal-to-insulator transition (MIT) in this case. Nevertheless, MIT has been experimentally observed for graphene sheets doped with  $\text{NO}_2$  [2], hydrogen [3], and boron [4]. It can be argued [5–7] that the “apparent” existence of extended states in doped graphene results from the long localization length of the material, which is often longer than the size of the experiment. Another explanation is that the finite-size scaling methods, which are often adopted in the analysis of 2D transport problems, impose restrictions on the Hilbert space that exclude information on the existence of some extended states.

The spectral approach used here has previously shown [8–10] that extended states exist in 2D systems, where the random variables (representing disorder) are chosen from a square probability distribution. This choice corresponds to the classical zero-temperature Anderson localization problem (first introduced in Anderson [11]). Here, we extend this study to the case of quantum percolation, which aim to model substitutional doping on the 2D honeycomb lattice. Our results confirm that the metal-to-insulator transition in this case should occur for doping  $\approx 0.3\%$ , which was experimentally observed in [3].

### 5.1 Discrete Percolation

Percolation theory is a simple (not exactly solved) probabilistic model for studying phase transitions in disordered media. Mathematically, it describes the behavior of connected clusters in a random topological space. Percolation was first introduced by Broadbent and Hammersley [12], who analyzed how the random properties of a porous medium influence the transport of a fluid moving through it. Since then, percolation theory has become a powerful tool in the study of conductivity in various

---

This chapter published as: E. G. Kostadinova, A. Cameron, F. Guyton, Liaw, C. D., Matthews, L. S., & Hyde, T. W. Transport in the two-dimensional lattice with substitutional disorder (submitted for review in *Phys. Rev. B*)

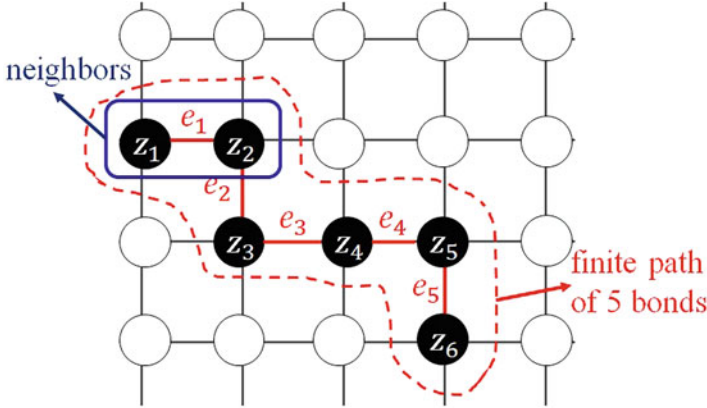


**Fig. 5.1** Visual representation of basic definitions in the discrete percolation problem on the 2D square lattice

materials. It has been shown [13, 14] that the Anderson localization belongs to the same universality class as the quantum percolation, which allows us to make parallels between the two problems.

The setup in the classical regime is as follows. Consider the  $d$ -dimensional integer lattice ( $d \geq 1$ ), which is the graph of the  $d$ -dimensional set of integers  $\mathbb{Z}^d$ . Each element of this lattice is a vertex and any two neighboring vertices are connected by a bond (or edge). A *path* is a finite or infinite alternating sequence  $(z_1, e_1, z_2, e_2, \dots)$  of vertices  $z_i$  and edges  $e_i$  such that  $z_i \neq z_j$  and  $e_i \neq e_j$  whenever  $i \neq j$  and such that  $e_i$  is the bond between the neighbors  $z_i$  and  $z_{i+1}$  for all  $i$ . The length of a path is the number of bonds it contains (Fig. 5.1).

In the site percolation problem, all bonds are considered open, while the vertices are, independently of each other, chosen to be open with probability  $p$  and closed with probability  $1 - p$ <sup>1</sup>. An open cluster is a set of open vertices. In the case of an infinite size lattice, one is interested in the probability that there exists an open cluster  $C(0)$  from the origin to infinity, i.e. the probability that the system percolates. The percolation probability (or percolation function)  $\theta(p)$  has limiting values  $\theta(p=0) = 0$  (all vertices closed) and  $\theta(p=1) = 1$  (all vertices open). Therefore, there exists a critical occupation probability  $p_c$  at which the system undergoes a phase transition. The precise value of  $p_c$  is dependent on the local structure of the graph (i.e. its geometry) and the type of problem considered (bond or site). However, the global behavior in the subcritical and supercritical phase is dependent only on the dimensionality of the system, which is called the *universality principle* in percolation [15].

In 2D, exact results have been obtained for the square lattice bond percolation [16] and for the triangular lattice site percolation [17]. Values of  $p_c$  for other 2D

<sup>1</sup>Alternatively, one can consider all vertices to be open and let the bonds be open or closed with a certain probability. This setup is called a *bond percolation* problem.

**Table 5.1** List of critical values  $p_c$  (and respective references) for various lattice dimensions and geometries. Here  $Z$  stands for number of nearest neighbors. Note that, in cases where  $p_c$  is obtained numerically (and not proven analytically), there may be multiple, slightly different results for the critical probabilities throughout the literature. Thus, the list of studies referenced here should not be considered exhaustive

Lattice type	$Z$	Site percolation	Bond percolation
1D	2	1	1
2D honeycomb	3	0.6962 [18]	0.6527 [19]
2D square	4	0.5927 [20]	0.5 [16]
2D triangular	6	0.5 [17]	0.3473 [19]
3D diamond	4	0.43 [21]	0.388 [22]
3D simple cubic	6	0.3116 [23]	0.2488 [24]
3D BCC	8	0.246 [25]	0.1803 [26]
3D FCC	12	0.198 [27]	0.120 [26]

geometries and higher dimensions have been obtained only numerically. Table 5.1 gives a summary of theoretical and numerical results in 1D, 2D, and 3D lattices of various geometry. Note that, in each case, the value of  $p_c$  decreases as the number of nearest neighbors  $Z$  increases, which is to be expected in the classical regime since a higher  $Z$  corresponds to more available paths. In the next section, we will see that this is not necessarily the case in the quantum regime, where quantum interference plays an important role. There are two important directions of study related to the critical phase: (1) investigate the properties of a system as  $p$  approaches  $p_c$  from above and below, and (2) study the effect of varying system parameters (such as dimension, size, and geometry) for a system at  $p = p_c$ .

It is expected [15] that around the critical point  $p = p_c$  many functions of interest exhibit power law behavior, whose critical exponents do not depend on the local properties of the lattice (by the universality principle). Thus, one can assume that a comparison of lattices with same dimension but different geometries will yield identical (or very close) critical exponents.

It is expected that in the critical phase, the probability of the existence of an open path from the origin to some distance  $r$  decreases polynomially as  $r^{-\alpha}$ . Smirnov et al. [28, 29] showed that the critical exponent for the site percolation problem on the square 2D lattice is given by  $\alpha = 5/48 \approx 0.104$ . By the universality principle, this result should hold for all other 2D lattices. However, this conjecture is not yet proven rigorously.

## 5.2 Formulation of the Transport Problem

Consider the 2D honeycomb lattice  $\Lambda$ , which is the graph  $G = (V, E)$  of the 2D set of vertices (or sites)  $V$  connected by edges (or bonds)  $E$ . Bonds represent the graph distance between pairs of nearest neighbors (vertices located at a Euclidean distance 1 apart from each other).

For the case examined here, one is interested in the critical amount of substitutional disorder (or doping) sufficient to induce a phase transition in the transport properties of the 2D honeycomb crystal. In the tight-binding approximation, the single-electron, noninteracting Hamiltonian on the 2D honeycomb lattice  $\Lambda$  has the form

$$H = \sum_{\substack{i,j \in \Lambda \\ i \neq j}} |i\rangle V_{ij} \langle j| + \sum_{i \in \Lambda} |i\rangle \epsilon_i \langle i|, \quad (5.1)$$

where  $|n\rangle$  are the standard basis vectors of the 2D space  $\Lambda$  and  $V_{ij}$  is the hopping potential between nearest neighbors. For any function of the vertices  $f: V \rightarrow R$  taking values in the 2D set of all integers  $\mathbb{Z}^2$ , the (discrete) Laplacian acting on  $f$  is given by

$$\Delta f = \sum_{e_{ij}=1} [f(v_i) - f(v_j)], \quad (5.2)$$

where  $e_{ij}$  is the edge between vertices  $v_i$  and  $v_j$  and the sum is over the nearest neighbors of vertex  $v_i$ . Thus, we see that the discrete Laplacian  $\Delta$  is the graph representation of the hopping potential term in Eq. (5.1).

The on-site energies  $\epsilon = \{\epsilon_i\}_{i \in \Lambda}$  form a set of independent variables chosen from an interval  $[a, b]$  according to a prescribed probability density distribution  $\chi(\epsilon)$ . The probability that  $\epsilon_i$  is selected from any subinterval  $[a', b'] \in [a, b]$  is given by the area under the curve between the points  $a'$  and  $b'$ , that is,

$$A = \int_{a'}^{b'} \chi(\epsilon) d\epsilon. \quad (5.3)$$

We assume that the on-site energies in the unperturbed crystal are zero and that the hopping potential is a constant (here  $V_{ij} = V = 1$ ). Then, assigning the variables  $\{\epsilon_i\}$  to the crystal sites corresponds to introducing impurities into the system. For this setup, the level of disorder can be varied by changing the width of the interval  $[a, b]$  or by altering the shape of  $\chi(\epsilon)$ . In the case, where there is only one atomic orbital per lattice site, the probability distribution of possible energy states in a single-species crystal at zero temperature can be represented by Gaussian function (Fig. 5.2a). In the presence of impurities, the shape of the distribution may change with the width of the peak broadening with increasing disorder.

In our previous work [8, 9], discussed in Chap. 3 and 4, we examined the Anderson localization problem, where the  $\{\epsilon_i\}$  are identically distributed in the interval of allowed energies (i.e. each value is equally probable to occur) using the square probability distribution

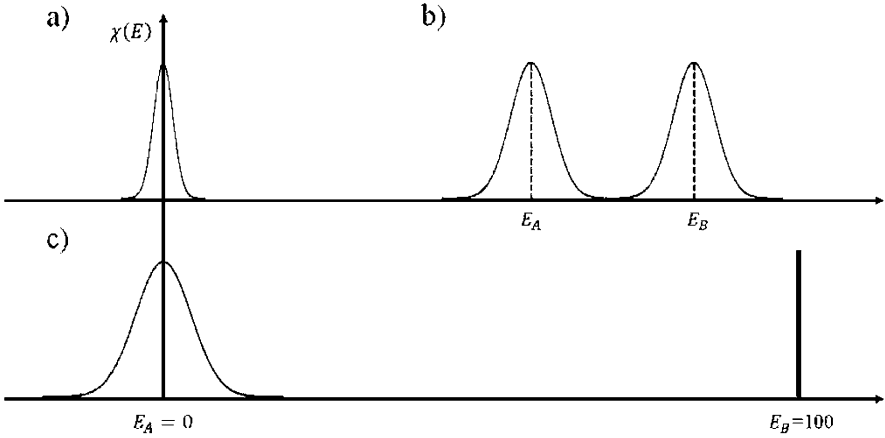


**Fig. 5.2** Graphs of a Gaussian distribution (a), bimodal distribution (b), and the modified bimodal distribution discussed in the text (c)

$$\chi(\epsilon) = \begin{cases} 0, & \epsilon \notin [a, b] \\ 1/W, & \epsilon \in [a, b] \end{cases} \quad (5.4)$$

In our numerical simulations, the area  $A$  defined in (5.3) is normalized to unity, i.e. every lattice site considered is assigned an energy value from the prescribed  $\chi(\epsilon)$ . Thus, for the distribution in (5.4), the level of disorder can be increased by increasing the width of the interval  $[a, b]$ , which is the common way to vary disorder in the Anderson localization problem. An important feature of this type of defect is randomness, such as random spacing of impurities or random arrangement of electronic/nuclear spins [11]. Although related, the Anderson-type defect is different from the substitutional disorder discussed here.

In the case of two-species mixtures, one can use the bimodal distribution (Fig. 5.2b), where the  $A$ -type atoms have a characteristic energy  $E_A$  (equal to the mean of the first peak) and  $B$ -type atoms have characteristic energy  $E_B$  (equal to the mean of the second peak). In the limit where  $E_B - E_A \rightarrow \infty$ , one atomic species acts like an open state, while the other atomic species acts like a perfect barrier. This scenario is modeled by the percolation problem.

### 5.2.1 Binary Alloy Model of Doping

Consider a 2D crystal composed of type  $A$  atoms with (most probable) energy  $E_A$  and type  $B$  atoms with (most probable) energy  $E_B$ , where  $E_A \neq E_B$ . The distribution of allowed energy states for such a system is a mixture of the form

$$\chi(\epsilon_i) = p\delta(\epsilon_i - E_A) + (1 - p)\delta(\epsilon_i - E_B), \quad (5.5)$$

where  $\delta(\epsilon_i - E_A)$  and  $\delta(\epsilon_i - E_B)$  are the unimodal probability distributions of the  $A$ -atoms and the  $B$ -atoms, respectively, and  $p$  is the mixing parameter. Here we consider a mixture of two Gaussian peaks

$$\delta(\epsilon_i - E_A) = \frac{1}{\sqrt{2\pi\sigma_1^2}} e^{-\left(\frac{\epsilon_i - E_A}{2\sigma_1^2}\right)^2} \quad (5.6a)$$

and

$$\delta(\epsilon_i - E_B) = \frac{1}{\sqrt{2\pi\sigma_2^2}} e^{-\left(\frac{\epsilon_i - E_B}{2\sigma_2^2}\right)^2}. \quad (5.6b)$$

In this case, the mixing parameter  $p$  corresponds to the concentration of  $A$ -atoms, while  $(1 - p)$  is the concentration of  $B$ -atoms. For appropriate choices of mixing parameter  $p$  and characteristic energies  $E_A$  and  $E_B$ , the binary alloy formulation can be used to represent a doped crystal with substitutional disorder. Assuming the same standard deviations  $\sigma_1 = \sigma_2 = \sigma$  for each distribution, one can vary both the width of the Gaussian peaks and the mixing parameter  $p$  until a critical behavior is observed.

## 5.2.2 Quantum Percolation Problem

As in the classical case, one can define a *quantum site percolation problem*. The key difference is that transport behavior in the quantum regime is influenced by scattering from defects and quantum interference, which can lead to localization of the quantum wave-particle even if all lattice sites are assumed open (in this limit, the quantum percolation becomes equivalent to the Anderson localization problem). Thus, transport in the quantum site percolation problem depends on two parameters: the concentration of open sites and the amount of lattice disorder.

The probability distribution for the quantum site-percolation problem can be obtained from Eq. (5.5) in the limit  $E_B \rightarrow \infty$  [30, 31], which gives a single Gaussian distribution function

$$\chi(\epsilon_i) = p\delta(\epsilon_i) = p \frac{1}{\sqrt{2\pi\sigma_1^2}} e^{-\left(\frac{\epsilon_i - E_A}{2\sigma_1^2}\right)^2}. \quad (5.7)$$

Without loss of generality, one can further choose  $E_A = 0$ , which centers the peak at the origin. In this formulation of the problem, the  $A$ -type atoms are open (or perfect acceptors), while the  $B$ -type atoms are closed (perfect barriers). Thus,

the electron moves only on a random assembly of  $A$ -atoms and the existence of extended or localized states is dependent on the variation of the concentration parameter  $p$ .

However, in a quantum mechanical system, there is a finite probability for tunneling to each lattice site and one cannot assume the existence of perfect barriers. Instead, the characteristic energy  $E_B$  should be represented by a high (but still finite) number. It is known [32] that when  $E_B - E_A > 2ZV$  (where  $Z$  is the number of nearest neighbors and  $V$  is the hopping potential), the spectrum of the Hamiltonian given in (5.1) splits into two sub-bands centered approximately around  $E_A$  and  $E_B$ . For the 2D honeycomb lattice used in our simulations, we let  $Z = 3$  and  $V = 1$ . Thus, a choice of  $E_B - E_A = 100$  ensures that the two bands are separate and far apart from one another, yet a finite distance away. In other words, lattice sites with energy  $E_B$  are unfavorable to occupy but do not represent forbidden states.

### 5.2.3 Relation Between Quantum Percolation and Anderson Localization

Let the critical probability in the percolation problem be denoted  $p_c$  in the classical regime and  $p_q$  in the quantum regime. Unlike the classical percolation problem, the quantum case accounts for the effect of quantum interference. As the particle passes along different routes in the disordered medium, it accumulates different phases. Interference of such phases can stop diffusion of the particle's wave function to a halt. It has been shown [13, 14] that the quantum percolation and the Anderson localization models belong to the same universality class of transport problems. In the subcritical phase of the quantum percolation problem (i.e.  $p < p_q$ ), it is known that  $\theta(p) = 0$  and  $C(0)$  is finite with probability 1. This corresponds to exponential localization with a localization length proportional to the size of the finite cluster. In the supercritical phase (i.e.  $p > p_q$ ),  $\theta(p) > 0$  and there is a nonzero probability that  $C(0)$  is infinite, which implies the existence of transport. Around the critical point  $p = p_c$  many functions of interest exhibit power law behavior, which is also characteristic for the transition region in the Anderson model. Although the correspondence between the critical amount of disorder  $W_c$  in the Anderson localization and the critical probability value  $p_q$  in the quantum percolation is not trivial, it can be expected that one is a function of the other (due to the equivalency of the two transport problems). Thus, it is not surprising that the question of whether a 2D system can percolate for  $p_q < 1$  has caused a decades-long debate closely related to the disagreement on the existence of extended states for nonzero disorder in the 2D Anderson problem.

For a 2D lattice of any geometry, it has been shown [14, 31, 33, 34] that the graph of  $\theta(p)$  is flat in the subcritical phase and at the critical point, i.e. for  $p \leq p_q$ . It is also expected that the phase transition from a finite to infinite cluster size in 2D has no jump discontinuities, although the shape of the graph of  $\theta(p)$  in the region  $p_q < p < 1$

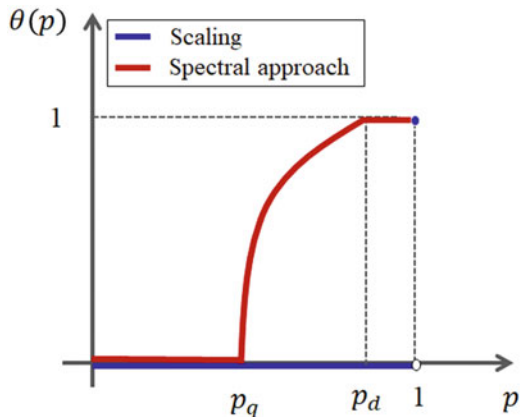
is still conjectural. The main source of disagreement is the exact value of  $p_q$ . Earlier numerical studies [34–36] based on finite-size scaling predicted that in the 2D scenario, the system can percolate only if all states are open, i.e. at  $p_q = 1$ . Later it was suggested [31] that percolation occurs for  $p < 1$  but only at energies sufficiently far away from the band center ( $E = 0$ ). Although the states near the center of the band were characterized by weaker than power-law localization, no clear evidence for crossover to percolation was established. Theoretical support for these results came from the scaling theory of localization [1]. Another part of the physics community argued that the 2D lattice can percolate for  $p_q < 1$  at all energies [37–40]. Nevertheless, different values of the critical  $p_q$  were obtained using different techniques. Table 5.2 presents a variety of  $p_q$  values obtained for the square lattice, which is the most studied two-dimensional geometry. In the honeycomb case examined here, most robust results are calculated for the classical percolation problem. In the quantum regime, it was suggested that the value of the percolation threshold varies with system size [45].

The primary question is whether there exists a value of  $p_q < 1$  that yields a nonzero probability function  $\theta(p)$ . If one shows that  $p_q = 1$ , the graph of  $\theta(p)$  becomes a flat line with a jump discontinuity at the critical point (as shown by the blue line in Fig. 5.3). In contrast, for the case where  $p_q < 1$ , one needs to further

**Table 5.2** List of various results for the critical probability value  $p_q$  in the 2D quantum site percolation problem on the square lattice

Authors	Method	$p_q$
Odagaki et al. [41]	Green’s function method	0.59
Koslowski and von Niessen [42]	Thouless-Edwards-Licciardello method	0.70
Srivastava and Chaturvedi [40]	Method of equations of motion	0.73
Daboul et al. [39]	Series expansion methods	0.74
Odagaki and Chang [43]	Real-space renormalization group method	0.87
Raghavan [44]	Mapping a 2D system into a one-dimensional system	0.95

**Fig. 5.3** The graph of  $\theta(p)$  vs.  $p$  according to scaling theory (blue line) and according to the spectral approach (red line). Note that below the critical point  $p_q$ , the function  $\theta(p) = 0$ , while above the critical point  $p_d$ , the function  $\theta(p) = 1$ . The shape of the graph in the transition region  $p_q < p < p_d$  is still conjectural



investigate the shape of the graph in the supercritical regime. Numerical studies yielding  $p_q < 1$  often do not provide rigorous predictions regarding the shape of the graph in the transition region, which makes them hard to apply to physical systems. Note that the existence of  $p_q < 1$  does not imply transport with probability 1; rather it suggests that in the interval  $p_q < p < 1$ , the function  $\theta(p)$  is increasing (probably) continuously from  $\theta(p_q) = 0$  to  $\theta(p) = 1$ . Thus, one cannot conclude with high certainty that the 2D system truly percolates in the supercritical regime.

The application of the spectral approach to the 2D quantum percolation problem provides an important improvement on this issue. In our previous work [8–10], we have shown the existence of extended states in a 2D infinite lattice with nonzero Anderson-type disorder. Similarly, the work presented in this chapter indicates that a 2D quantum system percolates for  $p_q < 1$ . However, unlike most methods previously mentioned, the spectral approach is designed to show the existence of extended states (or percolation) with probability 1. In other words, it identifies the critical value of  $p$  above which  $\theta(p) = 1$  (where the graph becomes a flat line). We call this value  $p_d$ , where  $d$  stands for delocalization. Note that  $p_q$  and  $p_d$  do not necessarily coincide as illustrated by the red line in Fig. 5.3.

### 5.3 Distribution of Variables

As mentioned in the previous sections, we applied the spectral method to the Hamiltonian in Eq. (5.1). In all simulations presented here, we assume  $\Delta = ZV$  (i.e. constant hopping potential over the nearest neighbors) and let  $\{\delta_i\}_{i \in \Lambda}$  be the standard basis vectors of the honeycomb lattice.<sup>2</sup> With this assumption, we recover the discrete random Schrödinger operator in Eq. (1.3), which is repeated below for convenience

$$H_\epsilon = -ZV + \sum_{i \in \Lambda} \epsilon_i \delta_i \langle \delta_i |. \quad (5.8)$$

The numerical analysis starts by generating one realization of the random variables  $\epsilon_i$  according to the prescribed probability distribution  $\chi(\epsilon)$ . Next, we fix a random base vector  $\delta_0$  and generate the sequence  $\{\delta_0, H\delta_0, H^2\delta_0, \dots, H^n\delta_0\}$ , where  $n = 4500$  corresponds to the number of iterations of the Hamiltonian and is used as a timestep. Then the sequence is orthogonalized and the distance value  $D$  at each timestep  $n$  is obtained using the distance formula (given by Eq. (3.12) in Chap. 3). Finally, we analyze the graph of  $D$  vs.  $n$  to determine the limiting behavior of  $D$  as  $n \rightarrow \infty$ .

---

<sup>2</sup>Note that the spectral approach only requires that  $v_0$  and  $v_1$  are any two (different) vectors in the Hilbert space of interest. The choice  $v_0 = \delta_0$  and  $v_1 = \delta_1$  ensures faster computation times and is not related to the generality of the spectral method.

The use of the modified bimodal distribution allows for introduction of two distinct types of defects: positional and substitutional. The positional disorder is controlled by the values of the mean energy  $E_B$  and the variance  $\sigma^2$  of the Gaussian peak, while doping is achieved by variation of the concentration<sup>3</sup>  $n_D$  of  $B$ -type lattice sites of energy  $E_B$ . In this section, we motivate the choice of  $E_B$ ,  $\sigma^2$ , and  $n_D$  for the present simulations. First, we perform a spectral analysis of the honeycomb lattice where the on-site energies are assigned from a single Gaussian peak with fixed variance but changing mean energy  $E_A$ . Then, we center the Gaussian peak at  $E_A = 0$  and alter its variance. Finally, for a given Gaussian distribution, we vary the concentration of lattice sites with energy  $E_B$ .

In this work, we model substitutional disorder using a modified bimodal distribution, in which one peak is a Gaussian centered at  $E_A = 0$  and the other peak is (approximately) a delta function located at  $E_B = 100$ . Here the delta function represents the dopant atoms characterized by a substantially higher average energy  $E_B$ . Since the introduction of substitutional disorder in a material is usually a controlled process, we do not consider a spread of possible energies for the  $B$ -type atoms. In other words, the defect is produced by a careful substitution of an  $A$ -type atom with a  $B$ -type atom, whose energy is controlled.

In Sect. 5.2, we argued that the chosen energy difference  $E_B - E_A = 100$  is sufficient to represent a quantum percolation problem, where the  $B$ -type atoms are unfavorable but not forbidden lattice sites. To ensure that the choice  $E_A = 0$  is appropriate, we applied the spectral approach to a normal distribution (single Gaussian peak) of fixed variance  $\sigma^2 = 0.4$  with mean values changing in the range  $E_A = 0 : 10 : 100$ . Figure 5.4 shows representative  $D_{hc}$ -value<sup>4</sup> plots for simulations with  $E_A = 0 : 20 : 100$ .

We see that for a fixed variance, the limiting behavior of  $D_{hc}$  does not change appreciably as one increases the mean value for the normal distribution. Specifically, even for the two extremes of the examined interval ( $E_A = 0$  and  $E_A = 100$ , marked in Fig. 5.4 with a solid red and black dotted line, respectively), the behavior of the distance parameters follows a very similar trend. This indicates that the spectral analysis is not affected by a change of the mean in the normal distribution. Thus, we conclude that, without loss of generality, the Gaussian peak in the modified bimodal distribution can be centered at  $E_A = 0$ . This approach is in agreement with other numerical simulations [30, 31], where a Gaussian distribution was used to model quantum percolation. This also makes sense in terms of probability theory, where the mean represents the most probable (or expected) value, which in this setup can be interpreted as the average ground state energy of the atoms in the unperturbed crystal.

To evaluate how changing the variance  $\sigma^2$  influences the transport behavior of a system, we performed a spectral analysis of a system characterized by a Gaussian

<sup>3</sup>Here  $n_D$  stands for the concentration of the  $B$ -type doping material and is equal to the probability for a closed state  $1 - p$  in the quantum percolation problem.

<sup>4</sup>Here the subscript  $hc$  in  $D_{hc}$  stands for *honeycomb*.

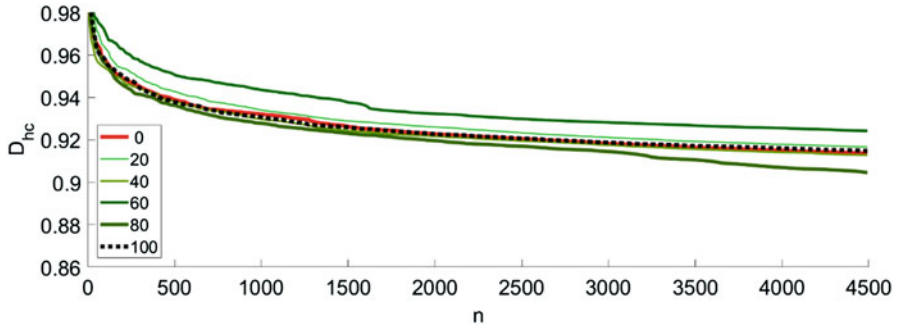


**Fig. 5.4** Distance time evolution plots for the Hamiltonian in Eq. (5.8), where the random variables are assigned according to a Gaussian distribution with fixed variance  $\sigma^2 = 0.04$  and changing mean values  $E_A$ . The  $D_{hc}$ -values for  $E_A = 0$  and  $E_A = 100$  are denoted in solid red and dotted black lines, respectively

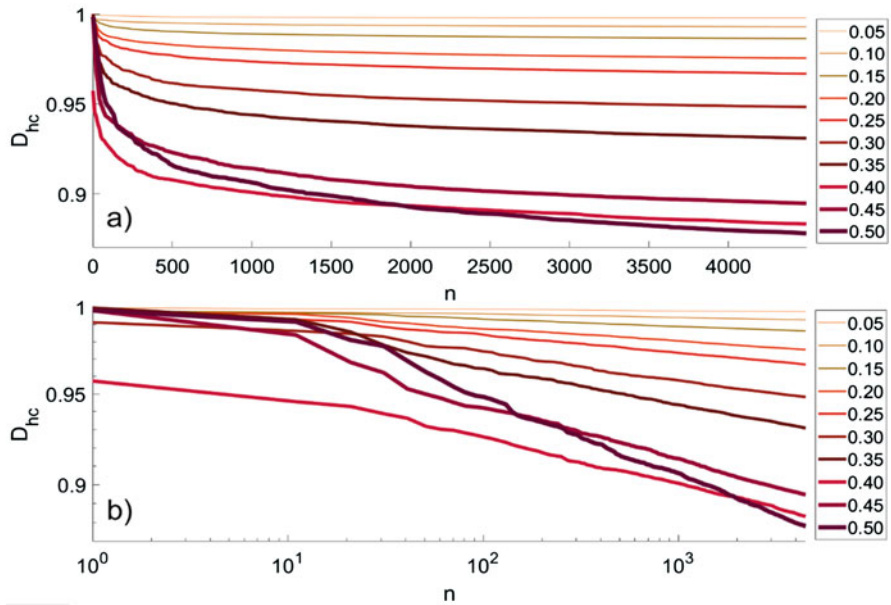


**Fig. 5.5** Distance time evolution plots (a) and the corresponding log-log plots (b) for the Hamiltonian in Eq. (5.8), where the random variables are assigned according to a Gaussian distribution with fixed mean  $E_A = 0$  and variance  $\sigma^2 = 0.05 : 0.05 : 0.50$

distribution with  $E_A = 0$  and  $\sigma^2 = 0.05:0.05:0.50$ . The distance plots in Fig. 5.5a show that for a fixed mean, as the variance increases, the slope of the  $D_{hc}$ -plots becomes increasingly negative. In the spectral approach, delocalization is established if  $D_{hc}$  approaches a nonzero positive value as  $n \rightarrow \infty$ . Thus, as the slope of the  $D_{hc}$ -plots

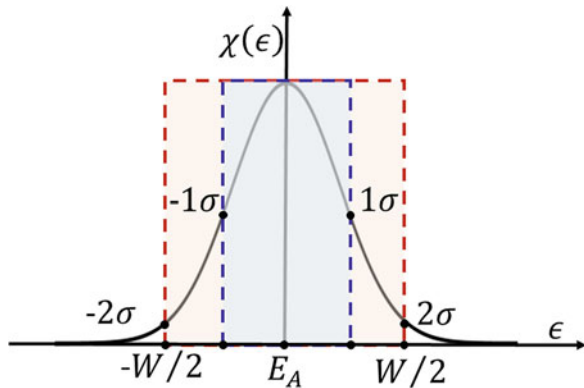
increases, the probability that  $D_{hc}(\infty) > 0$  decreases. Since the numerical simulations are finite ( $n = 4500$ ), the existence of extended states is most probable if a given plot decays exponentially.

In Fig. 5.5b, we see that for  $\sigma^2 \leq 0.15$  the log-log  $D_{hc}$ -plots are straight lines with almost no slope, which indicates exponential decay, while for  $\sigma^2 > 0.15$ , the negative slope of the lines monotonically increases with increasing  $\sigma^2$ . We can conclude that for a Gaussian distribution with a fixed mean  $E_A = 0$ , changes in the variance significantly affect the behavior of the distance parameter.

This is to be expected since, physically, the variance quantifies the deviation from the mean and can be interpreted as a type of disorder in the system. Note, however, that in this case, the spread of the Gaussian function represents a defect characteristic of the un-doped crystal and is thus related to the Anderson-type disorder. Although the focus of this work is substitutional defect, a realistic model of disorder in the crystal needs to account for lattice imperfections in the unperturbed crystal. Thus, it is useful to assume a value for  $\sigma^2$  that contributes to the total effect of impurities but does not dominate it. Since the normal distribution models a type of defect, which is similar to the Anderson-type disorder, we can get an estimate for the appropriate value of  $\sigma^2$  through a comparison with our previous study [9], where we have established that for the 2D honeycomb lattice with Anderson-type disorder (i.e. square distribution), extended states exist for  $W \leq 0.75$ .

An approximate relationship between the width of the square distribution  $W$  and the variance of the normal distribution  $\sigma^2$  is presented in Fig. 5.6. Since  $\approx 95\%$  of the normal distribution area falls within distance  $2\sigma$  from the mean, one can approximate the Gaussian by a square distribution with width  $W = 4\sigma$  (light pink square in Fig. 5.6) or  $W^2 = 16\sigma^2$ . Therefore, the critical value  $W \leq 0.75$  approximately corresponds to  $\sigma^2 \leq 0.035$ . The same calculation, performed with a square of width  $2\sigma$  (light blue square in Fig. 5.7) yields  $\sigma^2 \leq 0.14$ . Clearly, the pink square overestimates and the blue square underestimates the actual area of the Gaussian. Thus, it is appropriate to choose the variance from the range  $0.035 < \sigma^2 < 0.14$ . In the next section we choose  $E_A = 0$  and  $\sigma^2 = 0.05$  for the Gaussian peak of the modified bimodal distribution.

**Fig. 5.6** Visual representation of the connection between  $W$  of the square distribution and  $\sigma$  of the Gaussian distributions



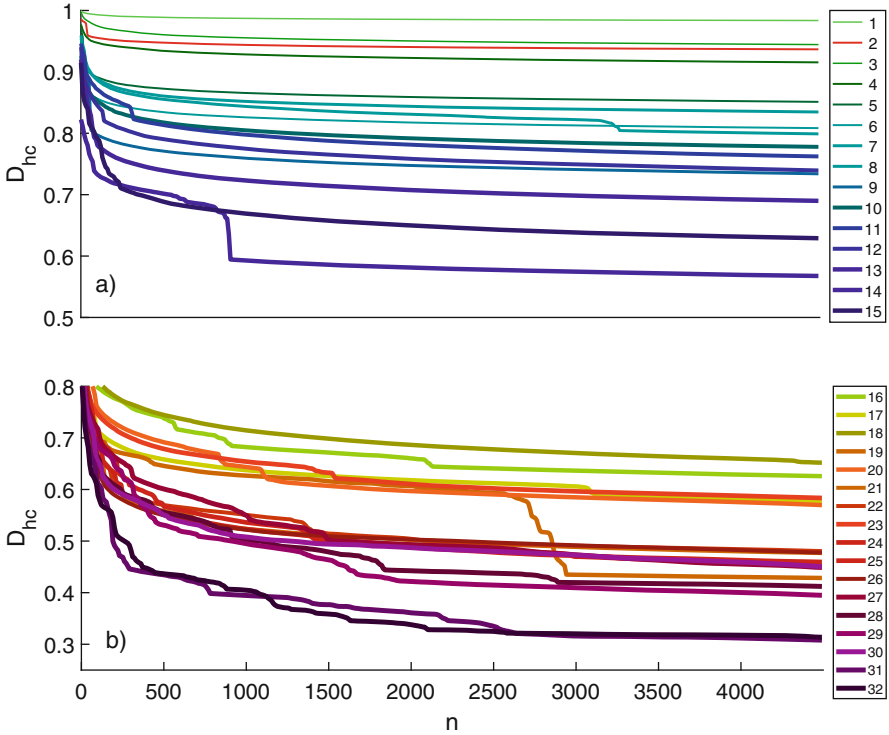


**Fig. 5.7** Distance time evolution plots for doping in the range  $n_D(\%) = 1 : 1 : 15$  (a) and  $n_D(\%) = 1 : 1 : 32$  (b)

## 5.4 2D Honeycomb Lattice with Substitutional Disorder

Consider the modified bimodal distribution consisting of a Gaussian peak (with mean  $E_A = 0$  and variance  $\sigma^2 = 0.05$ ) and a delta function at  $E_B = 100$ . Define  $n_G = p$  as the concentration of lattice sites with energy  $\epsilon_i$  selected from the Gaussian peak and  $n_D = 1 - p$  as the concentration of lattice sites with energy  $E_B = 100$ . In each numerical simulation, we first assigned all lattice sites energies from the normal distribution, which models a single-species crystal with small lattice imperfections (represented by the width of the Gaussian peak). Then, we simulate substitutional disorder by (randomly) assigning the energy  $E_B$  to a fraction of the lattice sites determined by the value  $n_D$ . In this study, the examined concentration of doping varied from  $n_D = 0$  to  $n_D = 32\%$ . To minimize numerical error, for each  $n_D$ , we generated 30 realizations of the on-site energies and averaged the resulting distance values. Figure 5.7 provides the time evolution plots of the (averaged)  $D_{hc}$  values in the range  $n_D(\%) = 1 : 1 : 32$ . As the amount of disorder increases, data fluctuations become prominent even for values of the disorder as small as 2% (bright red line on

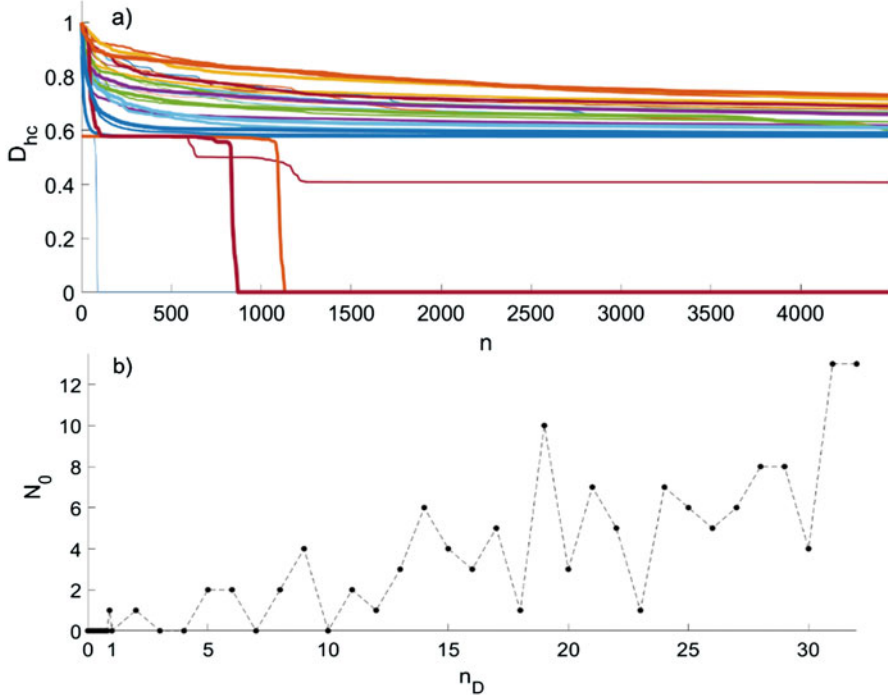


**Fig. 5.8** (a) Distance time evolution plots of the 30 realizations for the case  $n_D = 2\%$ . (b) Number of realizations that dropped to zero for each examined doping value

Fig. 5.7a). The sudden drops observed in the time evolution of some  $D_{hc}$  values indicate that the 30 realizations for the corresponding  $n_D$  varied significantly in their limiting behavior.

An increasing dissimilarity among the various realizations for a given  $n_D$  is proportional to an increasing uncertainty in the existence of extended states. The plot of the 30 realizations for  $n_D = 2\%$  (Fig. 5.8a) shows that several  $D_{hc}$  values drop rapidly to zero, in which case the spectral approach cannot establish the existence of extended states with probability 1. In Fig. 5.8b, we see that the number of realizations that drop to zero  $N_0$  increases with increasing doping value. As the plot of  $n_D$  vs.  $N_0$  indicates that no realizations for  $n_D(\%) = 0 : 0.1 : 0.8$  fall to zero, we expect that this is the appropriate range of doping where the spectral approach can establish delocalization with probability 1.

Note that, even for the cases where all realizations of a given  $n_D$  have a positive value at the last timestep of the simulation, i.e.  $D_{hc}(4500) > 0$ , we still need to extrapolate the limiting behavior of the distance parameter as  $n \rightarrow \infty$  to prove that extended states exist. To determine the limiting values of  $D_{hc}$  at infinity, we fit the data using the equation

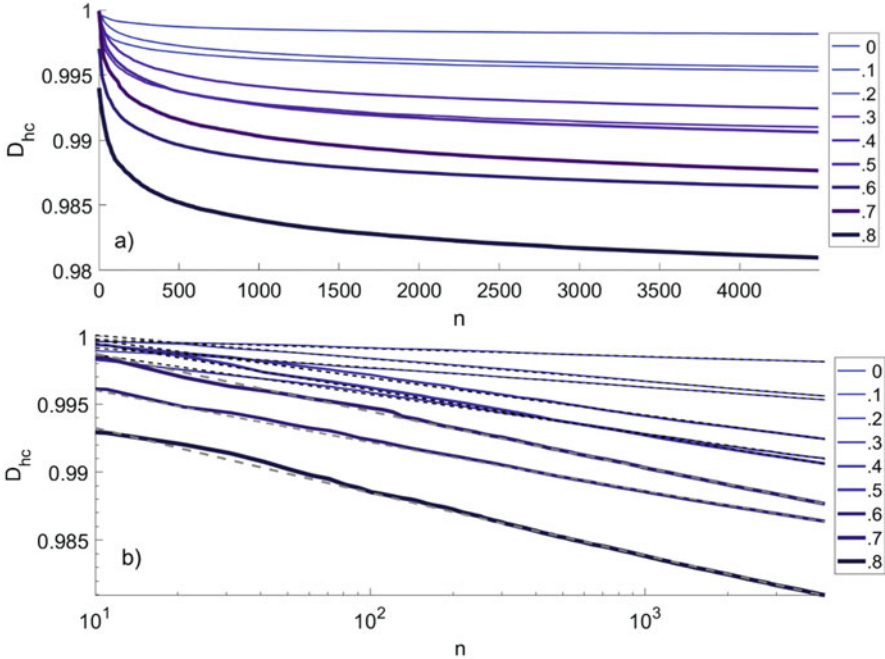
$$D_{hc} = mn^{-\alpha} + b, \quad (5.9)$$

where the first term shows how rapidly  $D_{hc}$  approaches a limiting value  $b$  as  $n \rightarrow \infty$ . Since all plots exhibit small fluctuations in the first thousand timesteps, we applied a nonlinear regression model to Eq. (5.9) using a weight function of the form  $w = 1/\sqrt{4500 - n}$ . In this way, the initial data fluctuations are minimized and the fitting results reflect more accurately the plots' behavior at large values of  $n$ .

In Fig. 5.9a, we show the distance plots and the corresponding log-log plots for the 2D honeycomb lattice with doping  $n_D(\%) = 0 : 0.1 : 0.8$ . As expected, the  $D_{hc}$  plots acquire greater negative slopes as the concentration of  $B$ -type atoms increases. For each doping concentration, we performed individual regression analysis to each of the 30 realizations. To evaluate the contribution of the exponential term in Eq. (5.9), we define the parameter

$$R = \frac{D_{hc}(4500) - b}{D_{hc}(4500)}, \quad (5.10)$$

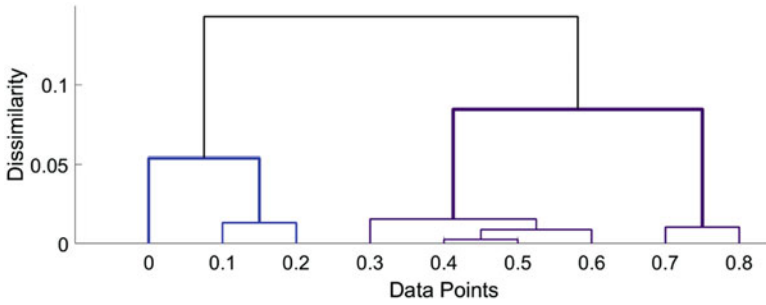
where  $D_{hc}(4500)$  is the distance value at  $n = 4500$ . The averaged values  $b$  and  $R$  are given in Table 5.3. The provided error estimate is the standard deviation from the



**Fig. 5.9** Distance time evolution plots (a) and the corresponding log-log plots (b) for the 2D honeycomb lattice with substitutional disorder in the range  $n_D(\%) = 0 : 0.1 : 0.8$ . The data shown is the average of 30 realizations for each value of  $n_D$

**Table 5.3** Equation parameters yielding best fits for various doping concentrations. The shaded area highlights the parameters for the critical value  $n_D = 0.3\%$ 

$n_D(\%)$	$b(\times 10^{-3})$	$R(\%)$
0	$985 \pm 9$	$1 \pm 1$
0.1	$955 \pm 74$	$4 \pm 7$
0.2	$944 \pm 22$	$5 \pm 2$
0.3	$921 \pm 103$	$7 \pm 10$
0.4	$926 \pm 37$	$7 \pm 4$
0.5	$918 \pm 61$	$7 \pm 6$
0.6	$914 \pm 57$	$7 \pm 6$
0.7	$881 \pm 66$	$11 \pm 7$
0.8	$881 \pm 78$	$10 \pm 8$

**Fig. 5.10** Dendrograms for the averaged values of  $b$ ,  $D(4500)$ , and  $R$  for doping in the range  $n_D(\%) = 0 : 0.1 : 0.8$ . The transition point between the two clusters is  $n_D = 0.3\%$ , in agreement with experimental results

mean in each group of 30 realizations. For all considered cases the root mean squared error from the fit equation was  $\sim 10^{-5}$  and the R-squared value was  $\approx 97\%$ , which indicates a good agreement with the weighted regression model. The nonlinear fits for each doping concentration are represented by black dashed lines in Fig. 5.9b. Table 5.3 shows that as doping concentration increases, the values of  $b$  decrease and the  $R$  contribution becomes more significant. For  $n_D = 0.3$  (shaded area in Table 5.3), the standard deviation from the mean increases about five times for both  $b$  and  $R$ , which suggests a transition in the behavior of the  $D_{hc}$  plots.

To confirm the existence of a transition point in the range  $n_D(\%) = 0 : 0.1 : 0.8$ , we study the dissimilarity among the averaged  $b$  and  $R$  values using a hierarchical clustering algorithm based on Ward's minimum variance method. The dendrogram in Fig. 5.10 shows the existence of two distinct clusters, corresponding to two different regimes in the limiting behavior of the distance plots. As expected, the transition between the two clusters occurs as one increases the doping from  $n_D = 0.2\%$  to  $n_D = 0.3\%$ . Thus, we conclude that  $n_D = 0.3\%$  is the critical

concentration of doping for which the spectral approach can no longer establish the existence of delocalization with probability 1. This agrees with the experiment by Bostwick et al. [3], who studied graphene samples doped with hydrogen.

## Bibliography

1. E. Abrahams, P. Anderson, D. Licciardello, T. Ramakrishnan, Scaling theory of localization. *Phys. Rev. Lett.* **42**(10) (1979)
2. S.Y. Zhou, D.A. Siegel, A.V. Fedorov, A. Lanzara, Metal to insulator transition in epitaxial graphene induced by molecular doping. *Phys. Rev. Lett.* **101**(8), 086402 (2008)
3. A. Bostwick et al., Quasiparticle transformation during a metal-insulator transition in graphene. *Phys. Rev. Lett.* **103**(5), 056404 (2009)
4. S. Agnoli, M. Favaro, Doping graphene with boron: a review of synthesis methods, physico-chemical characterization, and emerging applications. *J. Mater. Chem. A* **4**(14), 5002–5025 (2016)
5. I. Amanatidis, S.N. Evangelou, Quantum chaos in weakly disordered graphene. *Phys. Rev. B* **79**(20), 205420 (2009)
6. J.E. Barrios-Vargas, G.G. Naumis, Critical wavefunctions in disordered graphene. *J. Phys. Condens. Matter* **24**(25), 255305 (2012)
7. E. Amanatidis, I. Klefogiannis, D.E. Katsanos, S.N. Evangelou, Critical level statistics for weakly disordered graphene. *J. Phys. Condens. Matter* **26**(15), 155601 (2014)
8. E.G. Kostadinova, C.D. Liaw, L.S. Matthews, T.W. Hyde, Physical interpretation of the spectral approach to delocalization in infinite disordered systems. *Mater. Res. Express* **3**(12), 125904 (2016)
9. E.G. Kostadinova et al., Delocalization in infinite disordered 2D lattices of different geometry. *Phys. Rev. B* **96**, 235408 (2017)
10. C. Liaw, Approach to the extended states conjecture. *J. Stat. Phys.* **153**(6), 1022–1038 (2013)
11. P.W. Anderson, Absence of diffusion in certain random lattices. *Phys. Rev.* **109**(5), 1492 (1958)
12. S.R. Broadbent, J.M. Hammersley, Percolation processes: I. Crystals and mazes. *Math. Proc. Camb. Philos. Soc.* **53**(3), 629–641 (1957)
13. A. Mookerjee, T. Saha-Dasgupta, I. Dasgupta, Quantum transmittance through random media, in *Quantum and semi-classical percolation and breakdown in disordered solids*, ed. by B. K. Chakrabarti, K. K. Bardhan, A. K. Sen (Eds), (Springer, Berlin/Heidelberg, 2009), pp. 1–25
14. Y. Meir, A. Aharony, A.B. Harris, Delocalization transition in two-dimensional quantum percolation. *EPL Europhys. Lett.* **10**(3), 275 (1989)
15. G. Grimmett, Percolation and disordered systems, in *Lectures on probability theory and statistics*, ed. by P. Bernard (Ed), (Springer, Berlin/Heidelberg, 1997), pp. 153–300
16. H. Kesten, The critical probability of bond percolation on the square lattice equals 1/2. *Commun. Math. Phys.* **74**(1), 41–59 (1980)
17. J.C. Wierman, M.J. Appel, Infinite AB percolation clusters exist on the triangular lattice. *J. Phys. Math. Gen.* **20**(9), 2533 (1987)
18. Z.V. Djordjevic, H.E. Stanley, A. Margolina, Site percolation threshold for honeycomb and square lattices. *J. Phys. Math. Gen.* **15**(8), L405 (1982)
19. M.F. Sykes, J.W. Essam, Exact critical percolation probabilities for site and bond problems in two dimensions. *J. Math. Phys.* **5**(8), 1117–1127 (1964)
20. J.L. Jacobsen, Critical points of Potts and O(N) models from eigenvalue identities in periodic Temperley–Lieb algebras. *J. Phys. Math. Theor.* **48**(45), 454003 (2015)
21. X. Xu, J. Wang, J.-P. Lv, Y. Deng, Simultaneous analysis of three-dimensional percolation models. *Front. Phys.* **9**(1), 113–119 (2014)

22. M.F. Sykes, J.W. Essam, Critical percolation probabilities by series methods. *Phys. Rev.* **133** (1A), A310–A315 (1964)
23. M. Acharyya, D. Stauffer, Effects of boundary conditions on the critical spanning probability. *Int. J. Mod. Phys. C* **09**(04), 643–647 (1998)
24. J. Wang, Z. Zhou, W. Zhang, T.M. Garoni, Y. Deng, Bond and site percolation in three dimensions. *Phys. Rev. E* **87**(5), 052107 (2013)
25. C.D. Lorenz, R.M. Ziff, Universality of the excess number of clusters and the crossing probability function in three-dimensional percolation. *J. Phys. Math. Gen.* **31**(40), 8147 (1998)
26. C.D. Lorenz, R.M. Ziff, Precise determination of the bond percolation thresholds and finite-size scaling corrections for the sc, fcc, and bcc lattices. *Phys. Rev. E* **57**(1), 230–236 (1998)
27. M.F. Sykes, D.S. Gaunt, J.W. Essam, The percolation probability for the site problem on the face-centred cubic lattice. *J. Phys. Math. Gen.* **9**(5), L43 (1976)
28. S. Smirnov, Critical percolation in the plane: conformal invariance, Cardy’s formula, scaling limits. *Comptes Rendus Académie Sci. Ser. Math.* **333**(3), 239–244 (2001)
29. S. Smirnov, W. Werner, Critical exponents for two-dimensional percolation. *Math. Res. Lett.* **8**, 729–744 (2001)
30. G. Schubert, H. Fehske, Dynamical aspects of two-dimensional quantum percolation. *Phys. Rev. B* **77**(24), 245130 (2008)
31. M.F. Islam, H. Nakanishi, Localization-delocalization transition in a two-dimensional quantum percolation model. *Phys. Rev. E* **77**(6), 061109 (2008)
32. S. Kirkpatrick, T.P. Eggarter, Localized states of a binary alloy. *Phys. Rev. B* **6**(10), 3598–3609 (1972)
33. Y. Shapir, A. Aharony, A.B. Harris, Localization and quantum percolation. *Phys. Rev. Lett.* **49** (7), 486–489 (1982)
34. C.M. Soukoulis, G.S. Grest, Localization in two-dimensional quantum percolation. *Phys. Rev. B* **44**(9), 4685–4688 (1991)
35. Y. Avishai, J.M. Luck, Quantum percolation and ballistic conductance on a lattice of wires. *Phys. Rev. B* **45**(3), 1074–1095 (1992)
36. A. Mookerjee, I. Dasgupta, T. Saha, Quantum percolation. *Int. J. Mod. Phys. B* **09**(23), 2989–3024 (1995)
37. H.N. Nazareno, P.E. de Brito, E.S. Rodrigues, Quantum percolation in a two-dimensional finite binary alloy: Interplay between the strength of disorder and alloy composition. *Phys. Rev. B* **66** (1), 012205 (2002)
38. A. Eilmes, R. A. Römer, M. Schreiber, Exponents of the localization lengths in the bipartite Anderson model with off-diagonal disorder. *Phys. B Condens. Matter* **296**(1–3), 46–51 (2001)
39. D. Daboul, I. Chang, A. Aharony, Series expansion study of quantum percolation on the square lattice. *Eur. Phys. J. B Condens. Matter Complex Syst.* **16**(2), 303–316 (2000)
40. V. Srivastava, M. Chaturvedi, New scaling results in quantum percolation. *Phys. Rev. B* **30**(4), 2238–2240 (1984)
41. T. Odagaki, N. Ogita, H. Matsuda, Quantal percolation problems. *J. Phys. C Solid State Phys.* **13**(2), 189 (1980)
42. T. Koslowski, W. von Niessen, Mobility edges for the quantum percolation problem in two and three dimensions. *Phys. Rev. B* **42**(16), 10342–10347 (1990)
43. T. Odagaki, K.C. Chang, Real-space renormalization-group analysis of quantum percolation. *Phys. Rev. B* **30**(3), 1612–1614 (1984)
44. R. Raghavan, Study of localization in site-dilute systems by tridiagonalization. *Phys. Rev. B* **29** (2), 748–754 (1984)
45. C.M. Chandrashekar, T. Busch, Quantum percolation and transition point of a directed discrete-time quantum walk. *Sci. Rep.* **4**, 6583 (2014)

# Chapter 6

## Transport in 2D Complex Plasma Crystals



### 6.1 Complex Plasma Preliminaries

Plasma is a state of matter consisting of charged and neutral particles which exhibit collective behavior.<sup>1</sup> Plasma in the form of ionized gas can be found in numerous astrophysical objects, including stellar interiors and atmospheres, gaseous nebulae, and protoplanetary discs. Examples of plasma in the Solar System are the Earth's ionosphere, the Van Allen radiation belts, and the solar wind. On Earth, artificially produced plasma has numerous technological applications such as neon lights, plasma televisions, rocket propulsion, plasma etching, fusion energy research, etc. In laboratory conditions, plasmas are often produced using a low-pressure gas discharge (passing of strong electric currents through a neutral gas), resulting in a mixture of electrons, positively charged ions, and neutral atoms. Electrons in low-pressure gas discharge plasmas acquire high temperature and mobility (on the order of  $10^5 - 10^6$  K), while ion and neutral atoms are often assumed to have room temperature ( $\approx 300$  K). However, due to their small mass, electrons do not transfer much of their thermal energy as heat to the heavier plasma components or to the enclosing walls. Thus, this type of plasma is characterized as 'low-temperature plasma'.

In this chapter, we focus on the special case of laboratory complex plasma systems, which have attracted great attention in the past few decades. Complex (or dusty) plasmas are plasmas containing micron-sized solid or liquid particles (commonly referred to as dust) [1–4]. Upon interaction with the ionized environment, the macroscopic particles can acquire negative or positive charge depending

---

This chapter published as: Kostadinova, F. Guyton, A. Cameron, K. Busse, Liaw, C. D., Matthews, L. S., & Hyde, T. W. (2017). Transport properties of disordered 2D complex plasma crystal (recommended for publication in *Contrib. To Plasma Phys.*)

<sup>1</sup>The term 'collective behavior' implies that the dynamics of the plasma system is influenced not only by local interactions but also by the state of the plasma in remote regions. In other words, collective behavior necessarily implies the presence of long-range interactions.

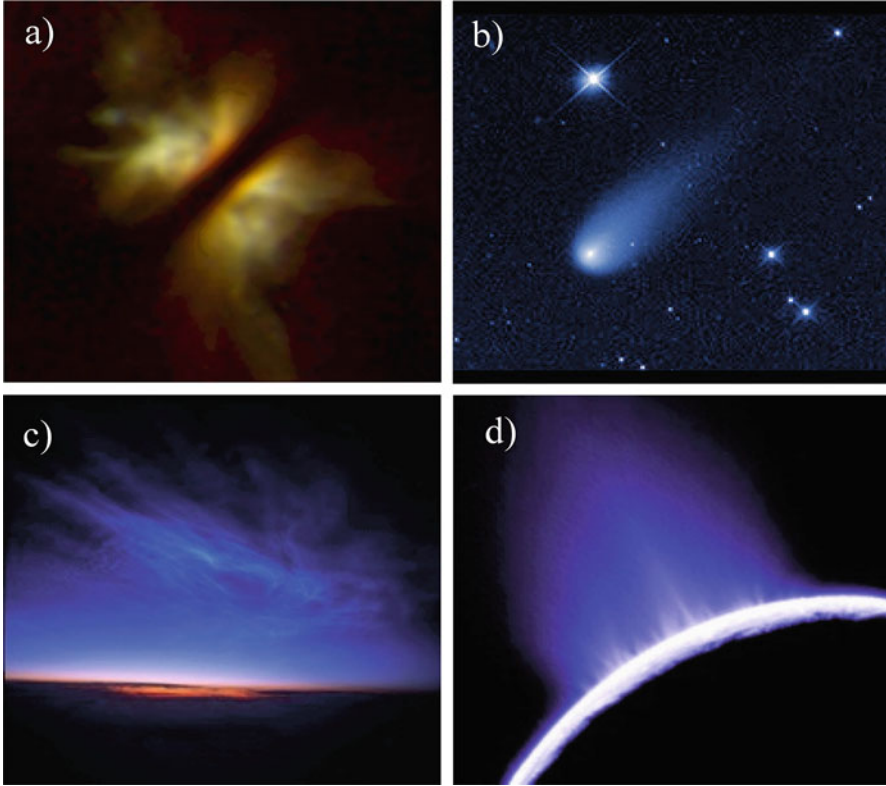


**Fig. 6.1** Astrophysical dusty plasmas. (a) Edge-on view of protoplanetary disk. Credit: D. Padgett (IPAC/Caltech), W. Brandner (IPAC), K. Stapelfeldt (JPL) and NASA, (b) Comet ISON Credit: NASA, ESA, and the Hubble Heritage Team (STScI/AURA) (c) Noctilucent clouds. Credit: John Boardman (d) Plumes of Enceladus Credit: NASA/JPL

on the charging mechanisms operating the plasmas. Dusty plasmas are characteristic of various space environments, such as protoplanetary discs, planetary rings, comet tails, interplanetary and interstellar clouds, and the Earth's atmosphere [5–7] (Fig. 6.1). Dust grains in ionized gas also form in the vicinity of artificial satellites and space stations [8, 9].

In chemically reactive plasmas on Earth, solid particles often form naturally within reactors; however, dust can also be injected into an experimental setup for dedicated study [10, 11]. The term ‘complex plasma’ is currently used to designate dusty plasmas that are specially prepared for investigation in the laboratory [12].

The dust grains used in controlled experiments can be non-conducting (dielectric) or conducting and be monodisperse or polydisperse (i.e., have size/shape distribution). The macroscopic particles acquire electrons and ions from the ionized gas, allowing them to be trapped by internal or external electric fields. In terrestrial experiments, the ionized environment is typically radio frequency (RF) or direct



**Fig. 6.2** Horizontal dust plasma crystal formed above the lower electrode of a GEC RF cell. Dust particles float at an equilibrium height where the gravitational force is balanced by electrostatic force due to external electric field. The confinement in the horizontal direction is provided by an inwardly directed force created by a ‘cut-out’ plate placed on the lower electrode. Image source: Center for Astrophysics, Space Physics, and Engineering Research, Waco, TX

current (DC) discharge plasma, where the primary dust-charging mechanism is the collection of electrons and ions. The net charge on the dust particles is negative due to the high electron thermal speed. The resulting intergrain force is dominated by the repulsive Yukawa (Debye-Hückel) potential given by

$$V(r) = \left( \frac{q}{4\pi\epsilon_0 r} \right) e^{-\frac{r}{\lambda_D}}, \quad (6.1)$$

where  $r$  is the distance from a particle with charge  $q$ ,  $\lambda_D$  is the scale length over which a charged grain is shielded by the plasma (called the Debye length), and  $\epsilon_0$  is the permittivity of free space.

In terrestrial experiments, dust particles are levitated against gravity with the help of external electric field. The grains can also be constrained in the radial direction by an inwardly-directed confinement force provided by an external potential. In such conditions, complex plasmas self-organize into dust liquids, 2D and 3D dust crystal lattices and 1D field-aligned dust chains. This feature allows researchers to examine a variety of collective phenomena, including structure formation, self-organization, phase transitions, waves, and instabilities). The first experimentally realized crystal-line complex plasma structure is the two-dimensional dust crystal (Fig. 6.2), which is the focus of this chapter [13, 14].

A variety of processes in complex plasma crystals have already been shown to be analogous to those found in other strongly correlated Yukawa systems (for instance, Wigner crystallization in 2D, quantum dot excitation, and excitonic condensation in symmetric electron-hole bilayers [15–19]). In this chapter, the dust crystal is proposed to be a toy model ‘toy’ model environment for the study of fundamental problems in transport theory.

## 6.2 Two-Dimensional Dust Crystal Analogue

As discussed in the previous chapters, the proper utilization of two-dimensional materials (such as graphene) relies on adequate understanding of conductivity in 2D disordered crystals. A useful tool in the study of transport problems is the use of 2D toy systems, or analogues, exhibiting similar properties to graphene (and graphene-like materials). These realizations of ‘artificial graphene’ are artificially prepared hexagonal or hexagonal-like lattices, designed to study the tunneling of electrons, atoms, and waves under controlled system conditions [20]. Previously, artificial graphene has been realized using ultracold atoms in optical traps [21], molecules assembled on metal surfaces [22], optical [23] and microwave [24] photonic crystals, and nanopatterned semiconductor surfaces [25]. Key advantages of graphene analogues include [20]: (1) control over a wide range of system parameters, (2) precise tunability of crystal disorder, (3) long length and time scales, and (4) interplay between transport and many-body effects. While the atomic and molecular lattices offer great tunability of system parameters and are characterized by longer time scales, they are effectively disorder free. Photonic crystals provide similar advantages with the added control over disorder but fail to exhibit long-distance interactions or many-body effects. These can be investigated using semiconductor analogues, which, however, do not allow for precise control over system parameters and disorder.

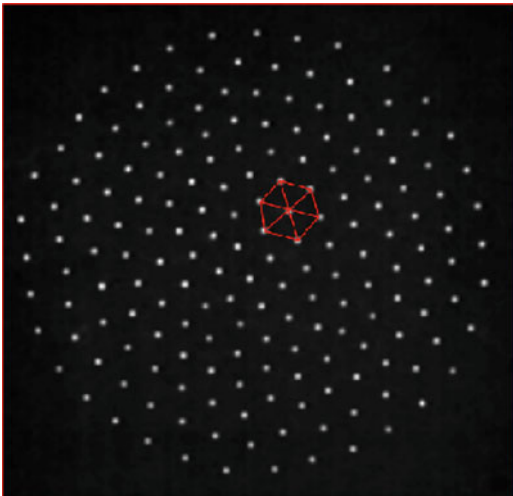
In Sect. 4.5, we argued that the disordered triangular and honeycomb lattice exhibit similar transport behavior due to planar duality. This indicates that a system characterized by triangular symmetry is a good candidate for a graphene analogue. In this chapter, we investigate numerically the transport properties of graphene-like lattices using a 2D complex plasma crystal as macroscopic analogue. Since electron-electron interaction in graphene has been shown to be very weak [26], many aspects of transport in the material can be studied with the help of a classical systems of similar geometry, such as the complex plasma crystal.

The 2D dust crystal consists of mutually-interacting micron-sized solid particles arranged in a single-layered triangular lattice that can be easily driven by external forces (Fig. 6.3). The average kinetic energy of the dust particles is determined by the balance of driving forces and dissipation. 2D complex plasma crystals have been previously used for the experimental study of condensed matter phenomena (such as crystallization [3, 27], melting [28, 29], dislocations in crystals [30, 31], solitons [32], etc.) at the kinetic level.

## 6.3 Transport in the Classical Regime

In the classical regime, Anderson-type problems can be studied using waves propagating in diffusive matter. Diffusion of both electron and electromagnetic waves through disordered medium obey Ohms law, where the conductance/transmission of

**Fig. 6.3** Top view of a single-layer complex plasma crystal. The red lines on the figure highlight the hexagonal symmetry of a single crystal cell. (Image source: Center for Astrophysics, Space Physics, and Engineering Research, Waco, TX)



the wave decreases linearly with the system length [33]. Experimental evidence for Anderson localization effects has been observed using both electromagnetic [33–40] and acoustic waves [41–45] showing that the Anderson model can be effectively studied in the classical regime. These experiments examine propagation of waves in a media with controlled number of random or ordered scattering centers and use the (modified) Ioffe-Regel criterion [46] for localization.

Both electromagnetic and acoustic waves can be induced in 2D complex plasma crystals, which makes them an ideal candidate for the study of Anderson-type problems. Here we consider the diffusion of coplanar lattice waves in a 2D disordered dust crystal in the regime where Hamiltonian interactions can be decoupled from non-Hamiltonian effects. In this case, the Hamiltonian part is represented by the wave interaction with hot-solid and topological defects in a system, while the non-Hamiltonian part arises as a long distance many-body effect, possibly resulting from the dust lattice coupling with the plasma environment. In our simulations, we introduce a coplanar wave excitation in the bulk of the crystal and record its space-time evolution. The data is then analyzed using the spectral approach, which can determine whether the wave reaches the exterior of the crystal or becomes localized due to spatial defects. Of specific interest is the case where long-distance lattice excitations are observed even when the spectral method does not indicate delocalization of the initial perturbation. In the decoupled Hamiltonian regime, such long-distance interactions can be contributed to the interaction with the plasma gas.

A common approach to the dynamics of a non-Hamiltonian problem is to assume that the system of interest is small and coupled to a much larger (but finite) volume, which acts like a thermal bath [47]. In this approximation, the time evolution is governed by a unitary transformation generated by a global Hamiltonian of the form

$$\mathbf{H} = \mathbf{H}_S + \mathbf{H}_B + \mathbf{H}_{SB} \quad (6.2)$$

where  $\mathbf{H}_S$ ,  $\mathbf{H}_B$ , and  $\mathbf{H}_{SB}$  are the Hamiltonians of the system, i.e., the bath, and the system-bath interaction, respectively. We introduce three important simplifications to this problem: (1) weak system-bath coupling, (2) fast bath dynamics (i.e.  $\mathbf{H}_B = 0$ ), and (3) an initially uncorrelated system and bath (i.e.  $\mathbf{H}_{SB} = 0$  at  $t = 0$ ). When all three approximations are satisfied, the time evolution of the density matrix for the system state  $\rho_S(t)$  is reduced to a differential equation of the form

$$\frac{d}{dt}\rho_S(t) = -\frac{i}{\hbar}[\mathbf{H}_S, \rho_S(t)] + \mathcal{L}_D\rho_S(t), \quad (6.3)$$

where  $\mathcal{L}_D$  is the generator of dissipative dynamics. Thus, transport in the open system can be approximated by transport in the closed system (first term of Eq. (6.3)) plus dissipation to the environment.

Here we examine a classical analogue of the quantum open system problem using a 2D dust crystal in contact with a plasma gas environment. The internal coupling between pairs of dust grains within the crystal is dominated by the repulsive screened Coulomb force, which is in general much larger than the averaged interaction with the plasma flow. In Earth-based experiments, dust structures are levitated against gravity with the help of a vertical electric field. At the same time, the ion flow from the bulk is known to produce a variety of effects such as wakefield focusing, shadowing forces, and dipole polarization of the grains. In most cases, such effects have not been shown to contribute appreciably to the interparticle potential in the horizontal plane. Thus, for the case of a 2D dusty plasma crystal, the in-plane system-bath coupling can be considered weak (when compared with the intergrain potential), which satisfies approximation (1). The requirement of fast bath dynamics given in (2) is easily met in our simulations, since the time scales of the dust lattice waves are considerably larger than the frequencies of plasma oscillations. Finally, the assumption in (3) can be (approximately) achieved in both numerical and experimental setups if the 2D crystal is in effective equilibrium at  $t = 0$ . Here, we define effective equilibrium with the environment as the state in which the velocity fluctuations of the dust grains are much smaller than the propagation velocity of the dust lattice wave.

With the above assumptions satisfied, we argue that transport phenomena in our simulations can be decoupled into two distinct contributions: a Hamiltonian interaction (modeled by an Anderson-type problem) and a non-Hamiltonian effect (resulting from the time-dependent interaction with the environment). In this analysis, the spectral theory will be employed to determine the contribution from the Anderson-type problem. The following section gives a brief overview of the logic behind the spectral approach to transport in 2D systems.

## 6.4 Numerical Simulations of Dust Particle Dynamics

To generate the complex plasma crystal, a self-consistent  $N$ -body code `Box_Tree` was employed. This code provides a user-specified coordinate system, dust particle size, charge, and density, Debye length, external potential, and interparticle forces.

**Table 6.1** Systems parameters used to generate dust crystal at stable equilibrium (reprinted with permission)

Size [N]	Mass [kg]	Charge [C]	Radius [m]	Conf. [Hz]	Defect [%]
$10^3$	$8.18 \times 10^{-13}$	$-2.45 \times 10^{-15}$	$5 \times 10^{-6}$	$5.4 \times 10^3$	5.3

This code has been used extensively to model the dynamics of charged dust in astrophysical environments [48–52] and in a GEC RF reference cell in Earth-based experiments [53–55]. `Box_Tree` also allows for control over confining potentials in the radial and vertical directions, gravity, ion drag, neutral gas drag, and thermophoretic forces.

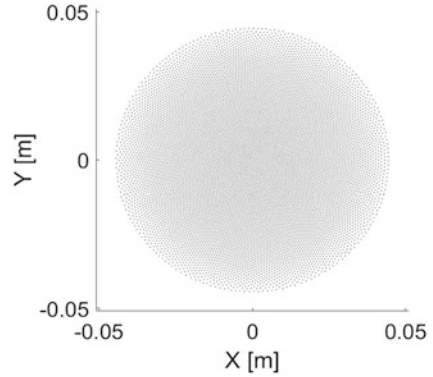
### 6.4.1 Dust Crystal Formation and Defect Types

In this study, we consider a two-dimensional crystal consisting of  $10^4$  identical spherical grains suspended in weakly ionized plasma gas. The numerically generated dust structure was obtained using system parameters that correspond to experimentally achievable conditions (see Table 6.1). To ensure that the examined crystal is approximately two-dimensional, we require that the dust grains are in effective equilibrium (i.e. have small average thermal velocities in each direction) and that the vertical extent of the structures is smaller than the average interparticle separation. Starting from initial random positions, the particles were allowed to approach equilibrium by including the effects of a drag force. At equilibrium, the average thermal velocity of the particles in the crystal were  $\sim 10^{-8} \text{ ms}^{-1}$  in the  $X$  and  $Y$  directions and  $\sim 10^{-16} \text{ ms}^{-1}$  in the  $Z$  direction indicating that the chosen crystal equilibrium is (effectively) static. These velocities are several orders of magnitude smaller than the thermal fluctuations usually observed in experimental conditions ( $\approx 10^{-4} \text{ ms}^{-1}$  [4]). However, in experiments where the dust grains only move distances smaller than the interparticle separation and have velocities randomly fluctuating in all directions, the damping due to thermal effects has small effect on lattice propagation in the strongly coupled system [56]. Thus, we expect that the main results from the presented study should be experimentally observable even in the presence of larger thermal velocities.

Figure 6.4 shows the spatial extent of the dusty structure in the horizontal direction. The observed radial symmetry is a result of the confinement force, applied in the horizontal direction (column five in Table 6.1). The crystal is levitated at a vertical position of  $\approx 5 \text{ mm}$  and has average interparticle spacing of  $\approx 300 \mu\text{m}$ , which agrees with experimentally obtained values [4]. The vertical spread of the crystal is less than the particle radius of  $r = 5 \mu\text{m}$ . Thus, we conclude that the numerically generated complex plasma structure in our simulations is two-dimensional.

To evaluate the amount of lattice defect in the dusty crystal, we employ a crystallinity code, which calculates the true number of nearest neighbors for each dust grain. This information is then used to determine the defect fraction  $D$  (defined

**Fig. 6.4** Spatial extent of the numerically generated dust crystal in the horizontal direction (reprinted with permission)



as the ratio of particles with nearest neighbors different than 6) and the complex bond-order parameter

$$G_6(i) = \frac{1}{6} \sum_{l=1}^{NN_i} e^{i6\Theta_i(l)}, \quad (6.4)$$

where,  $NN_i$  is the number of nearest neighbors of the  $i$ th particle and  $\Theta_i(l)$  is the angle of the  $l$ th nearest-neighbor bond measured with respect to the  $X$ -axis. The determination of the bond order in the crystallinity code relies on the Delaunay triangulation algorithm. Thus, when the code is applied to dust fluid structures with badly defined primitive cells, the Delaunay triangulation function returns an error due to ‘insufficient number of unique points’. In other words, in these structures, the function encounters numerous points laying on the same line, in which case, the triangulation does not exist. In this way, we can distinguish between strongly coupled and weakly coupled realizations of the dust structure.

The crystallinity code was also used to distinguish between the two main variations of spatial disorder (as defined by Thouless [57]): the hot solid type, and the topological disorder. In the static lattice approximation, the hot solid type disorder occurs when atoms are shifted from their regular position in the periodic lattice due to mechanical defect (static positional disorder) or due to the presence of another particle species (substitutional disorder). The examined hot solid type disorder in these simulations is mechanical. Figure 6.5a shows positions of various mechanical defects within the crystal, where in this case the definition of mechanical disorder coincides with the defect fraction  $D$ . For the lattice used in this study, we found that  $D = 5.3\%$ .

In the case of a topologically disordered system, the long-range symmetry in the atomic distribution is completely broken, i.e. uniform periodicity cannot be assumed throughout the lattice. Topological disorder can be represented by a system whose domains exhibit various orientation with respect to the  $X$ -axis (ranging from  $-\pi$  to  $\pi$  in radians). Figure 6.5b shows the formation of characteristic domains throughout

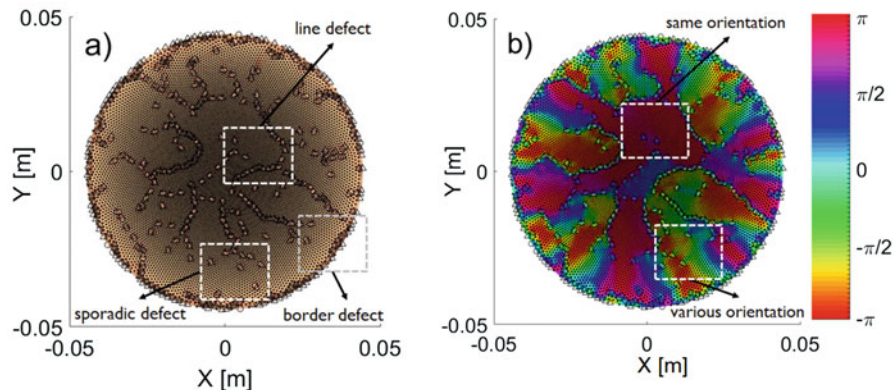


**Fig. 6.5** Lattice disorder in the form of mechanical hot solid type defect (a) and topological defect (b). The positions of the dust grains are marked by dots, with triangles marking particles with  $NN = 5$  and circles marking particles with  $NN = 7$  (reprinted with permission)

the dust structure. In areas where the cell orientation is the same, the color is uniform, whereas areas with changing cell orientation are characterized by color gradient.

### 6.4.2 Crystal Perturbation

After the crystal has reached equilibrium, the drag force is turned off and a lattice perturbation is induced by an in-plane Gaussian kick of a single particle. Variation of the kick strength, duration, and direction with respect to the X-axis allow for control over the frequency of the propagating lattice wave.

The lattice perturbation in our simulations is induced by an in-plane Gaussian kick of a single particle. Variation of the kick strength, duration, and direction with respect to the X-axis allow for control over the frequency of the propagating lattice wave. The magnitude of the perturbation can also be modified using the kick strength or the number of particles initially perturbed. The simulation additionally allows for wave excitation in various areas of the crystal, which can be used to study transport within a specific domain and interaction with the boundary. This paper shows two perturbations of different strength, which were induced in the center of the crystal. In each case, we generated a Gaussian kick at an angle of  $0.1336$  rad (with respect to the X-axis) and a kick duration of  $0.04$  s. The initial acceleration given to the perturbed particle was  $0.016 \text{ ms}^{-2}$  in case 1 and  $0.030 \text{ ms}^{-2}$  in case 2. (Note that in all Figures the two cases are labeled  $16 \equiv 0.016 \text{ ms}^{-2}$  and  $30 \equiv 0.030 \text{ ms}^{-2}$ .) The total simulation time was  $5$  s with an output timestep of  $\approx 17 \mu\text{s}$  (i.t. total number of timesteps  $n = 300$ ). Figure 6.6 shows maps of the particle trajectories up to the final timestep of the simulation. The trajectory maps in 3a and 3b indicate that in both cases particle excitation was not directly proportional

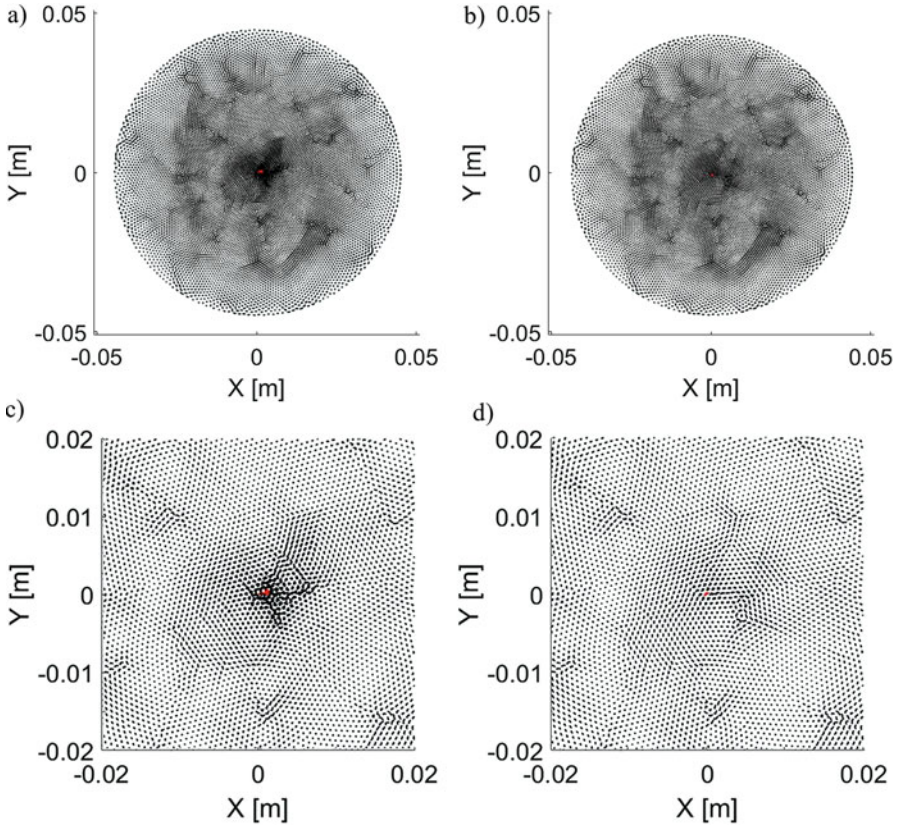


**Fig. 6.6** Final movie frames for two different crystal perturbations. Parts (a, b) show the extent of the perturbation throughout the crystal. Parts (c, d) are zoomed-in images of the lattice center, where the perturbation was induced. In all images, the trajectory of the perturbed particle is marked in red (reprinted with permission)

to distance from the kicked particle. Specifically, a comparison between Fig. 6.5a,b and Fig. 6.6a,b shows that the grains around defects were displaced more than the grains located in regions of higher crystallinity. This result makes sense as (by definition) particles located near mechanical defects will be shifted from their regular position and will therefore occupy additional unstable energy states.

Figure 6.6c,d show enlarged maps of the region around the perturbed particle. The small motion of particles at a distance  $\sim 10$  mm from the perturbed particle suggests that the initial wave perturbation did not spread considerably in the 2D plane. However, the excitation was ‘felt’ by particles far away from the center of the crystal. In Fig. 6.7, we present various plots of the total kinetic energy as a function of time and distance from the perturbed particle. The energy plots further suggest that the initial perturbation was damped out at a radial distance of  $\sim 1$  mm from the center. This

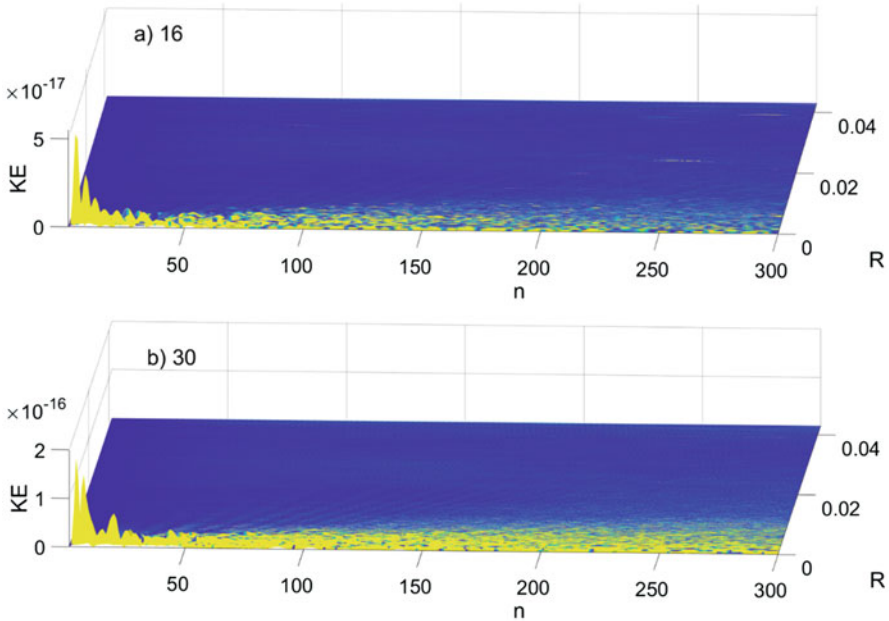


**Fig. 6.7** Plots of the total kinetic energy as a function of time and radial distance from the perturbed particle for the two kicks (reprinted with permission)

indicates that excitation around defects may contribute to long-range interactions. In the following section, we examine this assertion by using the spectral approach.

## 6.5 Spectral Analysis

The sequence  $\{v_0, H_\epsilon v_0, (H_\epsilon)^2 v_0, \dots, (H_\epsilon)^n v_0\}$  represents the dynamical evolution of the perturbed system. In the present case, the vector  $v_0$  corresponds to the initial kinetic energy of the crystal right after the Gaussian kick. Each successive term represents the spread of the energy to the nearest neighbors. The numerical equivalent to the operator sequence is given by

$$\left\{v_0, H_\epsilon v_0, (H_\epsilon)^2 v_0, \dots, (H_\epsilon)^n v_0\right\} \rightarrow \{KE_1, KE_2, KE_3, \dots, KE_n\} \quad (6.5)$$

where,  $KE_n$  is the total kinetic energy of the crystal at timestep  $n$ . The distance values for the two kicks are calculated using an orthogonalization procedure similar to the one employed in the previous chapters. Figure 6.8 shows a plot of the distance values at each iteration  $n$ . In both cases, the distance value limits to zero with time. According to the criterion given in Eq. (3.13), we cannot conclude that the perturbations reached the exterior of the crystal by the nearest-neighbor interaction. Thus,

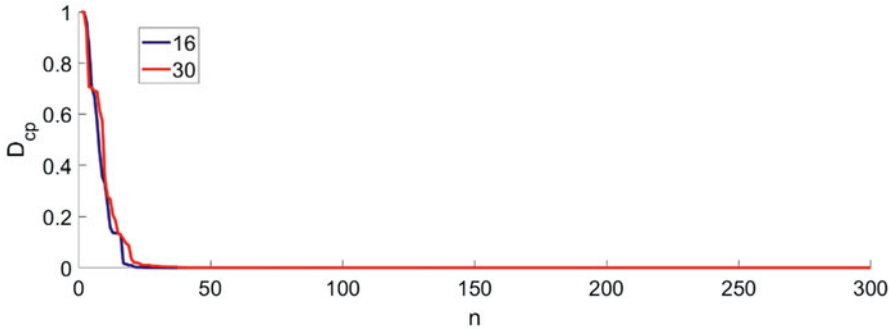


**Fig. 6.8** Limiting behavior of the distance values for the two kicks. The figure shows that in both cases  $D_{cp}$  drops down to zero within the first 50 timesteps, which indicates that the spectral approach cannot determine the existence of extended states with probability 1 (reprinted with permission)

we expect that the observed excitations in our simulations do not result from the classical Anderson-type transport. Instead, they can be contributed to a long-distance interaction.

## Bibliography

1. G. Hebner, M. Riley, D. Johnson, P. Ho, R. Buss, Direct determination of particle-particle interactions in a 2D plasma dust crystal. *Phys. Rev. Lett.* **87**(23), 235001 (2001)
2. K. Qiao, T.W. Hyde, Dispersion properties of the out-of-plane transverse wave in a two-dimensional Coulomb crystal. *Phys. Rev. E* **68**(4), 046403 (2003)
3. P. Hartmann et al., Crystallization dynamics of a single layer complex plasma. *Phys. Rev. Lett.* **105**, 115004 (2010)
4. P. Hartmann, A. Kovács, A. Douglass, J. Reyes, L. Matthews, T. Hyde, Slow plastic creep of 2D dusty plasma solids. *Phys. Rev. Lett.* **113**, 025002 (2014)
5. C.K. Goertz, Dusty plasmas in the solar system. *Rev. Geophys.* **27**(2), 271–292 (1989)
6. T.G. Northrop, Dusty plasmas. *Phys. Scr.* **45**(5), 475 (1992)
7. V.N. Tsytovich, Dust plasma crystals, drops, and clouds. *Phys.-Uspekhi* **40**(1), 53 (1997)
8. E.C. Whipple, Potentials of surfaces in space. *Rep. Prog. Phys.* **44**(11), 1197 (1981)
9. P.A. Robinson, P. Coakley, Spacecraft charging-progress in the study of dielectrics and plasmas. *IEEE Trans. Electr. Insul.* **27**(5), 944–960 (1992)
10. V.E. Fortov, A.G. Khrapak, S.A. Khrapak, V.I. Molotkov, O.F. Petrov, Dusty plasmas. *Phys.-Uspekhi* **47**(5), 447–492 (2004)
11. P.K. Shukla, A.A. Mamun, *Introduction to dusty plasma physics* (CRC Press, 2001)
12. V.E. Fortov, A.V. Ivlev, S.A. Khrapak, A.G. Khrapak, G.E. Morfill, Complex (dusty) plasmas: current status, open issues, perspectives. *Phys. Rep.* **421**(1–2), 1–103 (2005)
13. H. Thomas, G.E. Morfill, V. Demmel, J. Goree, B. Feuerbacher, D. Möhlmann, Plasma crystal: coulomb crystallization in a dusty plasma. *Phys. Rev. Lett.* **73**(5), 652–655 (1994)
14. Y. Hayashi, K. Tachibana, Observation of coulomb-crystal formation from carbon particles grown in a methane plasma. *Jpn. J. Appl. Phys.* **33**(Part 2, 6A), L804–L806 (1994)
15. A.V. Filinov, M. Bonitz, Y.E. Lozovik, Wigner crystallization in mesoscopic 2D electron systems. *Phys. Rev. Lett.* **86**(17), 3851–3854 (2001)

16. W.M. Itano, J.J. Bollinger, J.N. Tan, B. Jelenković, X.-P. Huang, D.J. Wineland, Bragg diffraction from crystallized ion plasmas. *Science* **279**(5351), 686–689 (1998)
17. O. Arp, D. Block, A. Piel, A. Melzer, Dust coulomb balls: three-dimensional plasma crystals. *Phys. Rev. Lett.* **93**(16), 165004 (2004)
18. M. Bonitz et al., Structural properties of screened coulomb balls. *Phys. Rev. Lett.* **96**(7), 075001 (2006)
19. S. De Palo, F. Rapisarda, G. Senatore, Excitonic condensation in a symmetric electron-hole bilayer. *Phys. Rev. Lett.* **88**(20), 206401 (2002)
20. M. Polini, F. Guinea, M. Lewenstein, H.C. Manoharan, V. Pellegrini, Artificial honeycomb lattices for electrons, atoms and photons. *Nat. Nanotechnol.* **8**(9), 625–633 (2013)
21. P. Soltan-Panahi et al., Multi-component quantum gases in spin-dependent hexagonal lattices. *Nat. Phys.* **7**(5), 434–440 (2011)
22. K.K. Gomes, W. Mar, W. Ko, F. Guinea, H.C. Manoharan, Designer Dirac fermions and topological phases in molecular graphene. *Nature* **483**(7389), 306–310 (2012)
23. Y. Plotnik et al., Observation of unconventional edge states in ‘photonic graphene’. *Nat. Mater.* **13**(1), 57–62 (2014)
24. M. Bellec, U. Kuhl, G. Montambaux, F. Mortessagne, Topological transition of Dirac points in a microwave experiment. *Phys. Rev. Lett.* **110**(3), 033902 (2013)
25. S.P. Scheeler et al., Plasmon coupling in self-assembled gold nanoparticle-based honeycomb islands. *J. Phys. Chem. C* **117**(36), 18634–18641 (2013)
26. J. González, F. Guinea, M.A.H. Vozmediano, Electron-electron interactions in graphene sheets. *Phys. Rev. B* **63**(13), 134421 (2001)
27. V.E. Fortov et al., Crystallization of a dusty plasma in the positive column of a glow discharge. *J. Exp. Theor. Phys. Lett.* **64**(2), 92–98 (1996)
28. R.A. Quinn, J. Goree, Experimental test of two-dimensional melting through disclination unbinding. *Phys. Rev. E* **64**(5), 051404 (2001)
29. T.E. Sheridan, Monte Carlo study of melting in a finite two-dimensional dusty plasma. *Phys. Plasmas* **16**(8), 083705 (2009)
30. V. Nosenko, S.K. Zhdanov, Dynamics of dislocations in a 2D plasma crystal. *Contrib. Plasma Physics* **49**(4–5), 191–198 (2009)
31. V. Nosenko, S. Zhdanov, G. Morfill, Supersonic dislocations observed in a plasma crystal. *Phys. Rev. Lett.* **99**(2), 025002 (2007)
32. S. Zhdanov et al., Dissipative dark solitons in a dc complex plasma. *EPL Europhys. Lett.* **89**(2), 25001 (2010)
33. D.S. Wiersma, P. Bartolini, A. Lagendijk, R. Righini, Localization of light in a disordered medium. *Nature* **390**(6661), 671–673 (1997)
34. R. Dalichaouch, J.P. Armstrong, S. Schultz, P.M. Platzman, S.L. McCall, Microwave localization by two-dimensional random scattering. *Nature* **354**(6348), 53–55 (1991)
35. A.A. Chabanov, M. Stoytchev, A.Z. Genack, Statistical signatures of photon localization. *Nature* **404**(6780), 850–853 (2000)
36. A.A. Chabanov, A.Z. Genack, Photon localization in resonant media. *Phys. Rev. Lett.* **87**(15), 153901 (2001)
37. M. Störzer, P. Gross, C.M. Aegerter, G. Maret, Observation of the critical regime near Anderson localization of light. *Phys. Rev. Lett.* **96**(6), 063904 (2006)
38. T. Schwartz, G. Bartal, S. Fishman, M. Segev, Transport and Anderson localization in disordered two-dimensional photonic lattices. *Nature* **446**(7131), 52–55 (2007)
39. F. Riboli et al., Anderson localization of near-visible light in two dimensions. *Opt. Lett.* **36**(2), 127 (2011)
40. J. Armijo, R. Allio, Observation of coherent back-scattering and its dynamics in a transverse 2D photonic disorder: from weak to strong localization. *Cond. Mat. Physicsphys.* (2015)
41. O. Richoux, V. Tourmat, T. Le Van Suu, Acoustic wave dispersion in a one-dimensional lattice of nonlinear resonant scatterers. *Phys. Rev. E* **75**(2), 026615 (2007)
42. O. Richoux, E. Morand, L. Simon, Analytical study of the propagation of acoustic waves in a 1D weakly disordered lattice. *Class. Phys.* **324**, 1983–1995 (2009)

43. H. Hu, A. Strybulevych, J.H. Page, S.E. Skipetrov, B.A. van Tiggelen, Localization of ultrasound in a three-dimensional elastic network. *Nat. Phys.* **4**(12), 945–948 (2008)
44. S. Faez, A. Strybulevych, J.H. Page, A. Lagendijk, B.A. van Tiggelen, Observation of multifractality in Anderson localization of ultrasound. *Phys. Rev. Lett.* **103**(15), 155703 (2009)
45. A.C. Hladky-Hennion, J.O. Vasseur, S. Degraeve, C. Granger, M. de Billy, Acoustic wave localization in one-dimensional Fibonacci phononic structures with mirror symmetry. *J. Appl. Phys.* **113**(15), 154901 (2013)
46. N. Mott, Metal-insulator transitions. *Phys. Today* **31**(11), 42–45 (1978)
47. R. Kosloff, Quantum thermodynamics: a dynamical viewpoint. *Entropy* **15**(6), 2100–2128 (2013)
48. L.S. Matthews, T.W. Hyde, Effect of dipole–dipole charge interactions on dust coagulation. *New J. Phys.* **11**(6), 063030 (2009)
49. L.S. Matthews, T.W. Hyde, Effects of the charge-dipole interaction on the coagulation of fractal aggregates. *IEEE Trans. Plasma Sci.* **32**(2), 586–593 (2004)
50. L.S. Matthews, T.W. Hyde, Charged grains in Saturn’s F-Ring: interaction with Saturn’s magnetic field. *Adv. Space Res.* **33**(12), 2292–2297 (2004)
51. L.S. Matthews, T.W. Hyde, Charging and growth of fractal dust grains. *IEEE Trans. Plasma Sci.* **36**(1), 310–314 (2008)
52. L.S. Matthews, T.W. Hyde, Gravitoelectrodynamics in Saturn’s F ring: encounters with Prometheus and Pandora. *J. Phys. Math. Gen.* **36**(22), 6207 (2003)
53. M. Sun, L.S. Matthews, T.W. Hyde, Effect of multi-sized dust distribution on local plasma sheath potentials. *Adv. Space Res.* **38**(11), 2575–2580 (2006)
54. L.S. Matthews, K. Qiao, T.W. Hyde, Dynamics of a dust crystal with two different size dust species. *Adv. Space Res.* **38**(11), 2564–2570 (2006)
55. K. Qiao, J. Kong, Z. Zhang, L.S. Matthews, T.W. Hyde, Mode couplings and conversions for horizontal dust particle pairs in complex plasmas. *IEEE Trans. Plasma Sci.* **41**(4), 745–753 (2013)
56. S. Nunomura, J. Goree, S. Hu, X. Wang, A. Bhattacharjee, Dispersion relations of longitudinal and transverse waves in two-dimensional screened Coulomb crystals. *Phys. Rev. E* **65**(6), 066402 (2002)
57. D.J. Thouless, Electrons in disordered systems and the theory of localization. *Phys. Rep.* **13**(3), 93–142 (1974)

# Chapter 7

## Conclusions



In this work we introduced the innovative spectral approach to delocalization in infinite disordered lattices. In the first three chapters, we reviewed the major theoretical and experimental developments related to the Anderson-type transport problems and discussed their relevance to physical systems. Then the mathematical formulation of the spectral method was provided together with a physical interpretation in the context of the classical model of Edward and Thouless. The spectral approach is an important contribution to localization theory because it can be applied to infinite systems of any dimension or geometry without the use of periodic boundary conditions or finite-size scaling. Our preliminary numerical simulations showed that delocalization, in the form of extended states, exists for  $W \leq 0.6$  in the 2D square lattice and for  $W \leq 5$  in the 3D diamond lattice. Since these results are based on conservative assumptions, the precise transition points for both cases may occur for higher values of the system disorder  $W$ . Specifically, in Chap. 4, we improved on our predictions for the square lattice case.

Identifying precise values of the disorder at the transition points in both 2D and 3D cases is beyond the scope of this work. However, it is important to emphasize that the spectral method and the analysis presented here can be used to define the critical value of  $W$  for which extended states cease to exist with probability 1. In contrast, the dynamical approach of scaling theory aims to identify the critical point where transition to pure localization occurs. As the two points do not necessarily coincide, one can speak of a transition region of disorder values, where the energy states are neither extended, nor exponentially localized. Mathematically, such solutions correspond to the (poorly behaved) singular-continuous pieces in the spectrum of the Hamiltonian. Thus, the proposed spectral method can be combined with the techniques developed in scaling theory in the study of the transition region. The possible connection between the singular-continuous part of the energy spectrum and wave-particle duality makes the transition region an interesting subject for both mathematicians and theoretical physicists.

The spectral method can be further employed in material science where accurate results in 1D and 2D disordered systems are crucial for the study of quasi-1D

graphene nanotubes and graphene sheets. Currently, both localization and transport have been shown to exist in graphene-based materials for weak disorder [1–4]. The transition from localized to extended states is still highly debated on theoretical grounds and there is disagreement on the value of the minimal conductivity [5]. Additionally, the localization lengths in graphene have been shown to be independent of system size for various strengths of the disorder [6], which contradicts the predictions of scaling theory [7]. Detailed numerical and experimental study employing the spectral approach can greatly contribute to such problems allowing for more accurate predictions related to the behavior of graphene-based materials.

In Chap. 4, we applied the spectral approach to delocalization in the 2D honeycomb, triangular, and square lattices. Our numerical simulations established that, in contrast to the predictions of scaling theory, extended states exist for nonzero disorder in all three lattices. The spectral approach, combined with nonlinear regression fitting and hierarchical clustering analysis indicates that delocalization occurs for  $W \leq 0.75$  in the honeycomb and triangular lattices, and  $W \leq 0.95$  in the square lattice. These results confirm that the existence of metal-to-insulator transition in 2D is characteristic of the dimension and is independent of the types of geometries considered here. We also showed that the spectral model correctly predicts the similarity in the transport properties of the honeycomb and the triangular lattices, which is to be expected from planar duality. This justifies the application of the spectral model to systems with triangular symmetries, which are commonly used as analogues to honeycomb lattices, such as graphene. We also observed that the abruptness of the transition from one transport regime to another is dependent on the lattice geometry.

The main goal of Chap. 4 was to identify the delocalization regime for the three 2D lattices, which was obtained by examining the two main clusters in each dendrogram in Fig. 4.5. However, the analysis can be extended by considering the substructure of the two main clusters in each geometry. Smaller clusters allow us to identify sub-regimes within the global transport behavior. In our future work, we will include more data points and consider greater values of the disorder, which will improve the accuracy of the statistical analysis and allow us to recognize a rich substructure of transport properties.

In Chap. 5, we used the spectral theory to establish the existence of extended states in a 2D honeycomb lattice with substitutional disorder. The examined transport problem is modeled by an Anderson-type Hamiltonian, where the hopping potential is represented by a constant nearest-neighbor interaction (tight-binding approximation) and on-site energies are random variables assigned according to a predetermined probability distribution  $\chi$ .

To model doping, we assumed a (modified) bimodal distribution consisting of a Gaussian peak and a Delta-type peak. The variables assigned from the Gaussian peak represent the fluctuations in the on-site energies of an unperturbed crystal. Physically, such fluctuations occur due to spatial lattice defects. Preliminary analysis of various normal distributions suggested that it is reasonable to use a Gaussian peak

with mean  $E_A = 0$  and variance  $\sigma^2 = 0.05$ . In all numerical simulations, we used a Delta peak at  $E_B \approx 100$  to represent the approximate energy of the doping atoms.

The defect concentration was varied between  $n_D = 0\%$  and  $n_D = 32\%$ . For  $n_D \geq 0.9\%$ , the spectral approach did not predict the existence of extended states with probability 1. Thus, we conclude that in this range the transport behavior of the system has transitioned into the localized regime. We applied a linear regression model and hierarchical clustering for small concentrations of the doping ( $n_D \leq 0.8\%$ ). The results indicate the existence of a transition point in the transport behavior of the system for  $0.2\% < n_D < 0.3\%$ , which agrees with previous experimental results [8].

The most important limitation of the work presented in Chaps. 3–5 is the finite character of the numerical simulations. The results from the present analysis can be improved by increasing the number of timesteps  $n$ , and the number of realizations of random energies for each value of the disorder. This will yield better estimates for the errors in the parameters  $b$  and  $R$ , used to determine the existence of transitions in the transport behavior of the system. A future goal of our research is to also optimize the choice of probability distribution  $\chi$  so that the spectral method can be used to model doping of different 2D materials with both atoms and molecules.

In Chap. 6, we presented a numerical study of in-plane dust lattice wave diffusion in a 2D disordered complex plasma crystal. We argue that the transport observed in the dust crystal can be decomposed into an Anderson-type wave delocalization and a long-distance interaction resulting from coupling to the plasma environment. Two examples were provided where a localized lattice perturbation was shown to induce long-distance excitations around lattice defects. In our future work, we will extend these numerical simulations to allow examination of various system regimes and types of perturbations. In this way, the contribution of the long-distance terms will be quantified using the thermodynamics of non-Hamiltonian systems. Finally, all numerical results will be compared to laboratory experiments employing perturbations through a complex plasma crystal.

## Bibliography

1. S.V. Morozov et al., Strong suppression of weak localization in graphene. *Phys. Rev. Lett.* **97**(1), 016801 (2006)
2. H. Suzuura, T. Ando, Weak-localization in metallic carbon nanotubes. *J. Phys. Soc. Jpn.* **75**(2), 024703 (2006)
3. V.I. Fal’ko, K. Kechedzhi, E. McCann, B.L. Altshuler, H. Suzuura, T. Ando, Weak localization in graphene. *Solid State Commun.* **143**(1–2), 33–38 (2007)
4. X. Wu, X. Li, Z. Song, C. Berger, W.A. de Heer, Weak antilocalization in epitaxial graphene: evidence for chiral electrons. *Phys. Rev. Lett.* **98**(13), 136801 (2007)
5. A. Lherbier, B. Biel, Y.-M. Niquet, S. Roche, Transport length scales in disordered graphene-based materials: strong localization regimes and dimensionality effects. *Phys. Rev. Lett.* **100**(3), 036803 (2008)

6. S.-J. Xiong, Y. Xiong, Anderson localization of electron states in graphene in different types of disorder. *Phys. Rev. B* **76**(21), 214204 (2007)
7. E. Abrahams, Scaling theory of localization: absence of quantum diffusion in two dimensions. *Phys. Rev. Lett.* **42**(10), 673–676 (1979)
8. A. Bostwick et al., Quasiparticle transformation during a metal-insulator transition in graphene. *Phys. Rev. Lett.* **103**(5), 056404 (2009)

# Appendix A: Basic Materials Science Terms

*Bravais lattice*—An infinite array of discrete points in three-dimensional space generated by a set of discrete transformation operations described by:  $\mathbf{R} = n_1\mathbf{a}_1 + n_2\mathbf{a}_2 + n_3\mathbf{a}_3$ , where  $n_i$  are any integers and  $\mathbf{a}_i$  are the primitive vectors, which lie in different directions and span the lattice. This discrete set of vectors must be closed under vector addition and subtraction. In physics, the Bravais lattice is usually used to model a periodic crystal structure. The Bravais lattice can be divided in Wigner-Seitz cells.

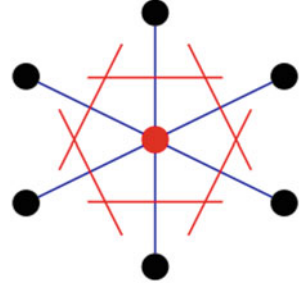
*Wigner-Seitz cell*—An example of a primitive cell, which is a unit cell containing exactly one lattice point. It represents the collection of points in space that are closer to that lattice point than to any other lattice point. Thus, the Wigner-Seitz cell is related to the notion of a neighborhood from topology. It can be mathematically shown that this cell spans the entire direct space without leaving any gaps or holes. It can be constructed by first picking a lattice point. After a point is chosen, lines are drawn to all nearby (closest) lattice points. At the midpoint of each line, another line is drawn normal to each of the first set of lines. The cell is the area enclosed by these lines (as shown in the shaded area in Fig. A.1).

*Reciprocal space*—In materials science, the reciprocal space (or reciprocal lattice) is the Fourier transform of another lattice (called the direct lattice). The direct lattice exists in real space, while the reciprocal lattice exists in momentum space (sometimes called K-space). The reciprocal lattice of the reciprocal lattice is the original direct lattice.

*Brillouin zone*—A uniquely defined primitive cell in reciprocal space. It is the equivalent of the Wigner-Seitz cell for the reciprocal space. The importance of the Brillouin zone stems from the Bloch wave description of waves in a periodic medium, in which it is found that the solutions can be completely characterized by their behavior in a single Brillouin zone.

*Fermi energy*—In quantum mechanics, the Fermi energy is the energy difference between the highest and lowest occupied single-particle states in a quantum system of non-interacting fermions at absolute zero temperature. In a Fermi gas (an ensemble of large number of fermions), the lowest occupied state is taken to

**Fig. A.1** Example of a Wigner-Seitz cell



have zero kinetic energy, whereas in a metal, the lowest occupied state is typically taken to mean the bottom of the conduction band.

*Fermi level*—At absolute zero there is no thermal energy, so electrons fill the band starting from the bottom with a sharp cutoff at the highest occupied energy level. This energy defines the Fermi energy. At finite temperatures, there is no sharply defined ‘most energetic electron’ because thermal energy is continuously exciting electrons within the band. The best that can be done is to define the energy level with a 50% probability of occupation, and set this as the Fermi level.

## Comparison Between Fermi Energy and Fermi Level

1. The Fermi energy is only defined at absolute zero, while the Fermi level is defined for any temperature.
2. The Fermi energy is an energy difference (usually corresponding to a kinetic energy), whereas the Fermi level is a total energy level including kinetic energy and potential energy.
3. The Fermi energy can only be defined for non-interacting fermions (where the potential energy or band edge is a static, well defined quantity), whereas the Fermi level (the electrochemical potential of an electron) remains well defined even in complex interacting systems, at thermodynamic equilibrium.

*Fermi surface*—An abstract boundary in reciprocal space useful for studying the properties of the material. At absolute zero temperature, the Fermi surface represents a sphere of radius  $p_F$ , which is obtained from the Fermi energy. A deformation of the Fermi sphere corresponds to a change in the properties of the material. Fermi surfaces are only defined for metals, i.e. when the Fermi level is in the band gap (there is no Fermi surface for insulators and semiconductors).

*Fermi liquid*—A theoretical model of interacting fermions that describes the normal state of most metals at sufficiently low temperatures. The interaction between the particles of the many-body system does not need to be small.

*Dirac point*—The Dirac points in graphene are six locations in momentum space, on the edge of the Brillouin zone, divided into two non-equivalent sets of three points.

The two sets are labeled  $K$  and  $K'$ . (I assume) the Dirac crossing energy is the energy at the Dirac points (also called Dirac points).

*Quasiparticle*—In physics, quasiparticles and collective excitations (which are closely related) are emergent phenomena that occur when a microscopically complicated system such as a solid behaves as if it contained different weakly interacting particles in free space. For example, as an electron travels through a semiconductor, its motion is disturbed in a complex way by its interactions with all of the other electrons and nuclei; however it approximately behaves like an electron with a different mass (effective mass) traveling unperturbed through free space. This “electron” with a different mass is called an “electron quasiparticle”. In another example, the aggregate motion of electrons in the valence band of a semiconductor or a hole band in a metal is the same as if the material instead contained positively charged quasiparticles called holes. Other quasiparticles or collective excitations include phonons (particles derived from the vibrations of atoms in a solid), plasmons (particles derived from plasma oscillations), and many others. These particles are typically called “quasiparticles” if they are related to fermions, and called “collective excitations” if they are related to bosons, although the precise distinction is not universally agreed upon. Thus, electrons and holes are typically called “quasiparticles”, while phonons and plasmons are typically called “collective excitations”.

*Annealing*—In metallurgy and materials science, annealing is a heat treatment that alters the physical and sometimes chemical properties of a material to increase its ductility (ability to deform under tensile stress) and reduce its hardness, making it more workable. It involves heating a material to above its recrystallization temperature, maintaining a suitable temperature, and then cooling. In annealing, atoms migrate in the crystal lattice and the number of dislocations decreases, leading to the change in ductility and hardness.

A *substitutionally disordered system* is one in which more than one atom is randomly distributed on an otherwise periodic lattice with translational invariance. To this category belong disordered alloys, mixed crystals and doped semiconductors.

A *positionally disordered system* is one in which the atomic positions are randomly distributed. In this category are classified liquid metals, some molecular liquids and amorphous metals.

A *topologically disordered system*, which was originally proposed to apply to amorphous semiconductors. In this kind of disordered system, the long-range order in the atomic distribution is completely broken while the short-range order (hereafter referred to as SRO) is maintained in the sense that the coordination number of each atom remains the same as in the case of a corresponding ordered crystal, although bond lengths and angles in a disordered system fluctuate. Essentially, this type of disorder is considered to belong to the category of positional disorder. However, since networks formed by the covalent bonds are regarded as playing a significant role in determining various physical properties of amorphous semiconductors, this type of disorder is distinguished from the more general “positional disorder” and is specifically called ‘topological disorder’.

# Appendix B: Mathematical Preliminaries

## Kindergarten Math

Informally, a *set* is a collection of objects. A *space* is a set with some added structure, i.e. members of a given space obey certain rules specific for that space. A *vector space* is a set, whose members are closed under finite vector addition (adding any finite number of members of the set will give a value that is also a member of the set) and scalar multiplication (multiplying any member of the set by a scalar will give a value that is also a member of the set). The real vector (or coordinate) space of  $n$ -dimensions is denoted as  $\mathbb{R}^n$ .

A *function* is a relation between a set of inputs and a set of outputs permissible for that function. The set of inputs (called the *domain* of the function) contains values for which the function is defined. To each member of the domain the function assigns an output value from the set of outputs. The set of outputs is called the *image* (or *range*) of the function. A *function space* is a set of functions of a given type, which relate a set  $X$  to a set  $Y$ , denoted by  $X \rightarrow Y$ .

Broadly speaking, a *map* (or mapping) is a synonym for a function.<sup>1</sup> A map  $f: X \rightarrow Y$  from a set  $X$  to a set  $Y$  is a function  $f$  such that for every  $x \in X$ , there is a unique object  $f(x) \in Y$ . An *operator* is a mapping from one vector space to another. In physics, an operator is a function from a space of physical states to another space of physical states. A *linear operator* is a mapping  $f$  from one vector space to another  $f: X \rightarrow Y$  that satisfies the following conditions

1. Additivity:  $f(x + y) = f(x) + f(y)$  for any two vectors  $x, y \in X$ ;
2. Homogeneity:  $f(\alpha x) = \alpha f(x)$  for any scalar  $\alpha$ .

---

<sup>1</sup>In category theory, a map is a *morphism*, which is a structure preserving operation that generalizes the idea of a function.

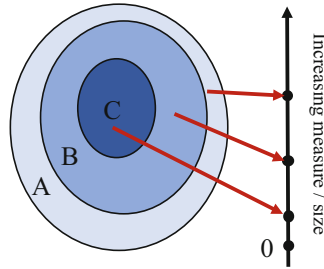


**Fig. B.1** Measure

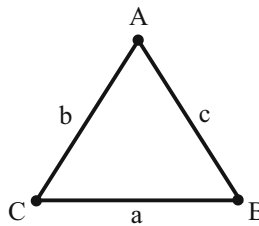


**Fig. B.2** Consider the set  $X$ , which contains the points  $A, B$ , and  $C$ , i.e.  $X = \{A, B, C\}$ . Define  $a, b$ , and  $c$  as the distances connecting the points  $A, B$ , and  $C$ . For a given subset of  $X$ , say  $\{A, B\}$ , the measure  $\mu(\{A, B\}) = 2$  tells us that  $\{A, B\}$  consists of two members, whereas  $\mu(X) = 3$  tells us that  $X$  consists of three members. These (counting) measures are nonnegative and obviously correspond to size

A *transformation* is a function that maps a set  $X$  onto itself, i.e.  $f : X \rightarrow X$ . The definition of a linear transformation is a linear mapping from one vector space to itself and satisfies the above definition.

## Measure Theory

*Measure theory* is the study of measures. In mathematical analysis, a *measure* on a set is a systematic way to assign a number to each suitable subset of that set, intuitively interpreted as its size. Informally, a measure is a generalization of the concepts of length, area, and volume. Measures have the property of being monotone in the sense that if  $C$  is a subset of  $B$ , which is a subset of  $A$ , the measure of  $C$  is less than or equal to the measure of  $B$  and the measure of  $B$  is less than or equal to the measure of  $A$  (Fig. B.1).

Only nonnegative measures can be related to size/volume of the corresponding subsets. Thus, for any subset  $M \subseteq X$  ( $M$  is contained in or equal to  $X$ ), we would like to have  $\mu(M) \geq 0$ . In general, there can be subsets for which trying to assign size/volume leads to a contradiction. For instance, in Fig. B.2,  $\mu(\{A, B\}) = 2$  is a counting measure, which gives the number of members in (or the cardinality of) the subset  $\{A, B\}$ . Such measure is defined for all subsets of  $X$ , including subsets containing only

one point. However, if the measure is defined as the distance between two points,<sup>2</sup> then  $\mu(\{A, B\}) = c$ . In this case, subsets consisting of one point cannot be assigned a meaningful size and are thus non-measurable.

Problems related to non-measurable subsets are avoided by restricting the suitable sets. This is accomplished using a sigma algebra  $\Sigma$ , which is the collection of all measurable subsets for a given measure on a set.

By definition [186] a sigma algebra  $\Sigma$  satisfies the following conditions

1. The empty set is in  $\Sigma$ ;
2. If a subset  $M$  is an element of  $\Sigma$ , then the complement of  $X$  and  $M$  (all the elements in  $X$  that are not contained in  $M$ ) is also contained in  $\Sigma$ , i.e. if  $M \in \Sigma$ , then  $X \setminus M \in \Sigma$ ;
3. For any collection of countable number of sets in  $\Sigma$ , their union must also be in  $\Sigma$ .

When the above three axioms are satisfied, the collection  $\Sigma$  of subsets of  $X$  is called a *sigma algebra* ( $\sigma$ -algebra) on the set  $X$  and the pair  $(X, \Sigma)$  is called a *measurable space* (assigning a measure to any subset in the space won't lead to a contradiction).

Formally [186], a *measure space* is described by the triple  $(X, \Sigma, \mu)$ , where  $X$  is a set,  $\Sigma$  is the sigma algebra of measurable sets, and  $\mu$  is a function that assigns nonnegative values to the subsets in  $\Sigma$ , i.e.  $\mu : \Sigma \rightarrow [0, \infty]$ . Additional requirements on  $\mu$  are:

1. The measure of the empty set is zero, i.e.  $\mu(\emptyset) = 0$ ;
2. The measure of the union of any given number of disjoint<sup>3</sup> sets in  $\Sigma$  should be the sum of their measures. In mathematical notation,  $\mu(\cup_{n \in \mathbb{N}} E_n) = \sum_{n=0}^{\infty} \mu(E_n)$ , where  $\langle E_n \rangle_{n \in \mathbb{N}}$  is a disjoint sequence of members in  $\Sigma$  and  $\mathbb{N}$  is the set of natural numbers.

In probability theory, the measure is chosen in such a way that  $\mu(X) = 1$  (the set  $X$  is measurable as it is the compliment of the empty set  $\emptyset$ ) and the measurable subsets (the subsets of  $X$  that form the  $\sigma$ -algebra) are interpreted as events which can be assigned probabilities.

---

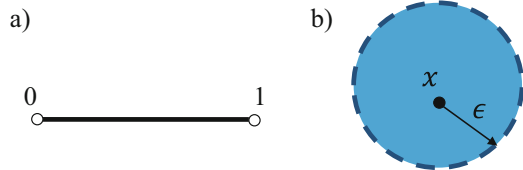
<sup>2</sup>Such choice of measure coincides with the notion of a metric in this specific example. However, a measure *should not* be confused with a metric on a given set. Intuitively, a measure on a set  $X$  is a function that assigns size/volume to its subsets, whereas a metric on  $X$  is a function that defines distances among the elements in the set. (See Sect. 1.2 for a formal definition of a metric space.)

<sup>3</sup>A sequence  $\langle E_n \rangle_{n \in \mathbb{N}}$  is disjoint if no point belongs to more than one  $E_n$ .

**Fig. B.3** A famous joke in topology says that a topologist is someone who cannot distinguish between a coffee cup and a donut. The picture on the left shows that a donut can be stretched into a coffee cup (and vice versa), which makes the two topologically equivalent objects (Picture found on the web)



**Fig. B.4** Examples of open sets in metric spaces: (a) the open interval  $(0, 1)$ ; (b) the  $\epsilon$ -ball around the point  $x \in X$



### Point-Set Topology

Broadly speaking, *topology* studies properties of spatial objects that are preserved under continuous deformations. The objects of topology can be geometrical curves and surfaces, phase spaces, space-time continuum, symmetry groups, etc. If one object can be continuously stretched to form another (without the use of tearing or gluing), the two objects are said to have the same topological properties (Fig. B.3).

Point-set topology (or general topology) investigates the properties of topological spaces through the study of open sets. *Open sets* generalize the idea of an open interval in the real line, i.e. a set is open if it does not contain any of its boundary points (Fig. B.4). The most general definition of open sets in topological spaces is fairly abstract and hard to visualize. Thus, we will start by introducing open sets in metric spaces.

By definition [187], a *metric space* is the ordered pair  $(X, \rho)$ , where  $X$  is a set and  $\rho$  is a function called a *metric* on the set. Applying  $\rho$  to any two members of the set returns a real value that corresponds to the distance between them, i.e.  $\rho : X \times X \rightarrow \mathbf{R}$ . Additional requirements on  $\rho$  are:

1. Positivity:  $\rho(A, B) \geq 0$  (with  $\rho(A, B) = 0$  for  $A = B$ );
2. Symmetry:  $\rho(A, B) = \rho(B, A)$ ; and
3. Triangle inequality:  $\rho(A, C) \leq \rho(A, B) + \rho(B, C)$ .

In a metric space  $X$ , define the  $\epsilon$ -ball ( $\epsilon > 0$ ) about a point  $x \in X$  to be the collection of all points  $y$  located a distance smaller than  $\epsilon$  away from  $x$ , i.e.  $B_\epsilon(x) = \{y \in X \mid \rho(x, y) < \epsilon\}$  (Fig. B.4b). Any subset  $M$  of  $X$  is said to be *open* if, for each point  $x \in M$ , there exists an  $\epsilon$ -ball about  $x$  that is completely contained in  $M$ .

Although the spaces of interest in this paper are all metric spaces, open sets can be more generally defined as subsets in topological spaces. Any object in topology is described by a *topological space*, which can be viewed as a set of points and neighborhoods (around these points) related by certain axioms. Formally [187], a topological space is the ordered pair  $(X, T)$ , where  $X$  is a set of points and  $T$  is a collection of open subsets of  $X$  that obey the following properties

1. The (trivial) subsets  $X$  and the empty set  $\emptyset$  are open, i.e.  $X, \emptyset \in T$ .
2. The intersection of any collection of open sets is open, i.e. if  $A, B \in T$ , then  $A \cap B \in T$ .
3. The union of any collection of open sets is open, i.e. if  $A, B \in T$ , then  $A \cup B \in T$ .

When the above requirements are fulfilled,  $T$  is a topology on the set  $X$ . Open sets in topological spaces are used to define nearness/distinguishability among points in space even if the metric is not well defined. This is achieved with the use of neighborhoods. Technically, a set  $N$  is a *neighborhood* of a point  $x \in X$  if there is an open set  $M$  such that  $x \in M$  and  $M \subset N$  ( $M$  is a subset of  $N$ ).

The functions (or transformations) in topology are those that operate on open sets and return images that are also open sets. Although such functions (called *open maps*) do not have to be continuous, the continuous open maps are the ones of greatest interest in topology. A map  $f$  between two topological spaces  $f: X \rightarrow Y$  is said to be *continuous* at a point  $x \in X$  if, given any neighborhood  $M$  of  $f(x) \in Y$ , there is a neighborhood  $N$  of  $x$  in  $X$  such that  $f(N) \subset M$  (applying  $f$  to any point in the neighborhood of  $x$  returns a value that is contained in the neighborhood of the image of  $x$ ) [187].

For a given topological space  $X$ , any set that can be formed from open (or closed) subsets through countable<sup>4</sup> union and countable intersection is called a *Borel set* [188]. An example of a Borel set is the set of all real numbers  $\mathbb{R}$ , which can be used to describe  $d$ -dimensional (finite or infinite) systems of countable lattice points (see next section on Group Theory). The collection of all Borel sets for a given topological space forms the *Borel sigma algebra*  $\mathcal{B}$  with a *Borel measure*  $\nu$  defined on all open sets. In other words, for every topological space  $X$  one can construct a Borel  $\sigma$ -algebra  $\mathcal{B}$ , which is the  $\sigma$ -algebra generated by all open sets in the space. To any Borel  $\sigma$ -algebra one can associate a corresponding Borel measure  $\nu$ , which (if compatible with the topology  $T$  of the set  $X$ ) makes the topological space  $(X, \mathcal{B}, \nu)$  measurable.

In measure theory, any measure defined on the open sets of the topological space, must also be defined on all Borel sets of that space. In probability theory, any given probability measure of the Borel  $\sigma$ -algebra is equivalent to a corresponding probability distribution of a given real random variable defined on the probability space.

---

<sup>4</sup>Here “countable” is used in the sense of either finite or countably infinite.

## Group Theory

In abstract algebra, *group theory* is the study of abstract and physical systems in which symmetry is present. The systems of interest in group theory are represented by the algebraic structures known as groups. A group is a finite or an infinite collection of elements together with a rule (called the group operation) that combines any two elements to form a third element in a way that satisfies a certain set of rules. Formally [189], a *group*  $G$  is a set equipped with an operation assigning to every (ordered) pair of elements, a third element, satisfying the following rules

1. Closure: If  $f, g \in G$ , then  $h = fg \in G$ ;
2. Associativity: If  $f, g, h \in G$ , then  $f(gh) = (fg)h$ ;
3. Identity property: There is an identity element,  $e$ , such that for all  $f \in G$ ,  $ef = fe = f$ ;
4. Inverse property: Every element  $f \in G$  has an inverse  $f^{-1}$ , such that  $ff^{-1} = f^{-1}f = e$ .

An important technique in group theory is representing the elements of a given group as linear transformations of vector spaces. A representation of a group  $G$  is a mapping  $D$  of the elements of  $G$  onto a set of linear operators with the following properties

1. The representation of the identity  $e$  is the identity operator  $I$  in the space on which the linear operators act, i.e.  $D(e) = I$ ;
2. The representation of the multiplication of elements in the group is the natural multiplication in the linear space on which the linear operators act, i.e. if  $g_1, g_2 \in G$ , then  $D(g_1, g_2) = D(g_1)D(g_2)$ .

A representation is *unitary* if every  $D(g_i)$  is unitary. If  $G$  is a finite group with identity  $e$  and with group composition  $(g_1, g_2) \rightarrow g_1, g_2$ , then a *linear representation*  $L$  of the group  $G$  in a given vector space  $V$  is a homomorphism on the vector space that preserves the linear structure. The *regular representation* of a group is the linear representation that satisfies  $D(g_1)|g_2\rangle = |g_1g_2\rangle$ , i.e. a linear representation generated when  $G$  acts on itself by translation. If you take the elements of a group and use them to form an orthonormal basis for a vector space, you.

An *Abelian group* is one in which the multiplication law is commutative, i.e.  $g_1g_2 = g_2g_1$ . An  *$n$ -dimensional free Abelian group* is an Abelian group with a basis, which makes it very similar to a vector space. Thus, a representation of a crystal lattice as a free Abelian group allows us to reduce many group-theoretic problems to problems in linear algebra. The group of all integers  $\mathbb{Z}$  is an example of a free Abelian group with the basis  $\{1\}$  and the addition as the group operation. A *lattice* in the  $n$ -dimensional real space  $\mathbb{R}^n$  is a subgroup of  $\mathbb{R}^n$ , which is isomorphic<sup>5</sup>

---

<sup>5</sup>In group theory, isomorphism is a one-to-one mapping of one group to another that preserves the multiplication law. In more general sense, isomorphism is a mathematical operation that admits an inverse.

to  $\mathbb{Z}^n$  and which spans the real vector space  $\mathbb{R}^n$ , i.e. the lattice is generated from all linear combinations with integer coefficients of the basis vectors of  $\mathbb{R}^n$ . The  $d$ -dimensional integer lattice has a natural basis consisting of the positive integer unit vectors, but it can have many other bases as well. The two-dimensional integer lattice is a free Abelian group with vector addition as the group operation and a basis  $\{(0, 1), (1, 0)\}$ .

A *symmetry group* of an object is the group of all transformations under which the object is invariant with composition as the group operation. In mathematics, physics and chemistry, a *space group* is the symmetry group of a configuration in space. Let a group  $G$  act on a set  $X$ . The *orbit* of an element  $x \in X$  is the set of elements in  $X$  to which the element  $x$  can be moved by the group action. The orbit of  $x$  is denoted by  $G \cdot x$ .

## Probability Theory

*Probability theory* is the branch of mathematics concerned with the analysis of random phenomena. In probability theory, a *probability space* (also called a probability triple) is a mathematical construct that models a real-world process in which the possible states of the system under consideration occur randomly. Each probability space  $(\Omega, \mathcal{F}, P)$  consists of the following components:

1. *Sample space*  $\Omega$ , which is the nonempty set of all possible outcomes.
2. *Event space*  $\mathcal{F}$ , which is a collection of events (subsets) of the sample space  $\Omega$ , where each event is a set containing zero or more outcomes.
3. *Probability function*  $P$ , which assigns probabilities to the events in the event space  $\mathcal{F}$ .

An *outcome*  $\omega$  is the result of a single execution of the model. Since individual outcomes might be of little practical use, more complex *events* are used to characterize given sets of outcomes. The collection of all such events is a  $\sigma$ -algebra  $\mathcal{F}$ . Finally, there is a need to specify each event's likelihood of happening. This is done using the *probability measure function*  $P$ .

Once the probability space is established, the model can be executed resulting in an outcome  $\omega$  from the sample space  $\Omega$ . All the events in  $\mathcal{F}$  that contain the selected outcome  $\omega$  are said to “have occurred”. The selection is performed in such a way that if the experiment were to be repeated an infinite number of times (i.e. infinite number of outcomes), the relative frequencies of occurrence of each of the events would coincide with the probabilities prescribed by the function  $P$ . (See Fig. B.5 for a simplified example.)

The probability space  $(\Omega, \mathcal{F}, P)$  is a type of a measure space where the measure is probability measure function and the measure of the whole set equals unit.

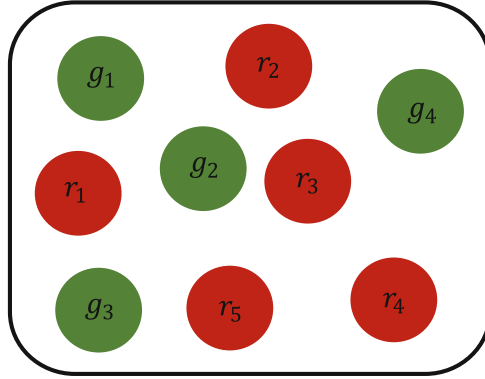


**Fig. B.5** Consider a container with four green balls and five red balls inside, i.e. sample space  $\Omega = \{g_1, g_2, g_3, g_4, r_1, r_2, r_3, r_4, r_5\}$ . Let us assume that an execution of the model amounts to drawing a single ball out of this container. Consider the subset of green balls  $A = \{g_1, g_2, g_3, g_4\}$  and the subset of red balls  $B = \{r_1, r_2, r_3, r_4, r_5\}$ . Subset  $A$  represents the event of drawing a green ball and it contains four outcomes. Similarly, subset  $B$  represents the event of drawing a red ball and it contains five outcomes. The two subsets  $A$  and  $B$  form the event space  $\mathcal{F}$  of the given problem, i.e.  $\mathcal{F} = \{A, B\}$ . If we draw a green (red) ball, event  $A$  ( $B$ ) is said to have occurred. The probability measure for event  $A$  is  $P(A) = 4/9$ , whereas the probability measure for event  $B$  is  $P(B) = 5/9$ .

*Conclusion: Based on the above definitions, we see that a transport problem in a (finite or infinite)  $d$ -dimensional lattice can be modeled with the help of a probability space  $\Omega = (\mathbb{R}, \mathcal{B}, \nu)$ , where  $\mathbb{R}$  is the set of all real numbers,  $\mathcal{B}$  is the Borel sigma algebra on  $\mathbb{R}$ , and  $\nu$  is the Borel probability measure.*

# Curriculum Vitae

EVDOKIYA (EVA) KOSTADINOVA  
Curriculum Vitae  
254 710 1135  
eva\_kostadinova@baylor.edu  
Baylor Research & Innovation Collaborative  
100 Research Pkwy, Waco, TX 76704, USA



## EDUCATION

### **Ph.D., Department of Physics, Baylor University, Exp. Graduation: Dec 2017**

- Dissertation: “Spectral Approach to Transport Problems in Two-Dimensional Disordered Lattices: Physical Interpretation and Applications”
- Advisor: Dr. T. Hyde
- Collaborators: Dr. L. Matthews, Dr. C. Liaw

### **B.S., Department of Physics, Furman University, Graduated: May 2014**

- Thesis: “Sensors for Extraterrestrial Robot Land Navigation”
- Advisor: Dr. D. Moffett
- Collaborators: Dr. J. Conrad

### **B.A., Department of Political Science, Furman University, Graduated: May 2014**

- Thesis: “Middle East and Islamic Studies Programs in the US in the Wake of the Arab Spring”

- Advisor: Dr. A. K. Yildirim
- Minor: Middle East and Islamic Studies

### **WORK EXPERIENCE**

- Assistant Research professor in CASPER Complex Plasma Group, Baylor University, Feb 2017–present
- Research assistant in Baylor University Complex Plasma Group, Baylor University, May 2016–Present
- Teaching assistant in Baylor University Physics Department, Baylor University, Sep 2014–May 2016
- Lab assistant in Furman University Physics Department, Furman University, Sep 2012–May 2014
- Physics tutor, Furman University, Sep 2012–May 2014
- Library Assistant in Inter Library Loan Department, Furman University, Sep 2010–May 2014

### **RESEARCH EXPERIENCE**

#### *Graduate Research:*

- Department of Physics, Baylor University, Sep 2014–Present (research advisor: Dr. T. Hyde)  
Topics: Spectral approach to Anderson-type transport problems in two-dimensional infinite disordered systems (physical interpretation and application to quantum and classical systems); Long-range attractive forces in plasma crystals; Disorder-induced phase transitions in complex plasmas; Complex plasma graphene analogues; Thermodynamics of finite non-Hamiltonian systems; Electrorheological dusty plasmas; Coulomb and Yukawa explosions; Dust chain formation and stability in microgravity.

#### *Undergraduate Research:*

- Madison Plasma Dynamo Experiment (MPDX), Department of Physics, University of Wisconsin (Madison), May–July 2013 (research advisor: Dr. C. Forest, post doctorate advisor: Dr. C. Cooper)  
Role: Designed, constructed and programmed a motion control system for robotic insertion of sweep probe used in plasma environment.
- Independent Study on Space Robotics, Physics Department, Furman University, January–May 2013 (research advisor: Dr. J. Conrad)  
Role: Conducted a study on types of sensors used in robot land navigation, their relative effectiveness in extraterrestrial conditions, and possible designs of sensor systems that optimize performance and reduce expenses. Constructed a fully autonomous robot to perform small obstacle avoidance;
- Fundamental topics in physics, Department of physics, Furman University, Jan–May 2013 (research advisor: Dr. W. Baker)  
Role: Developed a mathematical model to measure the amount of linear and angular momentum stored in the electromagnetic fields of a discharging parallel plate capacitor with a neodymium magnet positioned between its plates

- Hydration Status of Collagen as Revealed by Raman Spectroscopy, Department of Physics, Furman University, Jun–Aug 2011 (research advisor: Dr. D. Wang)  
Role: Investigated the capability of Raman spectroscopy in revealing the physiochemical status of collagen through analysis of bovine material samples (Sigma-Aldrich)

## JOURNAL PUBLICATIONS

- E G Kostadinova, C D Liaw, A S Hering, A Cameron, F Guyton, L S Matthews, & T W Hyde (2018). Spectral approach to transport in the 2D honeycomb lattice with substitutional disorder. *arXiv preprint arXiv:1711.09381*. (submitted to Physical Review B)
- E G Kostadinova, K Busse, N Ellis, J Padgett, C D Liaw, L S Matthews, & T W Hyde (2017). Delocalization in infinite disordered two-dimensional lattices of different geometry. *Physical Review B*, 96(23), 235408.
- E G Kostadinova, C D Liaw, L S Matthews, & T W Hyde (2016). Physical interpretation of the spectral approach to delocalization in infinite disordered systems. *Materials Research Express*, 3(12), 125904.

## CONFERENCE PROCEEDINGS

- E G Kostadinova, F Guyton, A Cameron, K Busse, C D Liaw, L S Matthews, & T W Hyde (2018) Transport properties of disordered two-dimensional complex plasma crystal, *Contrib. Plasma Phys.*, 58 (2–3), 209–216.

## CONFERENCE TALKS

- E G Kostadinova, J Padgett, K Busse, C D Liaw, L S Matthews, & T W Hyde, “Anomalous diffusion in microgravity complex plasma cloud”, *APS DPP*, Portland, OR, Nov 5–9, 2018
- E G Kostadinova, J Padgett, K Busse, C D Liaw, L S Matthews, & T W Hyde, “Anomalous diffusion in 1D dusty plasma structures: A fractional Laplacian model for strong correlations”, *15<sup>th</sup> Dusty Plasma Workshop*, Baltimore, MD, May 29–June 1, 2018
- E G Kostadinova, C D Liaw, L S Matthews, & T W Hyde, “Lattice wave transport in a 2D complex plasma graphene analogue”, *APS DPP Conference*, Milwaukee, WI, Oct 23–27, 2017
- E G Kostadinova, C D Liaw, L S Matthews, & T W Hyde, “Transport properties of disordered 2D complex plasma crystal”, *SCCS Conference*, Kiel, Germany, Jul 30–Aug 4, 2017
- E G Kostadinova, C D Liaw, L S Matthews, & T W Hyde, “Spectral Approach to Anderson Localization in 2D Complex Plasma Crystal”, *APS DPP Conference*, San Jose, CA, Oct 31–Nov 4, 2016

## POSTER PRESENTATIONS

- E G Kostadinova, K Busse, L S Matthews, & T W Hyde, “Dust chain formation in microgravity complex plasma”, *APS DPP*, Portland, OR, Nov 5–9, 2018

- E G Kostadinova, K Busse, C D Liaw, L S Matthews, & T W Hyde, “Nematic transition in microgravity complex plasma liquid crystals”, *15<sup>th</sup> Dusty Plasma Workshop*, Baltimore, MD, May 29–June 1, 2018
- E G Kostadinova, A Sheppard, “Women in Physics: Lise Meitner”, *Southeast Conference for Undergraduate Women in Physics*, University of Tennessee, Knoxville, TN, Jan 2012
- E G Kostadinova, B Mayberry, V Strait, W Smith, “Conservation of Momentum: Parallel Plate Capacitor Experiment”, *Fall Jointed Zone Meeting of the AAPT and the SPS*, Furman University, Greenville, SC, Oct 2013

### **HONORS and AWARDS**

- Springer Thesis award recognizing outstanding Ph. D. research, May 2018
- Baylor University Graduate School Fellowship, Aug 2014–Dec 2017
- Second place on Atmel Corporation National Robotics Competition at World Maker Faire, New York Hall of Science, Queens, NY, September 2012
- National Scholar Award of \$1,000 from the National Society of High School Scholars, May 2011
- Dean’s List – for students with GPA in the top 25% of their class, 2010, 2011, 2012, 2013
- National Society of High School Scholars Honorable Membership, May 2010–Present

### **SCIENTIFIC ORGANIZATIONS AND SOCIETIES**

- American Association of Physics Teachers, Member, Sep 2014–Present
- American Astronomical Society, Member, Sep 2013–Present
- American Physical Society (APS), Plasma Physics and Astrophysics, Member, Sep 2012–Present
- Society of Physics Students (SPS), Member, Sep 2010–2014
- Association for Women in Mathematics, Member, Sep 2016–Present
- National Society of High School Scholars (NSHSS), Honorable Member, May 2010–Present
- Sigma Pi Sigma Physics Honor Society, Honorable Member, Apr 2013–Present
- Pi Sigma Alpha Honor Society, Honorable Member, Jan 2014–Present

### **PUBLIC SERVICE AND OUTREACH**

- Judge coordinator for Code Red (high-school student science competition), Waco, TX, Nov 2017 and Nov 2016
- Workshop coordinator for APS DPP Conference, San Jose, CA, Oct 31–Nov 4, 2016
- Physics Department Representative in Baylor Graduate Students Association, Sep 2014–May 2017
- Graduate School Mentor in Baylor Mentor-Mentee Program, Sep 2015–Dec 2017
- President of Furman University Robotics Club, Sep 2012–May 2014
- Treasurer of Furman University Astronomy Club, Sep 2012–May 2014

- President of Furman University International Students Association, Mar 2012–May 2014
- Treasurer of Furman University International Students Association, Mar 2011–Mar 2012